Linear Stability Analysis of a Rijke Tube and Modeling of Turbulent Combustion Using Dynamic Well-Stirred Reactors

by

J. David Losh

Thesis submitted to the Faculty of the
Virginia Polytechnic Institute and State University
in partial fulfillment of the requirements for the degree of

MASTER OF SCIENCE

in

Mechanical Engineering

William R. Saunders, Chair
William T. Baumann
Uri Vandsburger

May 10, 2004
Blacksburg, Virginia

Keywords: Instability, Rijke, well-stirred reactor, combustion modeling

Linear Stability Analysis of a Rijke Tube and Modeling of Turbulent Combustion Using Dynamic Well-Stirred Reactors

by

J. David Losh

William R. Saunders, Chairman
Mechanical Engineering

Abstract

In the first part of this work, instability is correctly predicted for a Rijke tube with a new two-term acoustic forcing term derived from a one-dimensional flame dynamics model. The new two-term acoustic forcing term, which is comprised of the summation of chemical heat release rate and heat transfer due to convection, correctly predicts instability where older models of acoustic forcing based solely on chemical heat release rate incorrectly predicted stability. This stability analysis correctly predicts the inlet conditions of the instability in addition to the frequency of instability.

In the second part of this work, networks of dynamic well-stirred reactors are used to model qualitative behavior observed in turbulent combustion. First a model of dynamic well-stirred reactor is derived, and then several reactors are coupled together by recirculation. The dynamics of the various models are computed and assessed. The models exhibit interesting behavior that has been viewed experimentally including hysteresis and peaking in the dynamic response.

Acknowledgements

I would like to thank my parents, Larry and Mary Lana, for all their support throughout my life. They always encouraged my interests from soccer to science, and without that encouragement I would not have completed any of my education, much less this thesis.

I would like to thank the members of the VACCG for their all their support, especially Ludwig Haber for his guidance and mentoring.

Also, I would like to thank the friends I have had in Blacksburg during my time here: Leah, Rachel & Aaron, Sarah, Nick, Chris, and Rebecca. They have all helped, encouraged and listened. Also, I would like to thank my office mates, Anne and Jonathan, for hours of help, intellectual conversations and not so intellectual conversations. And a special thanks to Smee.

Most of all I would like to thank Dr. William T. Baumann for an enormous amount of support, advice, encouragement, and faith. He always displayed an upbeat, excited attitude and sense of humor about my research and my life in general. I wrote a thesis under his guidance, but most important I made a friend in one of the nicest and most intelligent people I have ever met. Giddy Up Doctor B.

Table of Contents

List of Figures

List of Tables

Nomenclature

Φ	equivalence ratio
ω_f	mass based reaction rate of fuel
ρ	density
α	percentage of recirculation
β	percentage of recirculation
τ	time delay
Y_i	mass fraction of the i-th species
$\dot{m}$	mass flow rate
V	volume of the reactor
Δh_r	enthalpy of formation
c_p	specific heat
T	temperature
MW	molecular weight
a	ratio of molecular weights
u	velocity
p	pressure
e	internal energy
q	heat release
q'''	heat release per unit volume
$\tilde{\bullet}$	unsteady portion of variable $\bullet$
$\bar{\bullet}$	steady portion of variable $\bullet$
ψ	basis function
k_i	wave number
γ	ratio of specific heats
φ	phase shift
$\bar{c}$	speed of sound
η_i	pressure due to the i-th mode

ω	natural frequency
x	spatial coordinate
ζ	damping coefficient
t	temporal coordinate
s	Laplace variable
k	thermal conductivity
ω_i	molar reaction rate of the i-th species
ε	emissivity
σ	Stefan-Boltzmann constant
h	convection heat transfer coefficient
A	area
$\dot{Q}_r$	heat release rate

1 Introduction

1.1 Background – Thermoacoustic Instabilities

Governmental regulations have forced gas turbine manufacturers to reduce the amount of pollution created by gas turbines. Much of this legal policy has concentrated on the reduction of nitrous oxides (NO_x) from the exhaust stream of turbines. One of several ways to reduce NO_x is to use lean premixed combustion. By using lean premixed combustion, the flame temperature is reduced, thus limiting the energy available to produce NO_x which has high activation energy. However, lean premixed combustion is highly susceptible to thermoacoustic instabilities because of smaller flame lengths leading to a highly localized heat release. These instabilities occur when the flame excites the acoustic natural frequencies of the combustor causing pressure oscillations inside the combustor, which in turn perturb the incoming premixed flow. The perturbed inlet flow causes fluctuations in the heat release, which cause greater pressure oscillations. This behavior creates a self-excited loop, which is illustrated in the block diagram shown in Figure 1.1.

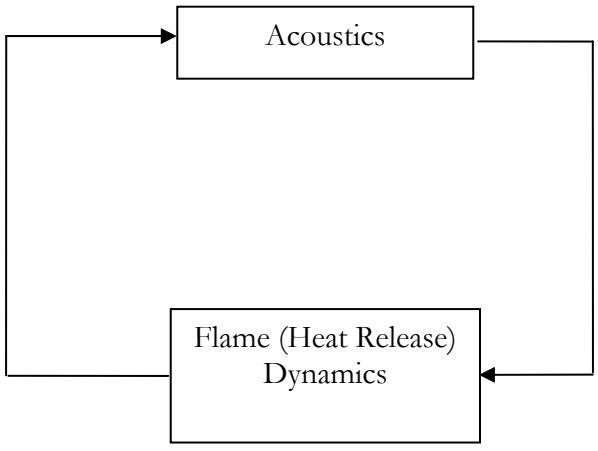

Figure 1.1: Self-excited thermoacoustic loop

The instability will eventually settle into a high amplitude limit cycle. This type of unstable behavior is detrimental to the combustor and turbine as a whole because the high amplitude pressure oscillations cause parts within the turbine to fatigue and eventually fail. This has led both academia and the private sector to pursue solutions, which will reduce or eliminate these oscillations as well as attempting to ultimately understand the nature of the problem.

1.2 Objectives

The goal of this work is to first establish that with accurate acoustic and heat release modeling the instability can be correctly predicted in a laminar flat flame case. A one-dimensional model developed by Ludwig Haber will be used to determine the heat release dynamics model [11]. A two-mode acoustics model will be developed here following the procedure of Annaswamy [3]. These two models will be combined to predict the stability of the system for a given mass flow and equivalence ratio.

The second goal of this work is to develop a reduced-order dynamic model that qualitatively reproduces features of flame dynamics documented in experiments. This model will be based on a dynamic version of the common well-stirred reactor (WSR). Multiple WSR's will be coupled together by recirculation in order to produce results of higher order. The ability of this WSR model to accurately model both heat release dynamics and other attributes of flame dynamics will be assessed.

1.3 Contributions of the Thesis

In the first section of this work, instability was correctly predicted by using a newly developed model of acoustic forcing in self excited Rijke tube model. This new model of

the acoustic forcing term includes both chemical heat-release rate and convection. This model was verified with PREMIX software modified by Ludwig Haber [11]. The model was combined with an acoustics model of the Rijke tube to study the stability of the closed-loop thermoacoustic combustion process. The model was able to correctly predict the flow rate and equivalence ratio (as well as the frequency) at which instability would occur. It was also shown that the use of chemical heat-release as a model of the acoustic forcing term incorrectly predicted a stable system for cases where instability has been observed experimentally.

In the second half of the thesis, it is shown that a dynamic well-stirred reactor network can capture qualitative behavior seen in turbulent combustors. These WSR networks are capable of modeling blowout. Bifurcation diagrams of the system's equilibrium points show that multiple equilibria exist for the same operating conditions. The model also exhibits widely different heat release dynamics for different equilibrium points. The model was capable of producing frequency responses that exhibited peaked behavior has seen in experimental data of turbulent rigs. The bandwidth associated with models that exhibit the same qualitative behavior seen in swirl-stabilized rigs is high however; models that exhibit a reasonable bandwidth lack the peaked behavior in the heat release dynamics that would match experimental results.

1.4 Thesis Organization

The remainder of this thesis describes the laminar instability analysis and the modeling completed using well-stirred reactors. Chapter 2 presents the literature related to both topics. Chapter 3 presents the basics of the combustion model used in finding the flame dynamics, the derivation of the acoustics model, the identification of the dominating terms of the heat addition term, and finally the linear stability analysis. Chapter 4 presents the dynamic well-stirred reactor modeling. First a single well-stirred reactor (WSR) model is developed as the basis of the later networks of well-stirred reactors. A network of two WSR's and then three WSR's will be developed and the

dynamics of each explored. The last chapter presents the conclusions of the laminar instability analysis as well as conclusions for the well-stirred reactor modeling. Future work suggestions are offered on both topics in the last chapter as well.

2 Literature Review

Chapter 2 presents a review of the literature already available about combustion instability, and specifically modeling techniques for both laminar and turbulent combustion. There is a plethora of literature and information on the Rijke tubes, first order modeling, and thermoacoustic instabilities. There also exists a large amount of literature pertaining to the modeling of turbulent flames and consequent instability. However there is not a large volume of work on dynamic well-stirred reactor models; also, the work available focuses on a single well-stirred reactor model. For each portion of the thesis, the very pertinent papers that were critical to the work in that section are included in the literature review with a detailed description of the contents of that paper.

2.1 Laminar Modeling Literature

2.1.1 [Haber and Vandsburger, 2003]

Haber [11] presented a model for OH* chemiluminescence that includes both the reaction between CH and molecular oxygen (O_2) as well as the reaction between formyl radicals (HCO) and oxygen atoms (O). The model was included in a modified version of the PREMIX code available in the CHEMKIN package. The modified code included a simplified model of heat transfer due to radiation as well as convective heat transfer from the gas to the ceramic honeycomb and from the gases to the chimney. The model incorporated the reactions from the detailed methane mechanism given in GRIMECH 3.0, [28]. The modeling results were then integrated over the computational domain in order to be compared with experimental results. This experimental data was taken from a laminar flat flame burner using chemiluminescence techniques [14]. The flame in the experiment was stabilized on a ceramic honeycomb plug with square channels in it. The fuel and air were premixed upstream of the honeycomb. The results showed that modeling the OH* reaction with the formation reaction through HCO better matched experimental data obtained for the study, thus validating the model.

2.1.2 [Annaswamy et al, 1995]

Annaswamy [3] presented a model incorporating feedback to illustrate a thermoacoustic instability process. The work derived a model of the acoustics within the system based on a one dimensional flow analysis. This portion resulted in a model of the response of the acoustics due to the forcing by the heat release rate due to combustion. This model was further simplified by using the Galerkin method, resulting in a one mode approximation of the unsteady pressure oscillations due to heat release rate. A flame dynamics model was developed as well. This flame model described the unsteady heat release rate due to velocity fluctuations. The two models were combined by transferring the model equations into the Laplace domain and writing the closed loop transfer function for the system as a whole. The authors then applied the Rayleigh criterion to discuss the instability of the model. A root-locus investigation of the sensitivity of several parameters was also performed. The derived model was compared to a numerical model of the Rijke tube.

2.2 Turbulent Modeling Literature

2.2.1 [Guckenheimer, 1984]

In Guckenheimer [10], a mathematical methodology for investigating bifurcation systems in a problem-independent manner is presented. This is done using "multiple bifurcation theory" developed by the author based on Catastrophe theory by Thom [29]. The method involves developing a "tableau" or picture representing all of the qualitative traits of the solutions to the equations. The picture shows the value of the design parameters where changes in the qualitative traits occur and labels the type of bifurcation exhibited by the particular section of the tableau. The work also outlines three examples where this method is employed to classify the different types of bifurcations seen in each problem. Of particular interest is the example problem involving the Continuous Stirred Tank Reactor (CSTR) which is the chemical engineering equivalent of the well-stirred reactor. The CSTR example illustrates the tableau method as the author locates the

bifurcations possible and illustrates their behavior via the tableau and associated phase portraits. The kind of behavior possible in a single dynamic CSTR is quite wide ranging.

2.2.2 [Lieuwen et al., 1998]

Lieuwen [20] investigated the role of variations in equivalence ratio, flow rate and temperature in causing thermoacoustic instabilities within a lean premixed combustor. The primary focus of the work was to model the magnitude of the reaction rate oscillations due to variations in the aforementioned parameters. The work presented an unsteady WSR combustion model that is based on the steady WSR. The authors also noted that while a constant pressure reactor seems a bad assumption, that after investigating other models with momentum and time varying pressure, it was found that the qualitative behavior did not differ between the three cases. The validity of the unsteady model was first checked against the steady state WSR model. This was done by "igniting" the unsteady WSR model by raising the inlet temperature and then checking the state steady portion of the solution with the steady state WSR solution. The model's response to variations in the inlet conditions showed that magnitude of the reaction rate for higher frequency inputs was larger than for 0 Hz (that is, the steady state). The model also exhibited a dynamic blowout point, which was due to large amplitude variations in the equivalence ratio. The authors also point out that the model acts as a low pass filter for equivalence ratio variations. The response due to variations in mass flow was also investigated for different mean equivalence ratios. The vulnerability of a combustor to instabilities due to inlet mass flow variations remains approximately constant with changes in mean equivalence ratio. The response due to variations in inlet temperature was also investigated. The model's response suggests that a combustor operating close to stoichiometric conditions is more susceptible to instabilities caused by inlet temperature variations than a combustor operating on a lean mixture. This work focused on the magnitude of the response of the reaction rate due to variations in inlet parameters but the authors admit that the phase information available via the WSR model is incorrect because of inherent assumptions which ignore mixing and convection processes. Thus

the model cannot actually determine the stability of a system, but it can determine whether a system is susceptible to instabilities based on the gain of the system.

2.2.3 [Park et al., 2002]

Park [24] presented a heat release dynamics model that incorporated a single well-stirred reactor (WSR). A linearized heat release model was developed using an unsteady version of the well-stirred reactor equations. The unsteady heat release model was linearized about equilibrium points in order to find the models linear heat release dynamics. An order analysis is then performed to eliminate unnecessary terms from the complicated equations. The model is then simplified to a first order transfer function of the form

$$\frac{\dot{Q}_r}{\dot{m}} = J(s) = \frac{\beta}{s+\alpha} \tag{2-1}$$

where α and β are found using equations involving the linearized form of the WSR equations. The physical meaning of these parameters is investigated: $\alpha = 0$ corresponds to the static blowout and $\beta = 0$ corresponds to the maximum steady heat release rate. It is also noted that at the maximum release rate, that is, when $\beta = 0$, the phase between $\dot{m}$ and $\dot{Q}_r$ changes by 180 degrees, an occurrence which could lead to instability. The effects of particular operating conditions on heat release dynamics are also investigated. The possibility of instability occurring because of the phase change mentioned earlier is explained: the Rayleigh Index is computed and shows that an unstable system is possible after the phase change occurs. Experimental evidence is presented that is in accordance with some of the phenomena exhibited by the model: the system becomes unstable has equivalence ratio is decreased, this instability is caused by a phase change just prior to blowout, and there is a narrow equivalence ratio band in which this instability can occur.

3 Linear Stability Analysis of a Rijke Tube Combustor

The accuracy of linear stability analysis techniques for predicting the expected occurrence of thermoacoustic instabilities in a combustion process is extremely dependent on the accuracy of describing the dynamic heat release rate coupling to the acoustic field. In the past five years, there have been numerous researchers who have investigated the important loop between the combustor vessel acoustic dynamics and the so-called "flame dynamics." Some of the investigations relied primarily on identifying the lightly damped acoustic field in a combustor and a simplified low-pass flame dynamics model (Annaswamy [3], Schreel [27]). Other researchers have attempted to use more complex flame dynamics models based on well-stirred reactor models (Fannin [8]) or CFD models (Kruger [16]). The ability to successfully predict the frequencies of thermoacoustic instabilities has often been linked to the acoustic resonance frequencies of the combustor because there is typically high loop gain and a quick 180° phase sweep, making these points likely place for instability. These frequencies are easy to determine a priori; therefore, predictions of thermoacoustic instability frequencies have correlated with measured instability frequencies because of the ease in determining the acoustic response of the combustor. A more stringent test of a closed loop model is its ability to predict at what operating conditions the system will go unstable.

In this section, a newly developed model of a two-part acoustic source term for a premixed laminar flat-flame burner is used to show that its use in a corresponding tube combustor linear stability analysis accurately reflects the loop gain and phase expected at measured instability frequencies. Computational methods that identify the acoustic source term, as discussed in Haber [11], are briefly reviewed in this paper. The essential difference between this acoustic source term and prior dynamic heat release models used in linear instability analyses is that the acoustic source term is not derived from an assumption that chemical heat release rate is the only source term for acoustic pressure waves in the combustor. The essential roles of chemical heat release, heat diffusion, radiative heat transfer and convective heat transfer are shown in terms of their impact on the "flame dynamics" transfer function computed for the stability analysis.

The loop-model considered in this paper consists of a one-dimensional acoustics model coupled with the new inclusive acoustic source model of heat release dynamics that utilizes the Premix software [13] and one-dimensional heat and mass transfer. This loop-model is shown schematically in Figure 3.1.

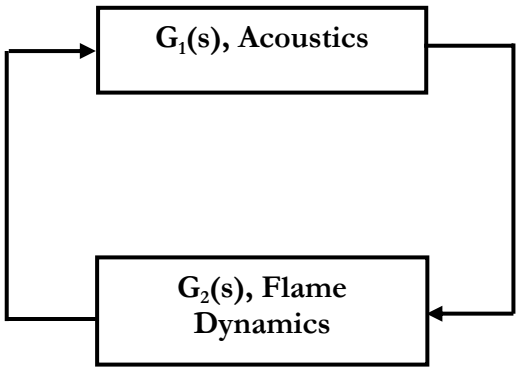

Figure 3.1: Systems block diagram of thermal-acoustic system.

The acoustics model is a two-mode variation on the acoustic model developed by Annaswamy [3]. The acoustics model and flame dynamics model interact in a closed loop as shown in Figure 3.1. Instability is correctly predicted for various operating conditions of a closed-open tube combustor using open-loop frequency response functions. It is also shown that for the same operating conditions a model that assumes that the acoustic forcing term is solely due to chemical heat-release rate, incorrectly predicts a stable system where experimental results have shown instability occurs. The new flame dynamics model introduced here clearly illustrates how the respective contributions of the individual energy transport phenomena change with frequency.

The setup of the experiment and simulations consists of an approximately six foot long open-closed tube, with a ceramic honeycomb flame stabilizer inserted approximately halfway in the tube. A premixed methane-air mixture is injected into the bottom of the tube and lit; the flame stabilizing above the honeycomb. The tube was designed so that the system would go unstable for specified conditions.

Section 3.1 presents the basics of the software used in finding the flame transfer function, $G_2(s)$. In Section 3.2, the acoustics model of the open-closed tube and the acoustic transfer function, $G_1(s)$ are derived. In Section 3.3, the acoustic forcing term is investigated more thoroughly, and the dominating terms that make up the acoustic forcing are identified. Section 3.4 presents the results of the stability analysis.

3.1 Combustion Model

A modified version of the Premix software ([11], [13], [28]) is used to simulate the combustion process. The modifications were done by Ludwig Haber. The Premix software uses a mechanism comprised of approximately 250 species for the combustion of methane in air at a specified equivalence ratio. The system is represented with a one dimensional model, whose results are adjusted to account for the area of the actual burner used in the laboratory. The model approximates the flow and associated heat transfers for one of the honeycomb passages. The model assumes a constant pressure over the entire domain; this is a reasonable assumption since the pressure fluctuations are small compared to the mean pressure within the combustor. A schematic of the model is shown in Figure 3.2.

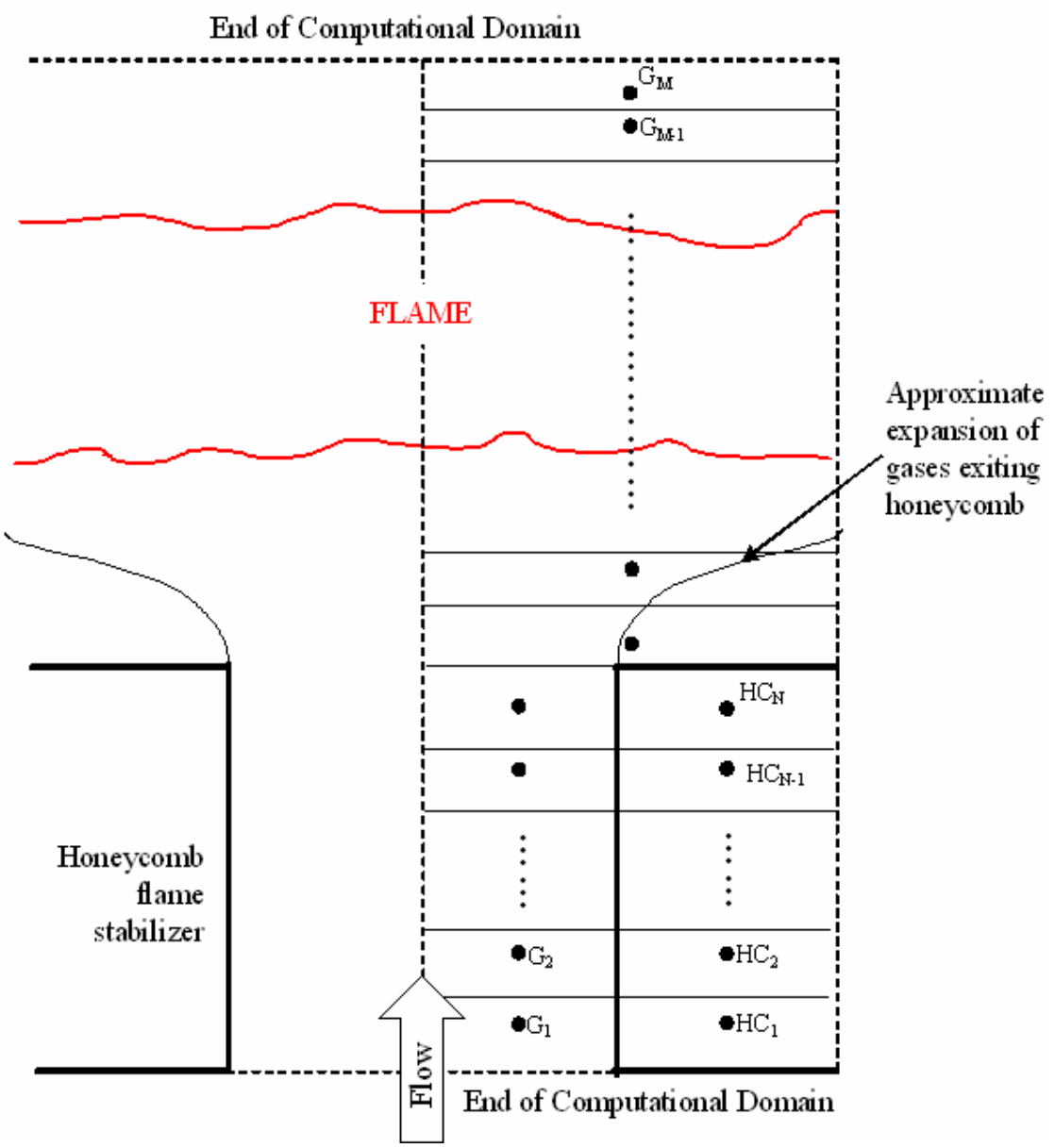

Figure 3.2: Schematic of one dimensional model. The schematic shows one of the many ports in the honeycomb.

HC_i – represents the i^{th} honeycomb node.
G_j – represents the j^{th} gas node.

In Figure 3.2, a cross-section of one of the ports in the honeycomb is shown with associated elements of honeycomb and gases also represented. The computational domain extends ten centimeters above the flame. The expansion of the gases at the exit of the honeycomb channel is modeled with a change in area term in the program. The one dimensional model accounts for the heat addition due to the combustion process, diffusion processes, convection, and radiation. The gas can exchange energy with the honeycomb stabilizer through both radiation and convection.

The boundary conditions must be determined for the model. The mass fractions and temperature of the entering gases are specified at node G_1. A radiation energy balance characterizes the boundary condition of the first honeycomb node, HC_1. The boundary condition of the last honeycomb node, HC_N, is also specified by a radiation energy balance. The exit boundary conditions specify that the mass fractions of the various species at the last node, G_M, must equal the mass fractions at the prior node, G_{M-1}; that is, the composition is frozen upon leaving the computational domain. Also the temperature boundary condition specifies that $\partial T/\partial x = 0$ at node G_M. The surrounding areas are assumed to be insulated.

While the model is only one dimensional, several steps have been taken to achieve better accuracy by modeling conglomerate heat transfer effects with effective areas or effective transfer coefficients. For instance, each honeycomb element receives a small amount of radiation from the entire flame, not just the elements above it. The program does take into account this radiation contribution from the entire flame, using effective areas. The program also accounts for the extra radiation and convection that the top of the honeycomb element receives due to more surface area, by estimating the expansion of the gases exiting the honeycomb. This estimate is used with the gas node temperatures to calculate an effective convection to the top of the honeycomb using an effective Nusselt number. The radiation to the top of the honeycomb is also included. Also, the convective heat transfer from the hot gases to the surrounding walls of the tube is accounted for by specifying that a fraction of heat is lost from each node to the walls, though only nodes near the walls would actually be responsible for this convective heat transfer in a higher dimensional model.

At each node of either a gas element or honeycomb element, a set of energy balance equations and species equations are solved. Based on the residuals of the energy balance, the temperature and mass fractions of the species at each node are iterated upon. An example energy balance for a gas node is

$$\rho A c_{p,i} \frac{\partial T_{G,i}}{\partial t} + \dot{m} c_{p,i} \frac{\partial T_{G,i}}{\partial x} = \left[\frac{\partial}{\partial x}\left(k_i A \frac{\partial T_{G,i}}{\partial x} \right) + A \sum_{i=1}^{W} \dot{\omega}_i h_i + h_{HC} P \left(T_{G,i} - T_{HC,j} \right) + \varepsilon \sigma P \left({T_{G,i}}^4 - T_s^4 \right) \right] \tag{3-1}$$

where ω_i is the molar reaction rate of the *i*-th species, h_i is the enthalpy of reaction of the *i*-th species, and they are summed over a total of *W* species. *P* is the perimeter of the channel; $T_{G,i}$ is the temperature of the gas at the *i*-th node; ε is the emissivity; σ is the Stefan-Boltzmann constant, h_{HC} is the convection heat transfer coefficient inside the honeycomb channel; *k* is the thermal conductivity of the gases or honeycomb. The term on the right side of the equation is the heat addition per unit length, q'. Pertinent values used in the energy equation are shown in Table 3-1.

Table 3-1: Values of properties used in altered PREMIX code

Property	Symbol	Units	Value
Nusselt Number	Nu	--	3.5
Emissivity (base)	ε	--	0.85, T < 900 K 1.253363 – 0.00044818(T), T > 900
Thermal conductivity of the honeycomb	k_{HC}	W/m-K	2.286
Specific heat of the honeycomb	$c_{p_{HC}}$	J/kg-K	852

The premix solver is used to iterate upon the temperatures as well as the species mass fractions by perturbing the temperatures and mass fractions and calculating residual sensitivities due to each perturbation. The sensitivities are then used to calculate the next

guess of temperature and species mass fraction. This process continues until the residuals of the energy balance are below a specified level. The program is capable of reporting the entire temperature profile at each time step, as well as specie mass fractions, densities, radiation, convection, and diffusion transfers for each element in the model.

The modified software model was verified by comparison with experiment in Haber [11].

3.2 Acoustics Model

The governing equations of the acoustics model are obtained from the conservation equations assuming one dimensional flow and that transport mechanisms are insignificant. Using Annaswamy [3] as a model, the conservation equations are

$$\frac{\partial \rho}{\partial t} + \frac{\partial (\rho u)}{\partial x} = 0 \tag{3-2}$$

$$\rho \frac{\partial u}{\partial t} + \rho u \frac{\partial u}{\partial x} = -\frac{\partial p}{\partial x} \tag{3-3}$$

$$\frac{\partial (\rho e)}{\partial t} + \frac{\partial (\rho u e)}{\partial x} = -p \frac{\partial u}{\partial x} + q''' \tag{3-4}$$

where t is time, x is the spatial dimension, ρ denotes the density, u denotes the velocity, p is the pressure, e is the internal energy and q''' is the heat flux into the system per unit volume, which consists of convection, radiation, thermal diffusion, and heat release due to combustion. In Eq. (3-4), q''' is the volumetric version q', shown earlier in (3-1). Assuming ideal gas, (3-4) becomes

$$\frac{\partial p}{\partial t} + u\frac{\partial p}{\partial x} + \gamma p\frac{\partial u}{\partial x} = (\gamma - 1)q'''$$

(3-5)

Separating variables into mean and perturbation components, pressure, density, velocity, and heat release rate become

$$\begin{aligned} p(x,t) &= \bar{p}(x) + \tilde{p}(x,t) \\ u(x,t) &= \bar{u}(x) + \tilde{u}(x,t) \\ \rho(x,t) &= \bar{\rho}(x) + \tilde{\rho}(x,t) \\ q'''(x,t) &= \bar{q}'''(x) + \tilde{q}'''(x,t) \end{aligned}$$

(3-6)

Assuming steady flow, (3-2), (3-3)and (3-5) become

$$\frac{d(\overline{\rho u})}{dx} = 0$$

(3-7)

$$\overline{\rho u}\frac{d\bar{u}}{dx} + \frac{d\bar{p}}{dx} = 0$$

(3-8)

$$\bar{u}\frac{d\bar{p}}{dx} + \gamma\bar{p}\frac{d\bar{u}}{dx} = (\gamma - 1)\bar{q}'''$$

(3-9)

Assuming small perturbations about the mean flow, the relations in (3-6) are substituted into (3-3) and (3-5), giving

$$\bar{\rho}\frac{\partial\tilde{u}}{\partial t} + \overline{\rho u}\frac{\partial\tilde{u}}{\partial x} + \bar{\rho}\tilde{u}\frac{d\bar{u}}{dx} + \tilde{\rho}\bar{u}\frac{d\bar{u}}{dx} + \frac{\partial\tilde{p}}{\partial x} = 0$$

(3-10)

$$\frac{\partial\tilde{p}}{\partial t} + \bar{u}\frac{\partial\tilde{p}}{\partial x} + \tilde{u}\frac{d\bar{p}}{dx} + \gamma\bar{p}\frac{\partial\tilde{u}}{\partial x} + \gamma\tilde{p}\frac{d\bar{u}}{dx} = (\gamma - 1)\tilde{q}'''$$

(3-11)

Under the assumption that the flame is localized spatially, the heat release rate can be expressed as

$$q'''(x,t) = \delta(x - x_f)q''(t)$$

(3-12)

where $q''(t)$ denotes the heat release rate per unit area, and δ is the Dirac delta function. In accordance with Annaswamy [3], the step change in pressure is considered negligible in comparison to the step change in mean velocity or mean density. Using this assumption, (3-10) and (3-11) become

$$\left(\frac{\partial^2 \tilde{p}}{\partial t^2} - \left(\bar{c}^2(x) - \bar{u}^2(x)\right)\frac{\partial^2 \tilde{p}}{\partial x^2}\right) + 2\bar{u}(x)\frac{\partial^2 \tilde{p}}{\partial x \partial t} = (\gamma - 1)\left(\frac{\partial \tilde{q}}{\partial t} + \bar{u}(x)\frac{\partial \tilde{q}}{\partial x}\right)$$

(3-13)

$$\frac{\partial \tilde{p}}{\partial t} + \bar{u}(x)\frac{\partial \tilde{p}}{\partial x} + \gamma \bar{p}\frac{\partial \tilde{u}}{\partial x} = (\gamma - 1)\tilde{q}$$

(3-14)

Again following Annaswamy [3], if we assume that the effect of the mean heat and the effect of the mean flow are negligible, then (3-13) and (3-14) simplify to

$$\left(\frac{\partial^2 \tilde{p}}{\partial t^2} - \bar{c}^2\frac{\partial^2 \tilde{p}}{\partial x^2}\right) = (\gamma - 1)\frac{\partial \tilde{q}}{\partial t}$$

(3-15)

$$\frac{\partial \tilde{p}}{\partial t} + \gamma \bar{p}\frac{\partial \tilde{u}}{\partial x} = (\gamma - 1)\tilde{q}$$

(3-16)

Next, the Galerkin method is used to separate the spatial and temporal dimensions [3]. The unsteady pressure, $\tilde{p}$, can be expressed as

$$\tilde{p}(x,t) = \bar{p}\sum_{i=1}^{n}\psi_i(x)\eta_i(t)$$

(3-17)

where the basis functions, $\psi_i(x)$, are of the form

$$\psi_i(x) = \cos(k_i x + \phi_{i0})$$

(3-18)

where ϕ_{i0} and the wave numbers, k_i, are evaluated based on the boundary conditions of the geometry studied. For the closed-open tube, the wave numbers are of the form

$$k_i = \frac{2i-1}{2L}\pi .$$

(3-19)

According to Annaswamy [3], the spatial mode shapes do not change substantially in the presence of a heat source; therefore, we can assume Eqs. (3-15) and (3-16) continue to give a solution in the form of Eq. (3-17). Using the form of Annaswamy et al, but for a two mode case, Eq. (3-17) becomes

$$\tilde{p}(x,t) = \bar{p}\sum_{i=1}^{2}\psi_i(x)\eta_i(t) = \bar{p}\left(\psi_1(x)\eta_1(t) + \psi_2(x)\eta_2(t)\right) = \tilde{p}_1 + \tilde{p}_2$$

(3-20)

where $\tilde{p}_1(x,t) = \bar{p}\,\psi_1(x)\eta_1(t)$ and $\tilde{p}_2(x,t) = \bar{p}\,\psi_2(x)\eta_2(t)$. Assuming the velocity perturbations from different pressure perturbations add linearly, we find the solution for $\tilde{p}_1$ and apply the form of the solution to $\tilde{p}_2$. Substituting $\tilde{p}_1(x,t) = \bar{p}\,\psi_1(x)\eta_1(t)$, Eq. (3-15) becomes

$$\bar{p}\,\psi_1(x)\ddot{\eta}_1 - \bar{c}^2\bar{p}\frac{\partial^2\psi_1}{dx^2}\eta_1(t) = (\gamma-1)\frac{\partial\tilde{q}}{\partial t}$$

(3-21)

Multiplying through by ψ_1 and integrating over the length of the combustor, *L*, Eq. (3-21) becomes

$$\ddot{\eta}_1 - \bar{c}^2 \eta_1 \frac{\int_0^L \psi_1 \frac{\partial^2 \psi_1}{dx^2} d\xi}{E} = \frac{(\gamma - 1)}{\bar{p}E} \int_0^L \psi_1(\xi) \frac{\partial \tilde{q}}{\partial t} d\xi$$

(3-22)

where $E = \int_0^L \psi_1{}^2(x) d\xi$ and the equation has been divided through by E and $\bar{p}$. Applying the assumption that the flame is localized spatially to the perturbation portion of the heat release, Eq. (3-12) implies

$$\tilde{q}'''(x,t) = \delta(x - x_f)\tilde{q}''(t)$$

(3-23)

Using Eq. (3-23), Eq. (3-23) becomes

$$\ddot{\eta}_1 + \omega_1{}^2 \eta_1 = \frac{(\gamma - 1)}{\bar{p}E_1} \psi_1(x_f) \dot{\tilde{q}}''(t)$$

(3-24)

where $\omega_i = k_i \bar{c}$. Eq. (3-27) can be manipulated and integrated similarly, yielding

$$\tilde{u}_1(x,t) = \left[\tilde{u}(0,t) - \frac{1}{\gamma k^2} \dot{\eta}_1(t) \frac{\partial \psi_1}{dx}(0) \right] + \frac{1}{\gamma k^2} \dot{\eta}_1(t) \frac{\partial \psi_1}{dx}(x) + \frac{\gamma - 1}{\gamma \bar{p}} \tilde{q}''(t) H\left(x - x_f\right)$$

(3-25)

where H is the Heaviside function, in which $H(x) = 1$ for $x > 0$, $H(x) = 0$ for $x \leq 0$. As Annaswamy et al show, the term in brackets in Eq. (3-25) equals zero. Also, we are examining the velocity perturbations at the flame, $x = x_f$, and thus the last term, due to the Heaviside function, is also zero. Eq. (3-25) then becomes

$$\tilde{u}_1(x,t) = \frac{1}{\gamma {k_1}^2}\dot{\eta}_1(t)\frac{\partial \psi_1}{dx}(x_f)$$

(3-26)

The first mode of the acoustics model is described by Eqs. (3-24) and (3-26), which relate the pressure oscillations due to the first mode, $\eta_1(t)$ and the velocity perturbations due to the first mode, $\tilde{u}_1(x,t)$, to the heat-release rate, $\dot{\tilde{q}}''(t)$. A similar set of equations can be written for the second mode as well

$$\ddot{\eta}_2 + {\omega_2}^2\eta_2 = \frac{(\gamma-1)}{\bar{p}E_2}\psi_2(x_f)\dot{\tilde{q}}''(t)$$

(3-27)

and

$$\tilde{u}_2(x,t) = \frac{1}{\gamma {k_2}^2}\dot{\eta}_2(t)\frac{\partial \psi_2}{dx}(x_f)$$

(3-28)

these equations relate the pressure oscillations due to the second mode, $\eta_2(t)$ and the velocity perturbations due to the second mode, $\tilde{u}_2(x,t)$, to the heat release rate, $\tilde{q}''(t)$. Eqs. (3-24), (3-26) – (3-28) are now transformed into the Laplace domain to describe the acoustics block of the block diagram shown in Figure 3.1. Using the Laplace operator, Eq. (3-24) and (3-26) become

$$s^2 N_1(s) + {\omega_1}^2 N_1(s) = \left(\frac{\gamma-1}{\bar{p}E_1}\psi_1(x_f)\right)\dot{\tilde{Q}}''(s)$$

(3-29)

$$\tilde{U}_1(s) = \frac{1}{\gamma {k_1}^2}sN_1(s)\frac{\partial \psi_1}{\partial x}(x_f)$$

(3-30)

Solving for the transfer function $\tilde{U}_1(s)/\dot{\tilde{Q}}''(s)$ yields

$$\frac{\widetilde{U}_1(s)}{\dot{\widetilde{Q}}''(s)} = \left(\frac{1}{\gamma k_1^{\,2}} \frac{\gamma - 1}{\overline{p} E_1} \psi_1(x_f) \frac{\partial \psi_1}{\partial x}(x_f) \right) \frac{s}{s^2 + 2\zeta\omega_1 s + \omega_1^{\,2}}$$

(3-31)

It should be noted that a damping term, $2\zeta\omega_1 s$, has been added to the transfer function in Eq. (3-31). This has been added because it is well known that there is acoustic damping which is not reflected in a simplified model. The damping for the studied Rijke tube was measured by Huang [12], and is included here, $\zeta = 0.01474$.

A similar transfer function was developed for the second mode

$$\frac{\widetilde{U}_2(s)}{\dot{\widetilde{Q}}''(s)} = \left(\frac{1}{\gamma k_2^{\,2}} \frac{\gamma - 1}{\overline{p} E_2} \psi_2(x_f) \frac{\partial \psi_2}{\partial x}(x_f) \right) \frac{s}{s^2 + 2\zeta\omega_2 s + \omega_2^{\,2}}$$

(3-32)

The entire acoustics model transfer function is simply the addition of the two transfer functions in Eqs. (3-31) and (3-32), thus the transfer function, $G_1(s)$ as shown in Figure 3.1, is

$$G_1(s) = \frac{\widetilde{U}(s)}{\dot{\widetilde{Q}}''(s)} = \frac{\widetilde{U}_1(s)}{\dot{\widetilde{Q}}''(s)} + \frac{\widetilde{U}_2(s)}{\dot{\widetilde{Q}}''(s)}$$

(3-33)

Using this representation of the acoustics model, the frequency response of the acoustics block can be obtained and is shown in Figure 3.3. The figure contains the frequency response for both a two mode model as well as a four mode model. The comparison shows that in the frequencies of interest (between 10 and 200 Hertz) the models are comparable and a four mode model is not required. Therefore the two mode model of the acoustics will be used for the rest of the linear stability analysis.

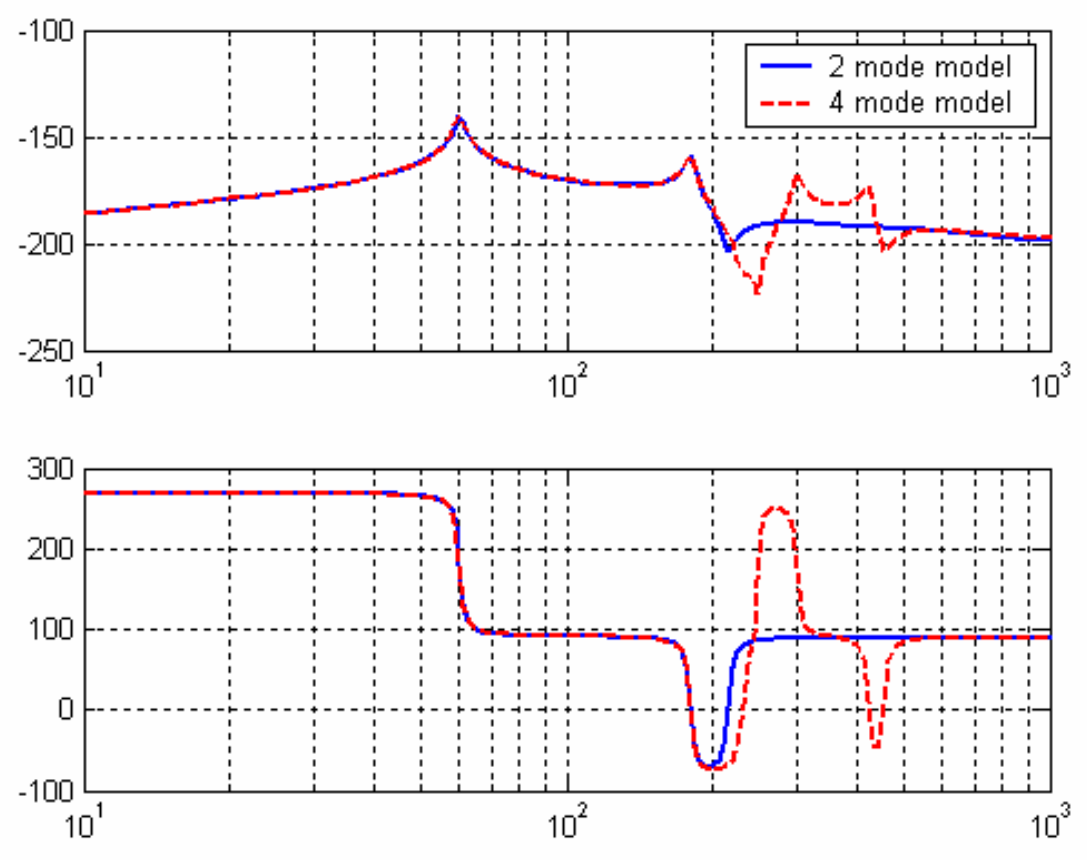

Figure 3.3: Frequency response of acoustics model.

Input: unsteady heat release rate (W/m^2); Output: unsteady velocity (m/s)

3.3 Identification of Dominating Terms in the Heat Addition Term

The frequency response of the flame model, with mass flow as the input and heat release as the output, was generated using the modified PREMIX program. The output of the program is actually heat release per unit length, and the results are integrated over the model domain to generate the graphs shown. An example of the open loop magnitude frequency response of the flame dynamics is shown in Figure 3.5, for the case of a flow rate of Q = 145 cc/sec and an equivalence ratio of Φ = 0.55. In the figures, and those following, CHR is chemical heat-release rate, Acoustic Forcing is the total heat addition

to the fluid, Total Convection is convective heat transfer, Diffusion is heat transfer due to diffusion processes, and Radiation is the heat transfer due to radiation heat transfer.

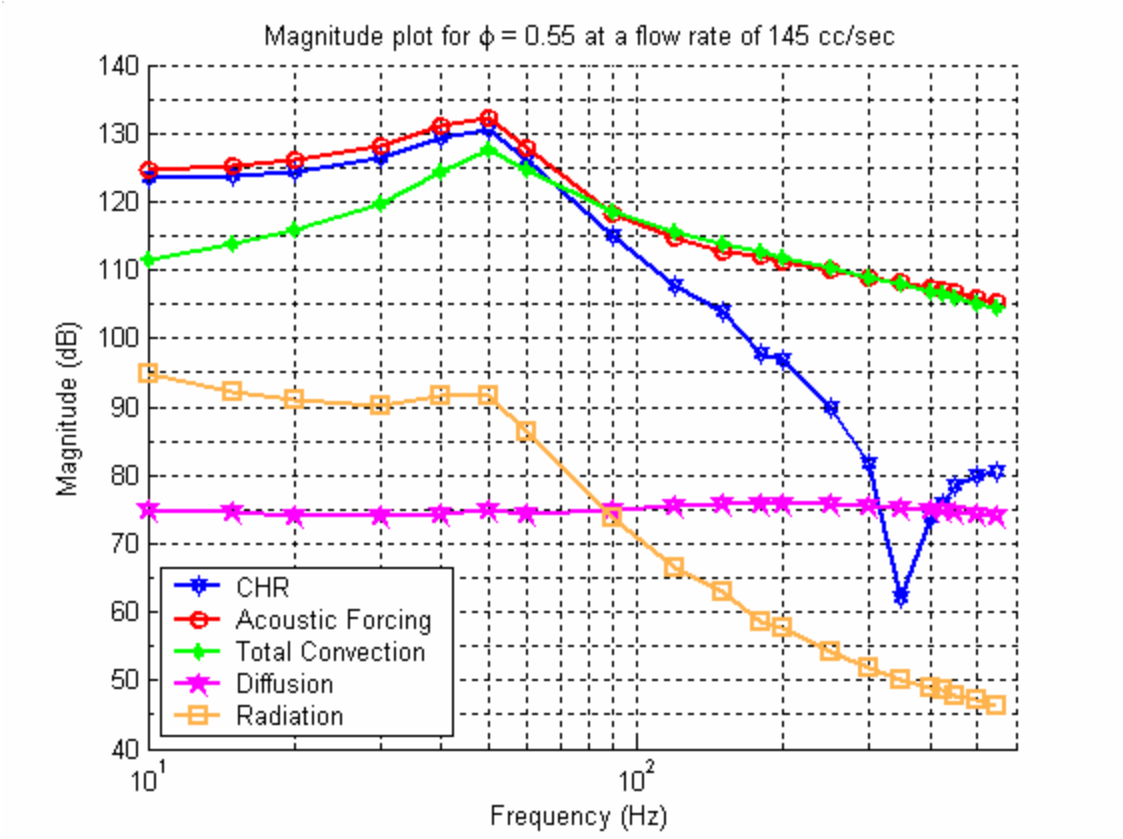

Figure 3.4. Magnitude response of acoustic forcing term and various components. Input: mass flow fluctuations, (kg/s); Output: heat release (J)

As can be seen in Figure 3.4, the relative magnitudes of diffusion and radiation indicate that these components are not important dynamic terms in the acoustic forcing. Chemical heat-release rate and convection, however, are important terms in the heat addition. This is contrary to the assumptions in our previous studies that assume chemical heat-release rate dominates the acoustic forcing term. However, Figure 3.4 shows that convection is not only an important factor in the acoustic forcing; it even dominates the forcing term for higher frequencies (above ~100 Hz). For this reason, convection and chemical heat-release rate will be included in the model of the acoustic forcing term. The frequency response of this two-term model of heat addition is shown along with the frequency

response of the actual acoustic forcing term, chemical heat-release rate and convection in Figure 3.5. In the figure, "2-term AF model" represents the two-term model of acoustic forcing as described above.

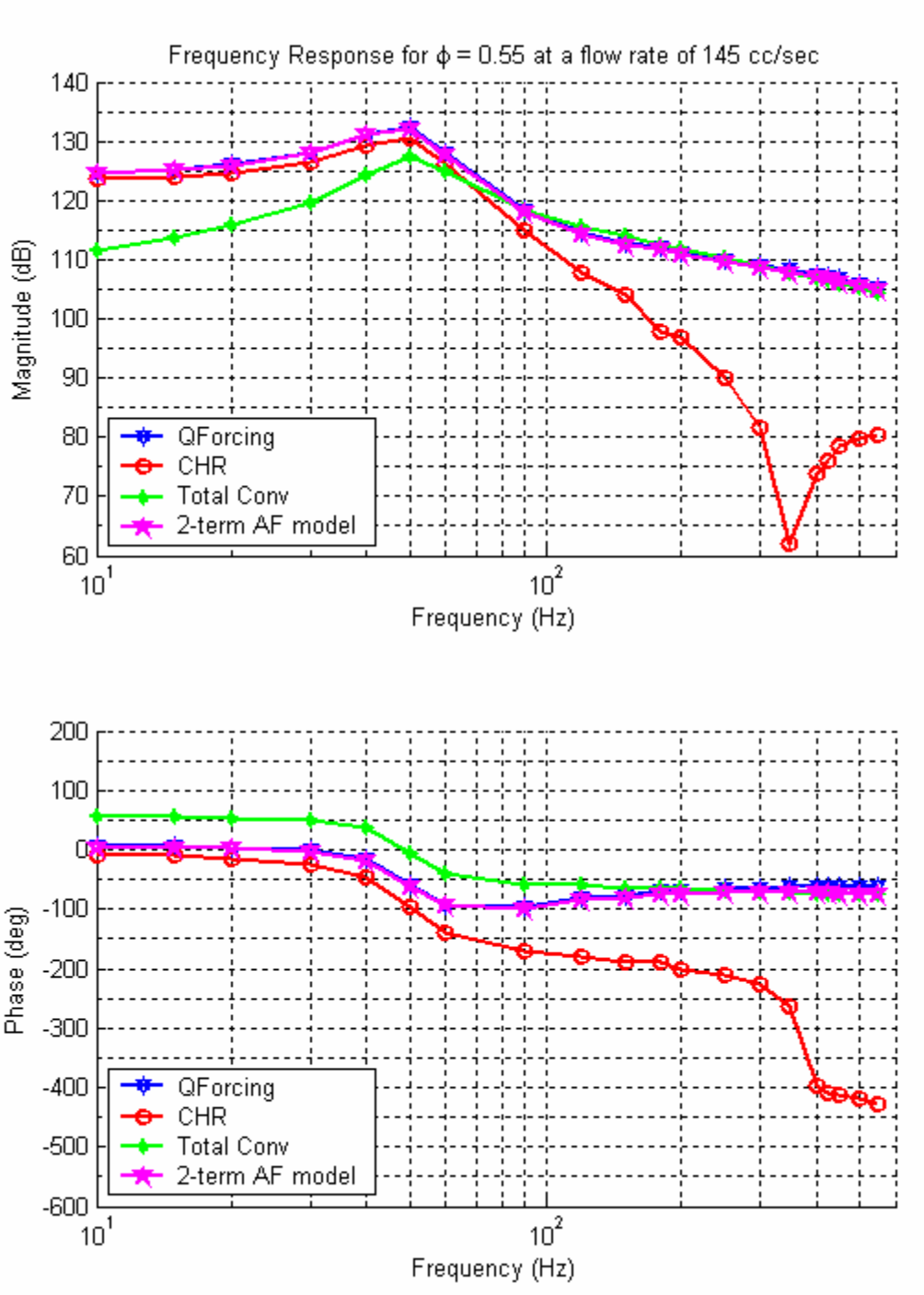

Figure 3.5. Frequency response for Φ = 0.55 and Q = 145 cc/sec.

Input: mass flow fluctuations, (kg/s); Output: heat release (J)

As Figure 3.5 shows, the two-term acoustic forcing model matches the total acoustic forcing term very well in both the magnitude and phase, thus validating the elimination of the other terms. Note in the figures that if the acoustic forcing term was taken to be just chemical heat-release rate, the CHR-based model and the acoustic forcing term would match relatively well until frequencies above 100 Hz. However, the CHR-based model would incorrectly predict the magnitude and phase above 100 Hz. Frequency response plots for other cases illustrating that convection is an important term in the dynamic acoustic forcing term are shown in Appendix A.

3.4 Closing the loop to predict instability.

The closed-loop stability of a system can be predicted using the frequency response of the open-loop system. The criterion for an open-loop system to go unstable is different for negative feedback versus positive feedback. For positive feedback, as in our case, the system is unstable if the open-loop frequency response exhibits a 360º phase crossing while the magnitude is greater than 0 dB. As mentioned before, the closed loop thermoacoustic process can be represented by the simplified block diagram in Figure 3.1, shown here in its entirety in Figure 3.6 Note the free differentiator that converts the heat release rate of the flame dynamics model to the change in heat release rate, which is the input to the acoustics model.

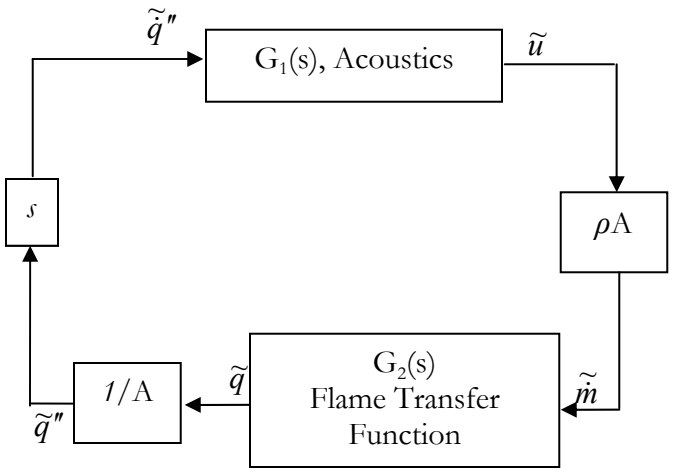

Figure 3.6. Complete systems block diagram of closed loop thermoacoustic process.

The open-loop frequency response of a model can be determined by the multiplication of the complex form of the frequency responses of the various components. This process is shown in Figure 3.7 assuming only chemical heat-release rate in the acoustic forcing term, as is normally assumed. The gains of the extra factors have been incorporated into the flame transfer function dynamics. The case shown is for a flow rate of 145 cc/sec and an equivalence ratio of 0.55. Figure 3.8 shows the open loop system with the two-term acoustic forcing term as derived earlier for the same equivalence ratio and flow rate. Examining Figure 3.7, the magnitude at the -360° phase crossing is less than 0 dB. Therefore using the stability criterion outlined above, the system would be considered stable. However this is contrary to experimental observations for this case. Also, it should be noted that the magnitude of the response at approximately 180 Hz (where instability is likely to occur based on the acoustics of the system) is slightly above zero, but the phase is approximately -450°. This indicates that the magnitude of the open loop frequency response is approximately correct, that is, it is above 0 dB where instability is expected; however, the phasing is incorrect.

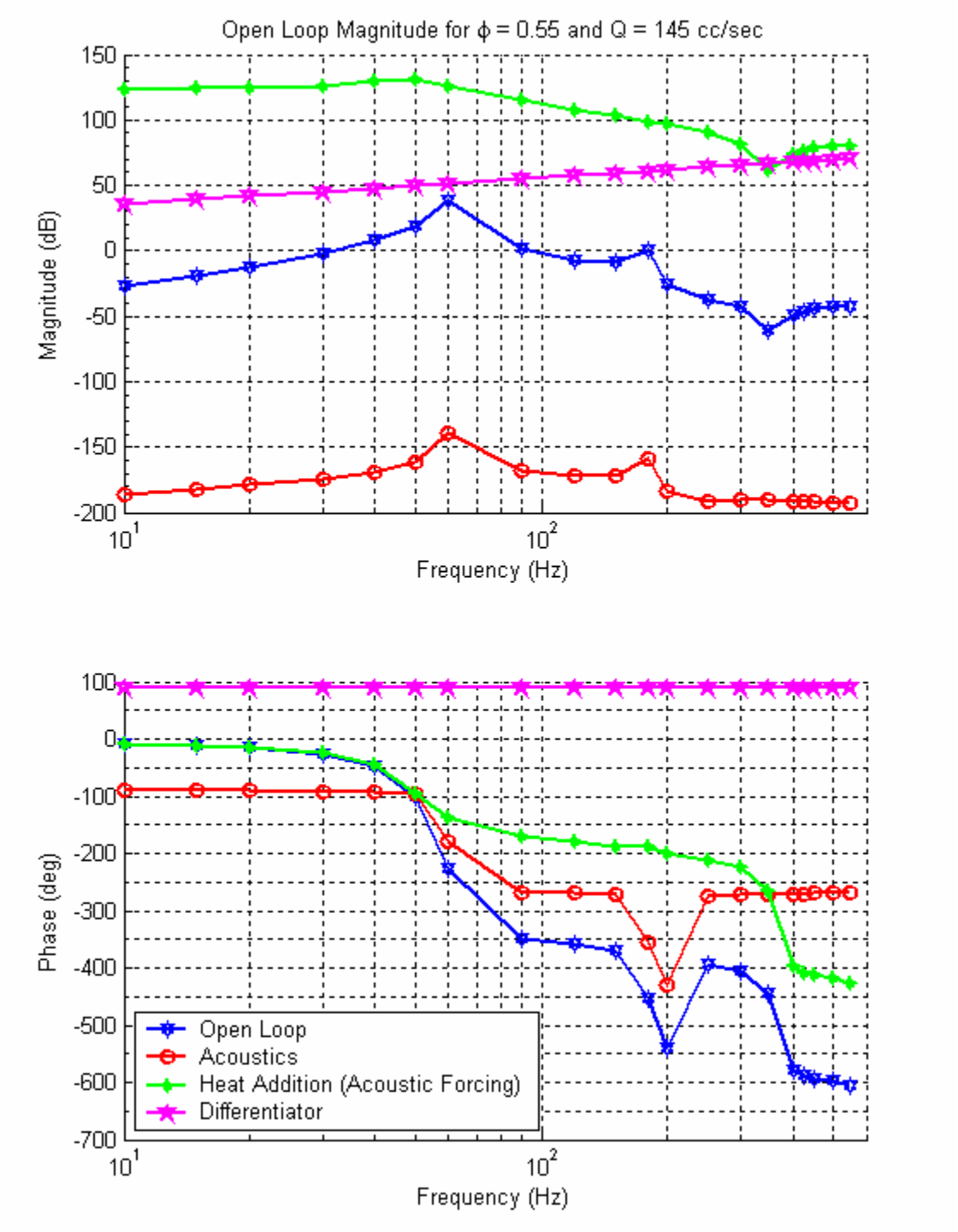

Figure 3.7: Open loop frequency response of system assuming acoustic forcing is CHR

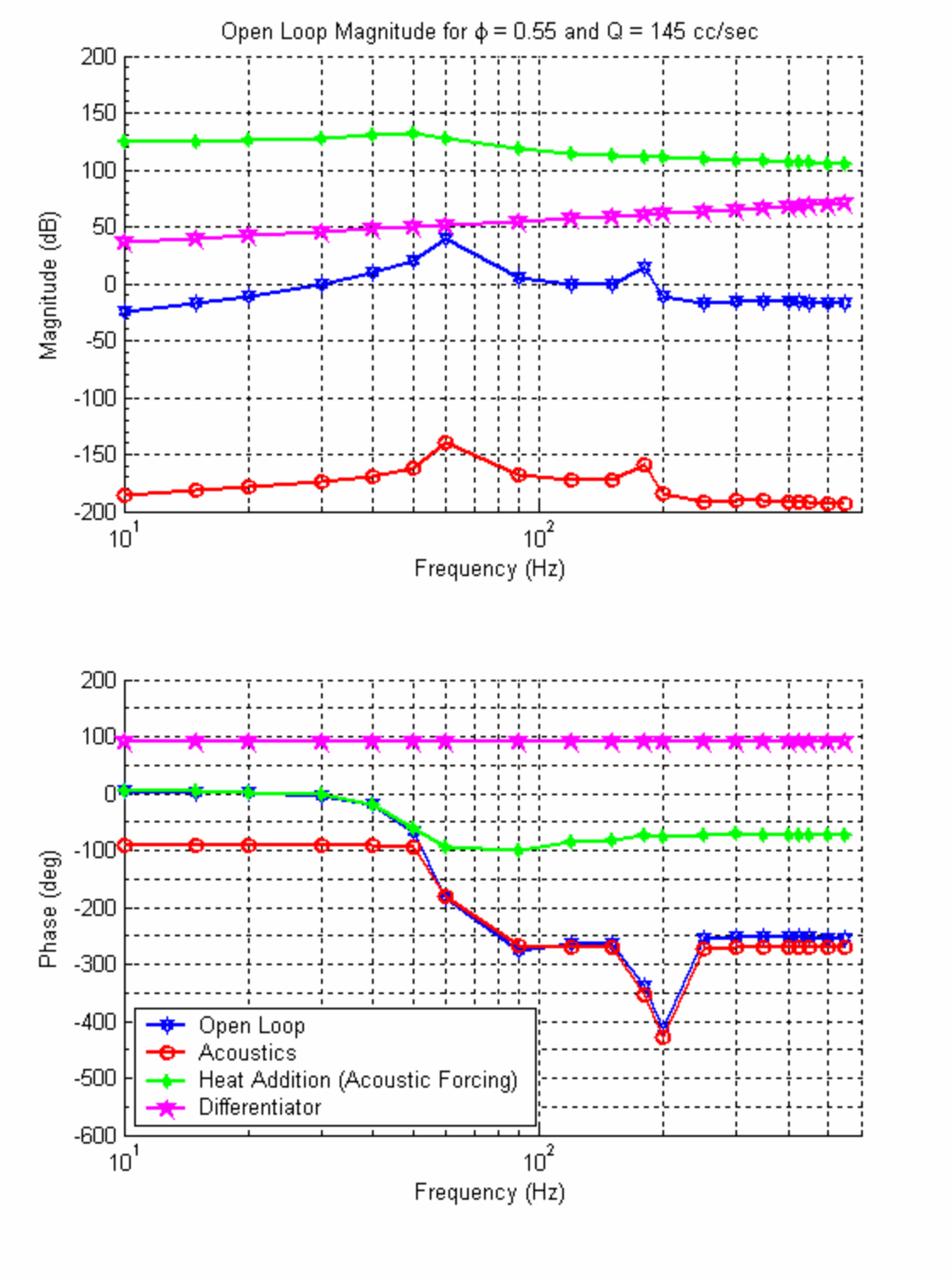

Figure 3.8: Open loop transfer function for system assuming acoustic forcing is the sum of CHR and convection

As Figure 3.8 shows, there is a phase crossing of 360º at approximately 180 Hz; the magnitude plot shows that at 180 Hz the system has a magnitude of approximately 14.5 dB. This means that the model predicts that the system will go unstable as was seen in experiment. Unfortunately, the model cannot predict the conditions at which the system will become stable. This is due to the inability of the Premix code to solve the equations for low mass flow rates or low equivalence ratios. However, if the mass flow rate is held constant and the equivalence ratio is lowered, the data does exhibit a trend that suggests the system will stabilize given low enough equivalence ratios. This trend is shown in Figure 3.9. This figure shows the frequency response of the open loop transfer function for a constant mass flow rate and varying equivalence ratio.

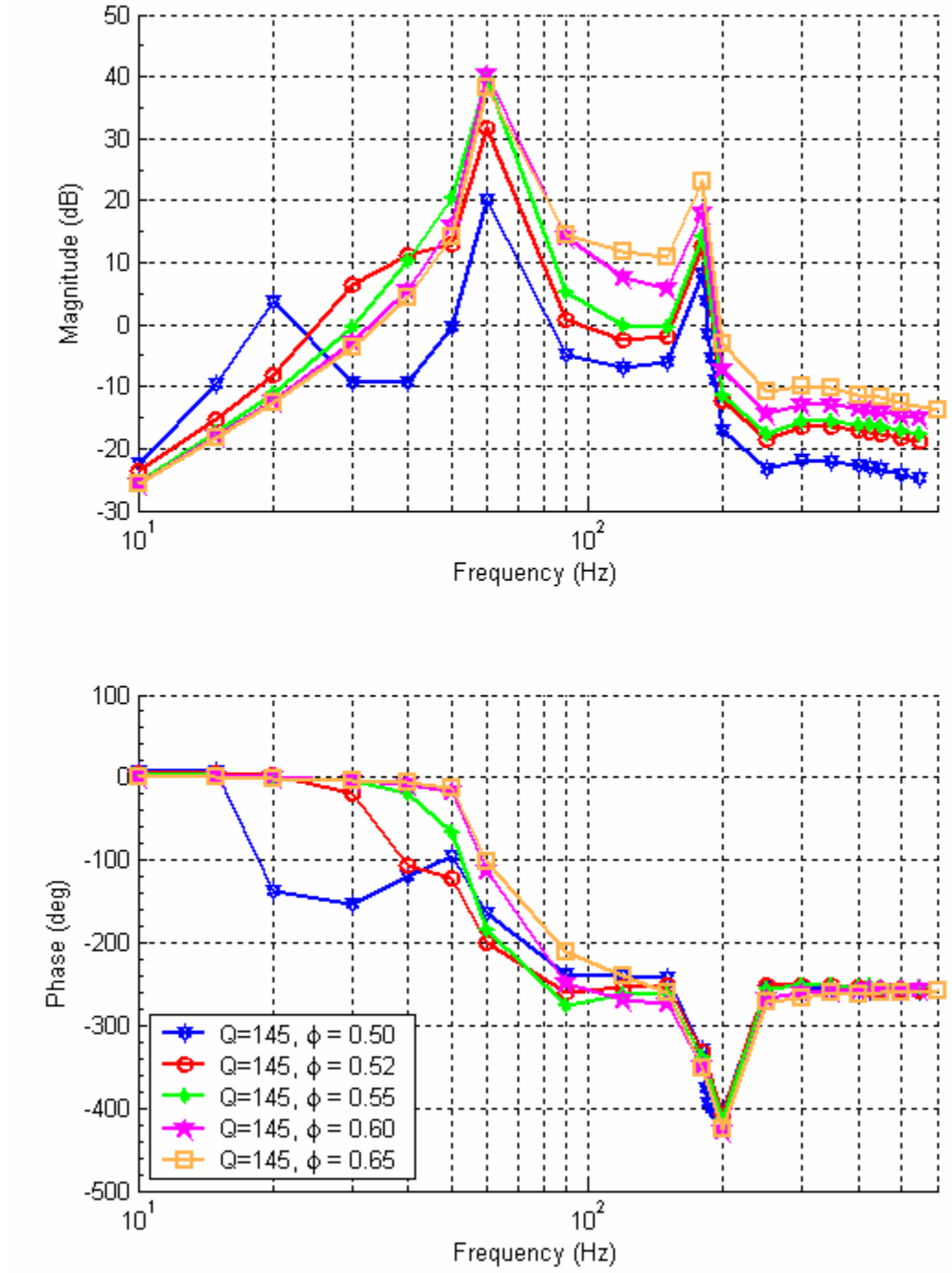

Figure 3.9: Open loop magnitude frequency response of system for varying equivalence ratio at a constant mass flow rate.

The magnitude of the system at the -360° phase crossing for each of the conditions shown in Figure 3.9 is detailed in Table 3-2. The data in Table 3-2 is extracted from an open loop frequency response that includes more data points.

Table 3-2: Magnitude at -360° phase crossing for varying equivalence ratio.

Flow rate (cc/sec)	Equivalence ratio (Φ)	Frequency of -360° crossing (Hz)	Magnitude at -360° crossing (dB)
145	0.65	180.7	21
145	0.60	180.2	17.7
145	0.55	181	13
145	0.52	181.4	11.2
145	0.50	182	4.65

As mentioned above, the phase of the open loop system is the portion of the frequency response which is in question. There are several sources of error within the analysis that could contribute to incorrectly modeling the system phase: the modeling of the expansion of the gases after exiting the honeycomb, the constant Nusselt number assumptions within the model, and the acoustics model derived earlier. As discussed earlier, the acoustics model used in the analysis only included two modes, but a four mode acoustics model was also developed and the results of the analysis did not change. Also, since the phase of the heat addition model is approximately constant in the frequency range of interest (170-200 Hz), the instability of the system is dependent on the frequency of the second acoustic mode. Thus a small change in the frequency of the acoustic mode will not make the difference between correctly predicting stability and incorrectly predicting instability for the Q = 145 cc/sec and Φ = 0.50 case. The effect of the damping was investigated and it was found that a 80% error was required to predict stability for the aforementioned case. Therefore the error in the open loop analysis is most likely not associated with the parameters of the acoustics model.

4 Modeling of Turbulent Combustion Using Dynamic Well-stirred Reactors

A number of researchers have used time-varying well-stirred reactor (WSR) models to provide very simple models of the unsteady heat release of turbulent flames [24], [20]. In Park [24], the authors show that for a single WSR model, where the input is mass flow variation and the output is heat release rate, the linearized dynamics are first order and just before blowout there is a sign change leading to a 180 degree phase shift in the dynamics. Recent measurements of the frequency response of the heat release (via OH* measurements) of a turbulent flame in response to mass flow variations show that the linearized dynamics are more complicated than those of a first-order system [14]. A typical frequency response for a turbulent flame of Khanna [14] is shown in Figure 4.2.

The objective of this section is to explore variations of a simple WSR model to determine if such models are capable of producing dynamics that are qualitatively similar to the observed dynamics. In particular, we consider variations involving recirculation, with and without time delay, and multiple WSR models coupled by recirculation. Since the linearized dynamics depend on the operating point, we first explore the equilibrium sets of our variations. For the multiple WSR models, the equilibrium curves have multiple points where jumps can occur, leading to interesting hysteretic phenomena. The linearized dynamics corresponding to the various equilibrium regions are explored and shown to produce dynamics that are not first order and are qualitatively similar to some of our observations. In addition, there are significant phase variations as a function of operating point that extend those seen in [24]. As pointed out in Park [24], these large changes in phase response with operating point could potentially explain why small changes in combustor operating conditions can cause instabilities to develop.

In Section 4.1, results of an experiment involving a swirl-stabilized turbulent flame will be presented as example of what the model will attempt to emulate. Section 4.2 will present a single well-stirred reactor model, the derivation of its equations, the linearization of those equations and the associated flame dynamics. Section 4.3 will

present the equations and results for a model using two coupled well-stirred reactors. Section 4.4 will present the equations and results for a model using three coupled well-stirred reactors.

4.1 Comparison with Experiment

The frequency response functions of a swirl-stabilized turbulent flame were completed by Khanna [14]. The experiment featured a variable swirl combustor capable of forcing the flame to the central recirculation zone, the outer recirculation zone, or the shear layer between the two zones, as shown in Figure 4.1. In a swirl stabilized flame, hot combustion products re-circulate to the inlet and heat the incoming mixture thus "hydrodynamically" stabilizing the flame [14]. Methane was used as the fuel in a fully premixed condition at equivalence ratios of $\Phi = 0.55, 0.6, 0.65$. The flow rate of the air was either 15 or 20 scfm; the swirl number was either 0.79 or 1.19. The heat release of the flame was characterized by OH* chemiluminescence measurements.

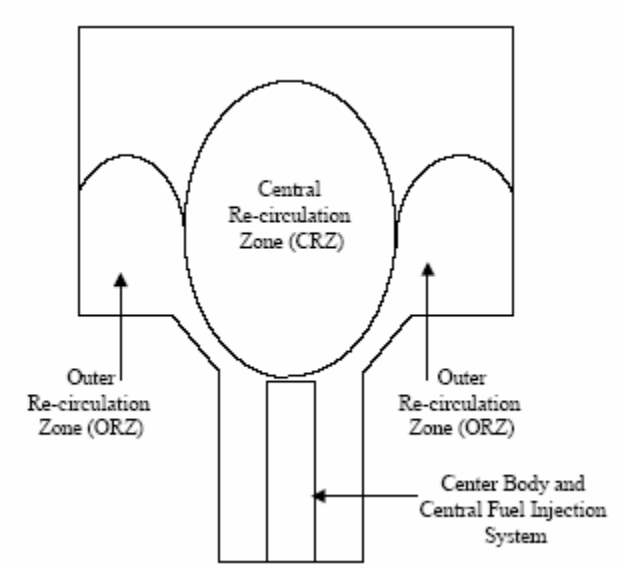

Figure 4.1: Schematic of variable swirl combustor [14]

A frequency response from the experimental data of the heat release of a turbulent swirling flame is shown in Figure 4.2. It can be seen that the response has a peak slightly above 100Hz and then drops off at approximately than 20dB/dec. The additional sharp

peaks appear to be traceable to the acoustic response of the combustion chamber. Since the linearized WSR model was first order, no peaking was possible and the drop off rate could not be more than 20dB/dec. The experimental frequency response also shows the phase dropping approximately 1000°. Time delay will have to be incorporated into the model in order to capture the shift in phase seen in the experiment.

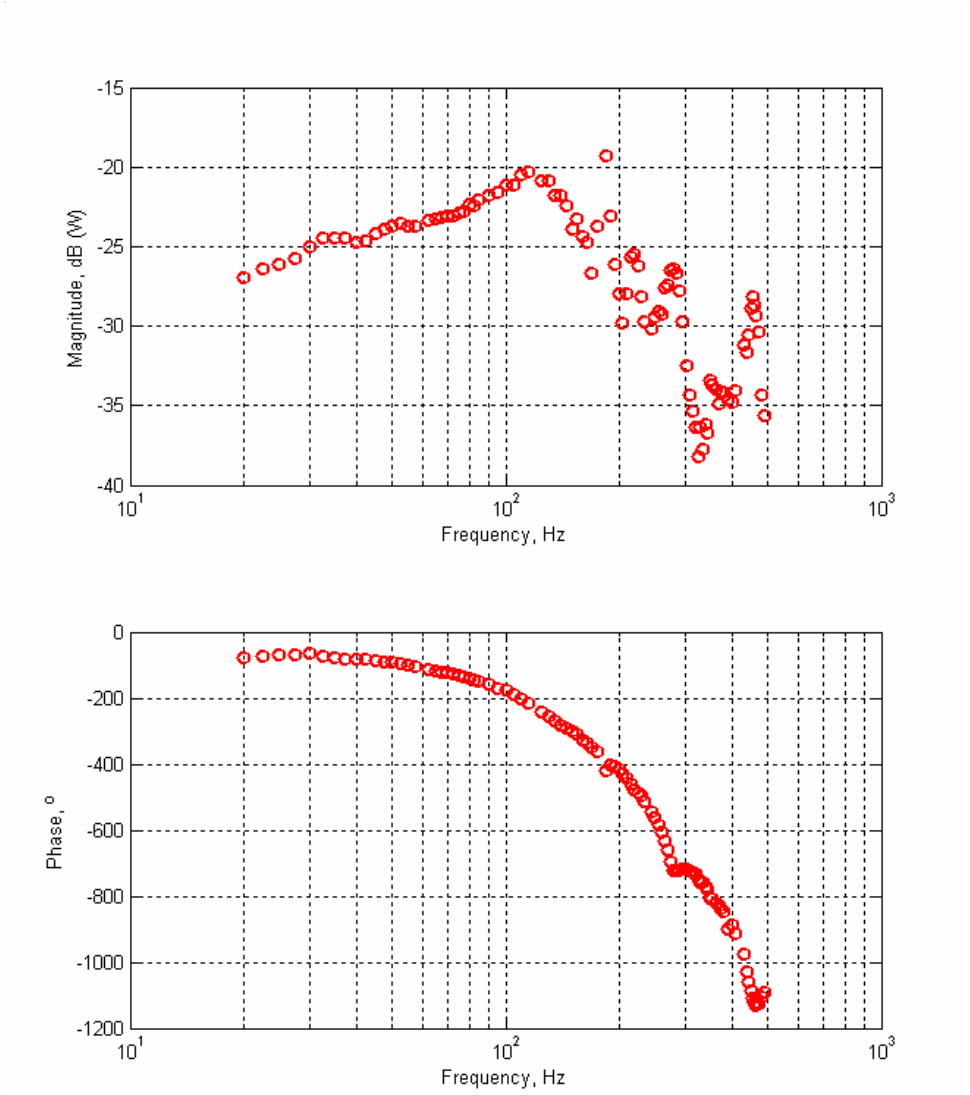

Figure 4.2: OH*-based heat release frequency response for a turbulent swirled flame, Q_{air} = 20 scfm, Φ = 0.65

4.2 Single WSR Model

4.2.1 Derivation of Equations

The basic schematic of a WSR is shown in Figure 4.3. Fuel and oxidizer enter the WSR and are assumed to instantly mix completely with the reactor contents so there is no variation in composition within the reactor volume. Products, fuel, and oxidizer exit the reactor in the same proportions as are present within the reactor. A fundamental

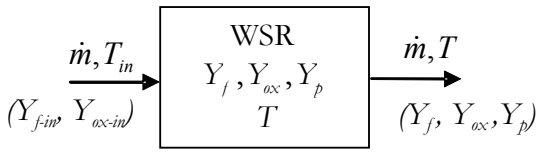

Figure 4.3: Block diagram of single well-stirred reactor

assumption is that the mass flow in is equal to the mass flow out of the reactor, so that mass does not accumulate. This forces the assumption of a fixed density within the reactor if the reactor volume is fixed.

The variables that need to be tracked in the reactor are the mass fractions of fuel, oxidizer and products, as well as the temperature. For simplicity, we will assume a global reaction mechanism

$$C_x H_y + \left(x + {}^{y}\!/_{4}\right)(O_2 + 3.76N_2) \Rightarrow xCO_2 + \left({}^{y}\!/_{2}\right)H_2O + 3.76\left(x + {}^{y}\!/_{4}\right)N_2 \tag{4-1}$$

With this assumption and the fact that the mass fractions must sum to 1, we only need to track the fuel and oxidizer mass fractions and the temperature. Conservation of mass leads to

$$\frac{dm_f}{dt} = \dot{m}_{f,in} - \dot{m}_{f,out} - \dot{\omega}_f V$$

(4-2)

where $\dot{\omega}_f$ is the fuel consumption rate in kg/m^{3}s. Converting to mass fractions and using the fact that $\dot{m}_{in} = \dot{m}_{out} = \dot{m}$ yields

$$\rho V \frac{dY_f}{dt} = \dot{m}(Y_{f,in} - Y_f) - \dot{\omega}_f V$$

(4-3)

Similarly for the oxidizer and products we have

$$\rho V \frac{dY_{ox}}{dt} = \dot{m}(Y_{ox,in} - Y_{ox}) - \dot{\omega}_f V a MW_{ox} / MW_f$$

(4-4)

$$\rho V \frac{dY_p}{dt} = -\dot{m} Y_p + \dot{\omega}_f V MW_p / MW_f$$

(4-5)

where $a = x + y/4$ comes from the stoichiometry of the reaction and we define the product such that one mole of fuel produces one mole of product. To get an equation for temperature, we start with conservation of energy

$$\frac{de}{dt} = \dot{m}_{in}\left(h_{in} - h_{out}\right)$$

(4-6)

Assuming constant and equal specific heats for the chemical components and zero enthalpy of formation for O_2 and N_2, leads to

$$\frac{d}{dt}\begin{pmatrix}\rho V Y_f (h_f^o + c_p (T - T_{ref}))\\ + \rho V Y_{ox} c_p (T - T_{ref})\\ + \rho V Y_p (h_p^o + c_p (T - T_{ref}))\end{pmatrix} = \dot{m}\begin{pmatrix}Y_{f,in}(h_f^o + c_p (T_{in} - T_{ref}))\\ + Y_{ox,in} c_p (T_{in} - T_{ref})\\ - Y_f (h_f^o + c_p (T - T_{ref}))\\ - Y_{ox} c_p (T - T_{ref})\\ - Y_p (h_p^o + c_p (T - T_{ref}))\end{pmatrix} \tag{4-7}$$

which simplifies to

$$\left(\rho V c_p \dot{T} + \rho V \dot{Y}_f h_f^o + \rho V \dot{Y}_p h_p^o\right) = \dot{m}(c_p (T_{in} - T) + (Y_{f,in} - Y_f) h_f^o - Y_p h_p^o) \tag{4-8}$$

Substituting for the mass fraction derivatives with respect to time gives

$$\begin{pmatrix}\rho V c_p \dot{T} + (\dot{m}(Y_{f,in} - Y_f) - \dot{\omega}_f V) h_f^o\\ + (-\dot{m} Y_p + \dot{\omega}_f V MW_p / MW_f) h_p^o\end{pmatrix} = \dot{m}(c_p (T_{in} - T) + (Y_{f,in} - Y_f) h_f^o - Y_p h_p^o) \tag{4-9}$$

which simplifies to

$$\rho V c_p \dot{T} = \dot{m} c_p (T_{in} - T) + \dot{\omega}_f V (h_f^o - (MW_p / MW_f) h_p^o) = \dot{m} c_p (T_{in} - T) + \dot{\omega}_f V \Delta h_r \tag{4-10}$$

where Δh_r is the heat of reaction per unit mass of fuel. The resulting time-varying equations for the WSR are thus

$$\frac{dY_f}{dt} = \frac{1}{\rho}\left(\frac{\dot{m}}{V}(Y_{f,in} - Y_f) - \dot{\omega}_f\right) \tag{4-11}$$

$$\frac{dY_{ox}}{dt} = \frac{1}{\rho}\left(\frac{\dot{m}}{V}(Y_{ox,in} - Y_{ox}) - \dot{\omega}_f a MW_{ox} / MW_f\right) \tag{4-12}$$

$$\dot{T} = \frac{1}{\rho}\left(\frac{\dot{m}}{V}(T_{in} - T) + \dot{\omega}_f \frac{\Delta h_r}{c_p}\right)$$

(4-13)

For a WSR with recirculation, the situation is depicted in Figure 4.4. A fraction α of the exiting mass is recirculated to the input after undergoing a time delay τ.

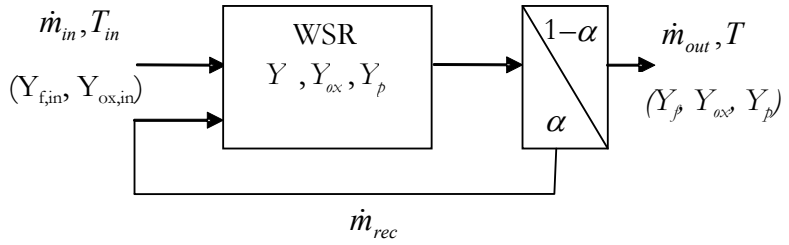

Figure 4.4: Block diagram of single WSR with Recirculation

To have no mass accumulation in the reactor, we require that $\dot{m}_{in}(t) = \dot{m}_{out}(t)(1-\alpha)$ so that

$$\dot{m}_{rec}(t) = \alpha \dot{m}_{out}(t) = \frac{\alpha}{1-\alpha}\dot{m}_{in}(t)$$

(4-14)

The equation for conservation of fuel mass is

$$\frac{dm_f}{dt}(t) = \dot{m}_{f,in}(t) + \dot{m}_{f,rec}(t) - \dot{m}_{f,out}(t) - \dot{\omega}_f(t)V$$

(4-15)

and converting to mass fractions yields

$$\rho V \dot{Y}_f(t) = \dot{m}_{in}(t)Y_{f,in} + \frac{\alpha}{1-\alpha}\dot{m}_{in}(t)Y_f(t-\tau) - \frac{1}{1-\alpha}\dot{m}_{in}(t)Y_f(t) - \dot{\omega}_f(t)V$$

(4-16)

or

$$\dot{Y}_f(t) = \frac{1}{\rho}\left(\frac{\dot{m}_{in}(t)}{V}\left(Y_{f,in} + \frac{\alpha}{1-\alpha}Y_f(t-\tau) - \frac{1}{1-\alpha}Y_f(t)\right) - \dot{\omega}_f(t)\right) \tag{4-17}$$

Similarly, the equation for the oxidizer is

$$\dot{Y}_{ox}(t) = \frac{1}{\rho}\left(\frac{\dot{m}_{in}(t)}{V}\left(Y_{ox,in} + \frac{\alpha}{1-\alpha}Y_{ox}(t-\tau) - \frac{1}{1-\alpha}Y_{ox}(t)\right) - \dot{\omega}_f(t)aMW_{ox}/MW_f\right) \tag{4-18}$$

Using a derivation similar to that above, the temperature equation is found to be

$$\dot{T} = \frac{1}{\rho}\left(\frac{\dot{m}(t)}{V}(T_{in} + \frac{\alpha}{1-\alpha}T(t-\tau) - \frac{1}{1-\alpha}T(t)) + \dot{\omega}_f(t)\frac{\Delta h_r}{c_p}\right) \tag{4-19}$$

Thus the WSR with recirculation is also characterized by three equations and it can be seen that it reduces to the standard WSR as either α or τ goes to zero. It suffices, then, to analyze only the WSR with recirculation and to recover the WSR results by letting α or τ go to zero.

In addition, at equilibrium the unknowns Y_f, Y_{ox}, and T are constant and so their values evaluated at $(t-\tau)$ are equal to their values at (t). This results in the equilibrium points of the WSR with recirculation being identical to the equilibrium points of the standard WSR.

4.2.2 Reducing the equations

Although there are three equations describing the WSR, the system is essentially first order. This is a consequence of several factors, including the fact that after initial transients the amount of oxidizer in the reactor should be directly related to the amount of fuel via stoichiometric arguments. To reduce the equations, define a state vector x and a constant vector v as

$$x = \begin{bmatrix} Y_f \\ Y_{ox} \\ T \end{bmatrix} \qquad v = \begin{bmatrix} -1 \\ -aMW_{ox} / MW_f \\ \Delta h_r / c_p \end{bmatrix}$$

(4-20)

The WSR equations can then be written as

$$\dot{x} = \frac{1}{\rho}\left(\frac{\dot{m}(t)}{V}(x_{in} + \frac{\alpha}{1-\alpha}x(t-\tau) - \frac{1}{1-\alpha}x(t)) + \dot{\omega}_f(t)v \right)$$

(4-21)

and it can be seen that the coupling between the equations is generated by the term $\dot{\omega}_f(t)v$. Define a transformation matrix T by

$$z = Tx = \begin{bmatrix} -aMW_{ox} / MW_f & 1 & 0 \\ \Delta h_r / c_p & 0 & 1 \\ 0 & 0 & 1 \end{bmatrix} x = \begin{bmatrix} Y_{ox} - aMW_{ox} / MW_f Y_f \\ T + Y_f \Delta h_r / c_p \\ T \end{bmatrix}$$

(4-22)

which has the property that

$$Tv = \begin{bmatrix} 0 \\ 0 \\ \Delta h_r / c_p \end{bmatrix}$$

(4-23)

The WSR equations in the z coordinates are

$$\dot{z} = \frac{1}{\rho}\left(\frac{\dot{m}(t)}{V}(z_{in} + \frac{\alpha}{1-\alpha}z(t-\tau) - \frac{1}{1-\alpha}z(t)) + \dot{\omega}_f(t)\begin{bmatrix} 0 \\ 0 \\ \Delta h_r / c_p \end{bmatrix} \right)$$

(4-24)

The first two components of the above equation are completely uncoupled and evolve according to the scalar equation

$$\dot{y} = \frac{1}{\rho}\frac{\dot{m}(t)}{V}(y_{in} + \frac{\alpha}{1-\alpha}y(t-\tau) - \frac{1}{1-\alpha}y(t))$$

(4-25)

This equation has a stable equilibrium point at $y(t) = y_{in}(t)$, which implies that after an initial transient the reactor variables satisfy the following equalities:

$$\begin{bmatrix} Y_{ox} - Y_f aMW_{ox}/MW_f \\ T + Y_f \Delta h_r / c_p \end{bmatrix} = \begin{bmatrix} Y_{ox,in} - Y_{f,in} aMW_{ox}/MW_f \\ T_{in} + Y_{f,in}\Delta h_r / c_p \end{bmatrix}$$

(4-26)

Since the right hand side of the above equation is constant, we can use these equations to express Y_f in terms of T and Y_{ox} in terms of Y_f, and hence in terms of T. This enables us to write an expression for $\dot{\omega}_f$ solely in terms of T and thus the WSR system is governed by the scalar equation

$$\dot{T} = \frac{1}{\rho}\left(\frac{\dot{m}(t)}{V}(T_{in} + \frac{\alpha}{1-\alpha}T(t-\tau) - \frac{1}{1-\alpha}T(t)) + \dot{\omega}_f(T(t))\frac{\Delta h_r}{c_p}\right)$$

(4-27)

where the input to the system is $\dot{m}(t)$ and the output is the heat release rate

$$\dot{Q}_r = \dot{\omega}_f(t)\Delta h_r .$$

(4-28)

The rate at which fuel is consumed (kg/m^{3}sec) is given by the Arrhenius form

$$\dot{\omega}_f = Ae^{T_a/T}(\rho Y_f)^{n_f}(\rho Y_{o_2})^{n_{O_2}}$$

(4-29)

4.2.3 Linearization of Nonlinear Equations

To determine the equilibrium points, we can look for a constant solution to the differential equation (4-27) which, together with (4-26), yields the algebraic equations

$$Y_{ox,eq} = Y_{ox,in} + Y_{f,eq} aMW_{ox} / MW_f - Y_{f,in} aMW_{ox} / MW_f \tag{4-30}$$

$$Y_{f,eq} = \frac{c_p}{\Delta h_r}(T_{in} - T_{eq}) + Y_{f,in} \tag{4-31}$$

$$0 = \frac{\dot{m}_{eq} c_p}{V \Delta h_r}(T_{in} - T_{eq}) + \dot{\omega}_f(T_{eq}) \tag{4-32}$$

One way to solve these equations is to pick an equilibrium value of the input, $\dot{m}_{eq}$, and then solve the nonlinear third equation for T_{eq}. Graphically, this would amount to plotting the linear term $\frac{\dot{m}_{eq} c_p}{V \Delta h_r}(T - T_{in})$ and the nonlinear term $\dot{\omega}_f(T)$ as functions of T and looking for the intersections. This clearly shows that there can be up to three solutions for T_{eq} including the zero solution, and also that as the equilibrium mass flow increases, a point is reached at which two solutions disappear and the only solution is the zero solution. This corresponds to the blow off point.

Despite the insight gained by the above method, it is easier numerically to simply pick an equilibrium temperature, T_{eq}, solve equation (4-31) for $Y_{f,eq}$, solve equation (4-30) for $Y_{ox,eq}$, and then finally solve equation (4-32) for $\dot{m}_{eq}$.

Once the equilibrium point has been determined, the linearization can be computed by first determining the row vector

$$\nabla \dot{\omega}_{f,eq} = \left. \frac{\partial \dot{\omega}_f}{\partial x} \right|_{eq} \tag{4-33}$$

The linearization then becomes

$$\dot{T}' = \frac{1}{\rho}\left(\frac{\dot{m}_{eq}}{V}\left(\frac{\alpha}{1-\alpha}T'(t-\tau) - \frac{1}{1-\alpha}T'(t)\right) + \frac{\Delta h_r}{c_p}\left[\frac{\partial \dot{\omega}_f}{\partial Y_f}\frac{\partial Y_f}{\partial T} + \frac{\partial \dot{\omega}_f}{\partial Y_{O_2}}\frac{\partial Y_{O_2}}{\partial Y_{ox}}\frac{\partial Y_{ox}}{\partial T} + \frac{\partial \dot{\omega}_f}{\partial T}\right]_{eq} T'(t) + \frac{(T_{in} - T_{eq})}{V}\dot{m}'(t) \right) \tag{4-34}$$

which reduces to

$$\dot{T}' = \frac{1}{\rho}\left(\frac{\dot{m}_{eq}}{V}\left(\frac{\alpha}{1-\alpha}T'(t-\tau) - \frac{1}{1-\alpha}T'(t)\right) + \nabla \dot{\omega}_{f,eq}\begin{bmatrix} -1 \\ -aMW_{ox}/MW_f \\ \Delta h_r / c_p \end{bmatrix} T'(t) + \frac{(T_{in} - T_{eq})}{V}\dot{m}'(t) \right) \tag{4-35}$$

The linearization of the output equation is

$$\dot{Q}_r' = \Delta h_r \left[\frac{\partial \dot{\omega}_f}{\partial Y_f}\frac{\partial Y_f}{\partial T} + \frac{\partial \dot{\omega}_f}{\partial Y_{O_2}}\frac{\partial Y_{O_2}}{\partial Y_{ox}}\frac{\partial Y_{ox}}{\partial T} + \frac{\partial \dot{\omega}_f}{\partial T}\right]_{eq} T'(t) = \nabla \dot{\omega}_{f,eq}\begin{bmatrix} -c_p \\ -ac_pMW_{ox}/MW_f \\ \Delta h_r \end{bmatrix} T'(t) \tag{4-36}$$

4.2.4 Results

A map of the possible equilibrium points as a function of mass flow rate for a one well-stirred reactor system is shown in Figure 4.5 (Φ=0.65, T_{inlet} = 600 K). The solid portion of the graph represents stable equilibria; the dotted line represents unstable equilibria. The transition from stable to unstable equilibria is the mass flow rate at which blowout occurs. The two points shown on the graph refer to the equilibrium points used for generating the graphs shown in Figure 4.6 and Figure 4.7. The pertinent constants used in the modeling are shown below in Table 4-1; the constants listed there are also used in the modeling in Sections 4.3 and 4.4.

In Figure 4.6 and Figure 4.7, and for the frequency responses shown in the remainder of this document, the input was fluctuation in mass flow rate (kg/s) and the output was heat release rate (W/m^3).

Table 4-1: Property values used in WSR modeling

Property	Symbol	Units	Value
Inlet Temperature	T_{in}	K	600
Specific heat	c_p	J/kg-K	2200
Heat of reaction	Δh_r	kJ/kg	50016
Pre-exponential factor	A	$(gmol/cm^3)^{1-m-n}$	2.0×10^{22}
Activation Energy	E_a	kcal/gmol	40
Activation Temperature	T_a	K	20128.82
Fuel concentration exponent	m	--	1
Oxygen concentration exponent	n	--	2

As mass flow rate increases, the stable equilibrium temperature decreases, as can be seen in Figure 4.5. Also, the bandwidth of the system decreases as the mass flow rate increases. This can be seen by comparing Figure 4.6 and Figure 4.7. Figure 4.6 shows the frequency response of a one WSR system with a small mass flow rate. The frequency response shown in Figure 4.7 is for a one WSR system near blowout with a high mass flow rate. It should be noted that the frequency response in Figure 4.7 not only has a smaller bandwidth, but the phase of the response has also been shifted by 180°. This behavior was also seen in Park [24], and was attributed to the heat release reaching a maximum. The change in phase of the frequency response always precedes blowout as mass flow rate is increased. Figure 4.7 shows that it is possible obtain a WSR system which has approximately the same bandwidth as those seen in experiments. However,

they also demonstrate that a single WSR system without recirculation will not be able to approximate the phase shown in the experiments.

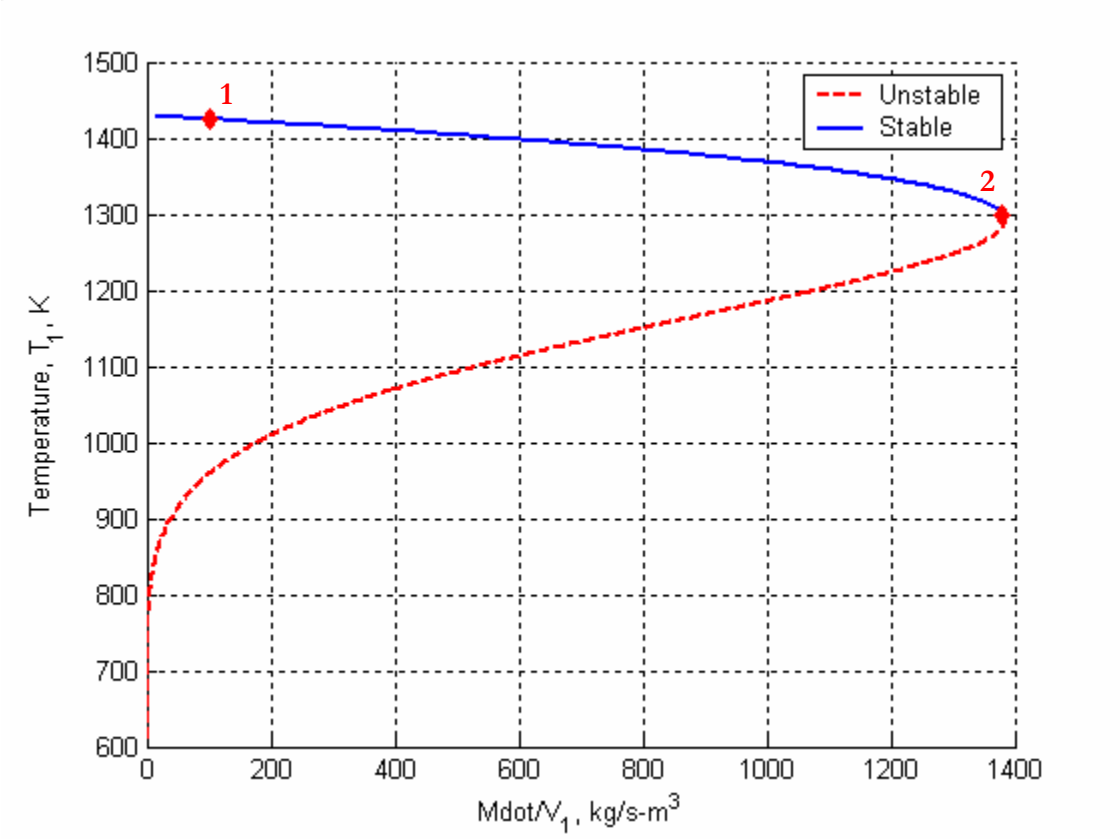

Figure 4.5: Bifurcation diagram of a one WSR system showing possible equilibrium points.

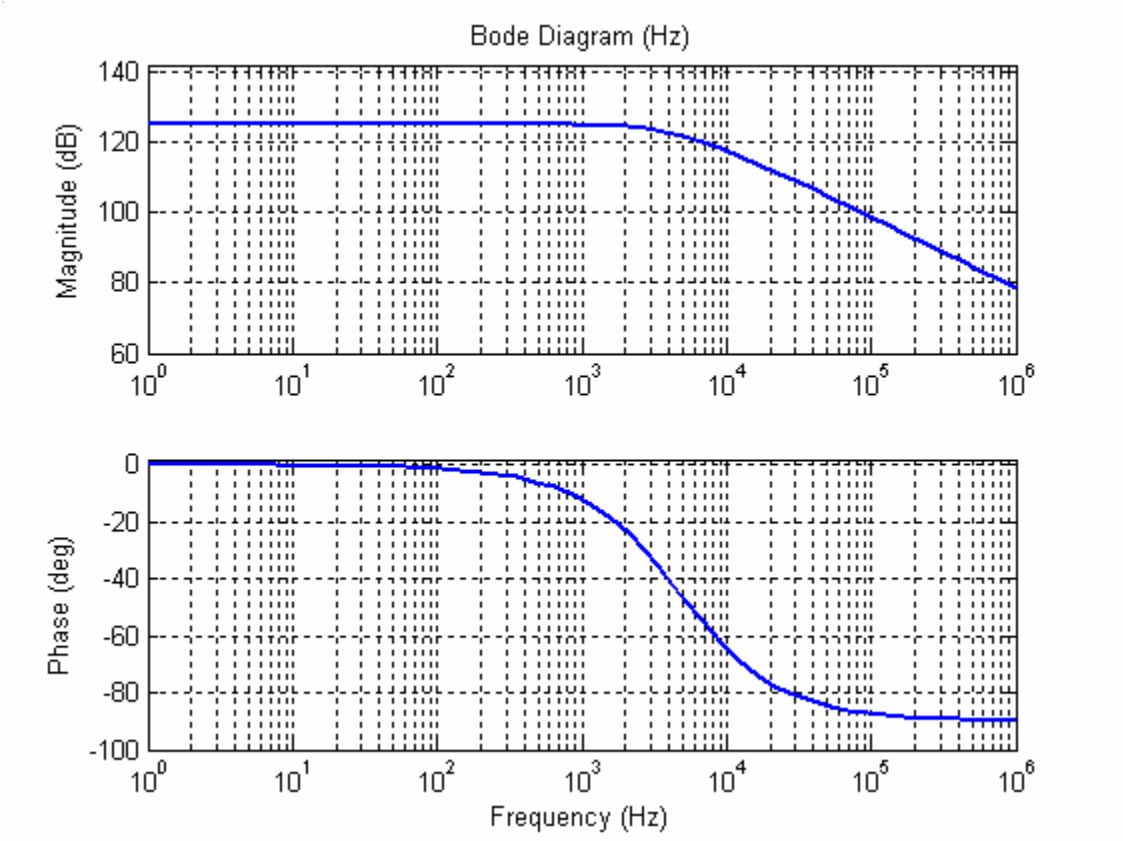

Figure 4.6: Frequency response of WSR without recirculation, Φ=0.65, $\dot{m}/V = 102$ **kg/s (point 1 in Figure 4.5)**

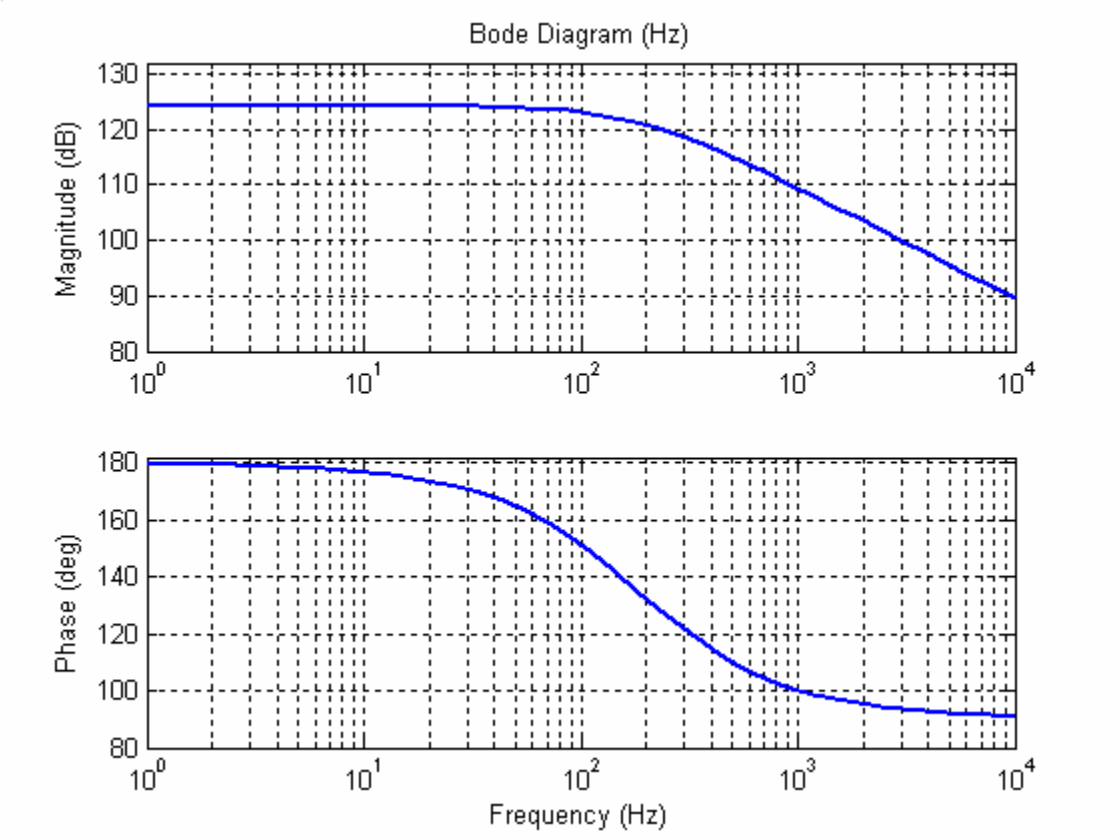

Figure 4.7: Frequency response of one WSR without recirculation, Φ=0.65, $\dot{m}/V$ =1380 kg/s (point 2 in Figure 4.5)

The response of a WSR with time delay on the recirculation loop is shown in Figure 4.8. In a WSR model with recirculation and time delay, the time delay in denoted by τ, and the amount of recirculation is denoted by α. The response of a single WSR with only recirculation and no time delay is not shown because the response is the same as a WSR with no recirculation. This is because due to the assumptions made in deriving the models, the equations for one WSR with only recirculation reduce to the equations of a single WSR without recirculation. The bandwidth of a one WSR model with time delay can also be made to have a bandwidth on the order of 200 Hz. The recirculation adds some ripples to the response, but cannot produce a major effect. Varying the parameters of these reactors does not appear to produce changes significant enough to match the experimental results.

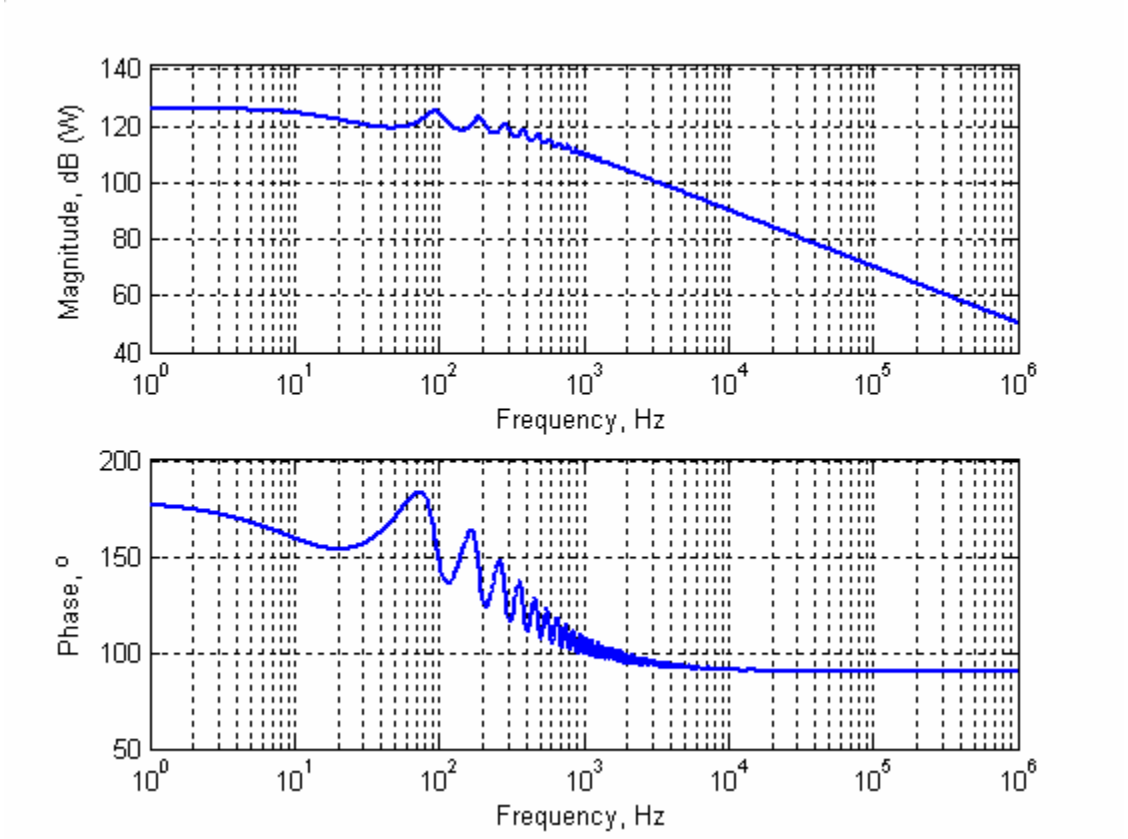

Figure 4.8: Frequency response of WSR with Recirculation, *Φ=0.65,*

$\dot{m}/V = 1380$ **kg/s, α = 20%, τ = 0.01 seconds.**

4.3 Two Coupled Well-Stirred Reactor System

To investigate situations capable of dynamics of order higher than first, the case of two WSR's coupled by a feedback loop was considered. The block diagram of the system is shown in Figure 4.9. In this case, the output of the first reactor goes directly to the second reactor and a fraction of the output of the second reactor is recirculated to the first reactor. Since the reactors are coupled, it should be possible to achieve equilibrium states that would be impossible with a simple series connection of reactors.

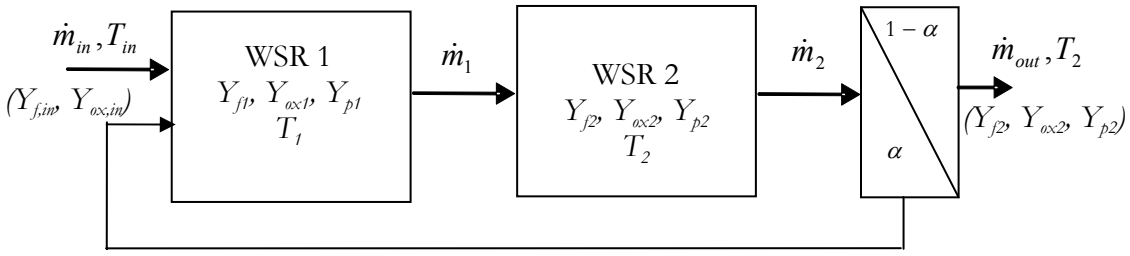

Figure 4.9. Block diagram of two WSR's coupled by recirculation.

4.3.1 Derivation of Equations

To derive the equations for this system, first note that a mass flow balance requires

$$\dot{m}_{in} + \alpha\dot{m}_2 = \dot{m}_1 = \dot{m}_2 \tag{4-37}$$

In reactor 1, mass conservation of fuel requires that

$$\rho_1 V_1 \dot{Y}_{f1} = \dot{m}_{in} Y_{f,in} + \alpha\dot{m}_2 Y_{f2} - \dot{m}_1 Y_{f1} - \dot{\omega}_{f1} V_1 \tag{4-38}$$

and a similar equation holds for the oxidizer. An energy balance requires that

$$\rho_1 V_1 c_p \dot{T}_1 = \dot{m}_{in} c_p T_{in} + \alpha\dot{m}_2 c_p T_2 - \dot{m}_1 c_p T_1 + \dot{\omega}_{f1} V_1 \Delta h_r$$

(4-39)

The second reactor has equations similar to the single WSR considered previously, with input consisting of the output of reactor one (Y_{f1}, Y_{ox1}, T_1) with a mass flow rate of $\dot{m}_{in}(t)/(1-\alpha)$.

The equations for the entire system are given by

$$\dot{Y}_{f1}(t) = \frac{1}{\rho_1}\left(\frac{\dot{m}_{in}(t)}{V_1}\left(Y_{f,in} + \frac{\alpha}{1-\alpha}Y_{f2}(t-\tau) - \frac{1}{1-\alpha}Y_{f1}(t)\right) - \dot{\omega}_{f1}(t)\right)$$

(4-40)

$$\dot{Y}_{ox1}(t) = \frac{1}{\rho_1}\left(\frac{\dot{m}_{in}(t)}{V_1}\left(Y_{ox,in} + \frac{\alpha}{1-\alpha}Y_{ox2}(t-\tau) - \frac{1}{1-\alpha}Y_{ox1}(t)\right) - \dot{\omega}_{f1}(t)aMW_{ox}/MW_f\right)$$

(4-41)

$$\dot{T}_1(t) = \frac{1}{\rho_1}\left(\frac{\dot{m}_{in}(t)}{V_1}(T_{in} + \frac{\alpha}{1-\alpha}T_2(t-\tau) - \frac{1}{1-\alpha}T_1(t)) + \dot{\omega}_{f1}(t)\frac{\Delta h_r}{c_p}\right)$$

(4-42)

$$\dot{Y}_{f2}(t) = \frac{1}{\rho_2}\left(\frac{\dot{m}_{in}(t)}{V_2(1-\alpha)}\left(Y_{f1}(t) - Y_{f2}(t)\right) - \dot{\omega}_{f2}(t)\right)$$

(4-43)

$$\dot{Y}_{ox2}(t) = \frac{1}{\rho_2}\left(\frac{\dot{m}_{in}(t)}{V_2(1-\alpha)}\left(Y_{ox1}(t) - Y_{ox2}(t)\right) - \dot{\omega}_{f2}(t)aMW_{ox}/MW_f\right)$$

(4-44)

$$\dot{T}_2(t) = \frac{1}{\rho_2}\left(\frac{\dot{m}_{in}(t)}{V_2(1-\alpha)}(T_1(t) - T_2(t)) + \dot{\omega}_{f2}(t)\frac{\Delta h_r}{c_p}\right)$$

(4-45)

4.3.2 Reducing the equations

These equations can be reduced to just a pair of equations by proceeding as for the case of one WSR. Define

$$x_i = \begin{bmatrix} Y_{fi} & Y_{oxi} & T_i \end{bmatrix}^T$$

(4-46)

Then we can write the above equations as

$$\dot{x}_1(t) = \frac{1}{\rho_1}\left(\frac{\dot{m}_{in}(t)}{V_1}\left(x_{in} + \frac{\alpha}{1-\alpha} x_2(t-\tau) - \frac{1}{1-\alpha} x_1(t) \right) - \dot{\omega}_{f1}(t) \begin{bmatrix} 1 \\ aMW_{ox} / MW_f \\ -\Delta h_r / c_p \end{bmatrix} \right)$$

(4-47)

$$\dot{x}_2(t) = \frac{1}{\rho_2}\left(\frac{\dot{m}_{in}(t)}{V_2(1-\alpha)}\left(x_1(t) - x_2(t) \right) - \dot{\omega}_{f2}(t) \begin{bmatrix} 1 \\ aMW_{ox} / MW_f \\ -\Delta h_r / c_p \end{bmatrix} \right)$$

(4-48)

Using the same transformation as before gives

$$\dot{z}_1(t) = \frac{1}{\rho_1}\left(\frac{\dot{m}_{in}(t)}{V_1}\left(z_{in} + \frac{\alpha}{1-\alpha} z_2(t-\tau) - \frac{1}{1-\alpha} z_1(t) \right) - \dot{\omega}_{f1}(t) \begin{bmatrix} 0 \\ 0 \\ -\Delta h_r / c_p \end{bmatrix} \right)$$

(4-49)

$$\dot{z}_2(t) = \frac{1}{\rho_2}\left(\frac{\dot{m}_{in}(t)}{V_2(1-\alpha)}\left(z_1(t) - z_2(t) \right) - \dot{\omega}_{f2}(t) \begin{bmatrix} 0 \\ 0 \\ -\Delta h_r / c_p \end{bmatrix} \right)$$

(4-50)

It can be seen that the first two components in each of the above equations evolve independently of the third components, although the first component of z_1, z_{11}, is linked to the first component of z_2, z_{21}, and similarly for the second components. The equations for each set of components are identical and are given, in the first case, by

$$\begin{bmatrix} z_{11}(t) \\ z_{21}(t) \end{bmatrix} = \dot{m}_{in}(t) \begin{bmatrix} -\dfrac{1}{\rho_1 V_1(1-\alpha)} & 0 \\ \dfrac{1}{\rho_2 V_2(1-\alpha)} & -\dfrac{1}{\rho_2 V_2(1-\alpha)} \end{bmatrix} \begin{bmatrix} z_{11}(t) \\ z_{21}(t) \end{bmatrix} + \dot{m}_{in}(t) \begin{bmatrix} 0 & \dfrac{\alpha}{\rho_1 V_1(1-\alpha)} \\ 0 & 0 \end{bmatrix} \begin{bmatrix} z_{11}(t-\tau) \\ z_{21}(t-\tau) \end{bmatrix} + \begin{bmatrix} \dfrac{\dot{m}_{in}}{\rho_1 V_1} \\ 0 \end{bmatrix} z_{in,1}$$

(4-51)

For the case $\tau = 0$, it is straightforward to see that the above equation is asymptotically stable and converges to the equilibrium point

$$\begin{bmatrix} z_{11}(t) \\ z_{21}(t) \end{bmatrix} = \begin{bmatrix} z_{in,1} \\ z_{in,1} \end{bmatrix}$$

(4-52)

Considering both sets of equations, the components $z_{11}, z_{21}, z_{12}, z_{22}$ converge to an equilibrium point and, in terms of the original variables, the following algebraic relationships result:

$$\begin{bmatrix} -(aMW_{ox}/MW_f)Y_{f1} + Y_{ox1} \\ (\Delta h_r / c_p)Y_{f1} + T_1 \\ -(aMW_{ox}/MW_f)Y_{f2} + Y_{ox2} \\ (\Delta h_r / c_p)Y_{f2} + T_2 \end{bmatrix} = \begin{bmatrix} -(aMW_{ox}/MW_f)Y_{f,in} + Y_{ox,in} \\ (\Delta h_r / c_p)Y_{f,in} + T_{in} \\ -(aMW_{ox}/MW_f)Y_{f,in} + Y_{ox,in} \\ (\Delta h_r / c_p)Y_{f,in} + T_{in} \end{bmatrix}$$

(4-53)

The remaining dynamic equations are given by

$$\dot{T}_1(t) = \frac{1}{\rho_1}\left(\frac{\dot{m}(t)}{V_1}(T_{in} + \frac{\alpha}{1-\alpha}T_2(t) - \frac{1}{1-\alpha}T_1(t)) + \dot{\omega}_{f1}(T_1(t))\frac{\Delta h_r}{c_p} \right)$$

(4-54)

$$\dot{T}_2(t) = \frac{1}{\rho_2}\left(\frac{\dot{m}(t)}{V_2(1-\alpha)}(T_1(t) - T_2(t)) + \dot{\omega}_{f2}(T_2(t))\frac{\Delta h_r}{c_p} \right)$$

(4-55)

with the total heat release rate given by

$$\dot{Q}_r = \Delta h_r(\dot{\omega}_{f1} + \dot{\omega}_{f2})$$

(4-56)

4.3.3 Linearization of Nonlinear Equations

To find the possible equilibrium points of the system it is easiest to pick values for T_1 and T_2, and then solve for the required values of $\dot{m}(t)/V_1$ and the volume ratio V_2/V_1. This approach will produce all possible equilibrium points for this configuration of WSR's. The linearization of the above equations about an equilibrium point proceeds analogously to the single WSR case and results in

$$\dot{T}_1' = \frac{1}{\rho_1}\left(\frac{\dot{m}_{eq}}{V_1}\left(\frac{\alpha}{1-\alpha}T_2'(t) - \frac{1}{1-\alpha}T_1'(t)\right) + \nabla\dot{\omega}_{f1,eq}\begin{bmatrix} -1 \\ -aMW_{ox}/MW_f \\ \Delta h_r / c_p \end{bmatrix} T_1'(t) + \frac{\dot{m}'(t)}{V_1}\left(T_{in} + \frac{\alpha}{1-\alpha}T_{2,eq} - \frac{1}{1-\alpha}T_{1,eq}\right)\right) \tag{4-57}$$

$$\dot{T}_2' = \frac{1}{\rho_2}\left(\frac{\dot{m}_{eq}}{V_2(1-\alpha)}\left(T_1'(t) - T_2'(t)\right) + \nabla\dot{\omega}_{f2,eq}\begin{bmatrix} -1 \\ -aMW_{ox}/MW_f \\ \Delta h_r / c_p \end{bmatrix} T_2'(t) + \frac{\dot{m}'(t)}{V_2(1-\alpha)}\left(T_{1,eq} - T_{2,eq}\right)\right) \tag{4-58}$$

The linearization of the output equation is

$$\dot{Q}_r' = \nabla\dot{\omega}_{f1,eq}\begin{bmatrix} -c_p \\ -ac_pMW_{ox}/MW_f \\ \Delta h_r \end{bmatrix} T_1'(t) + \nabla\dot{\omega}_{f2,eq}\begin{bmatrix} -c_p \\ -ac_pMW_{ox}/MW_f \\ \Delta h_r \end{bmatrix} T_2'(t) \tag{4-59}$$

4.3.4 Results

A map of the possible stable equilibrium temperatures of the system for a fixed amount of recirculation (in this case, α = 30% and Φ = 0.7) is shown in Figure 4.10. This map is generated by computing the linearized system, corresponding to the possible equilibrium temperatures, and determining the system's stability. A plot of the stability boundary in the $T_1 - T_2$ plane leads to the graph shown below in Figure 4.10.

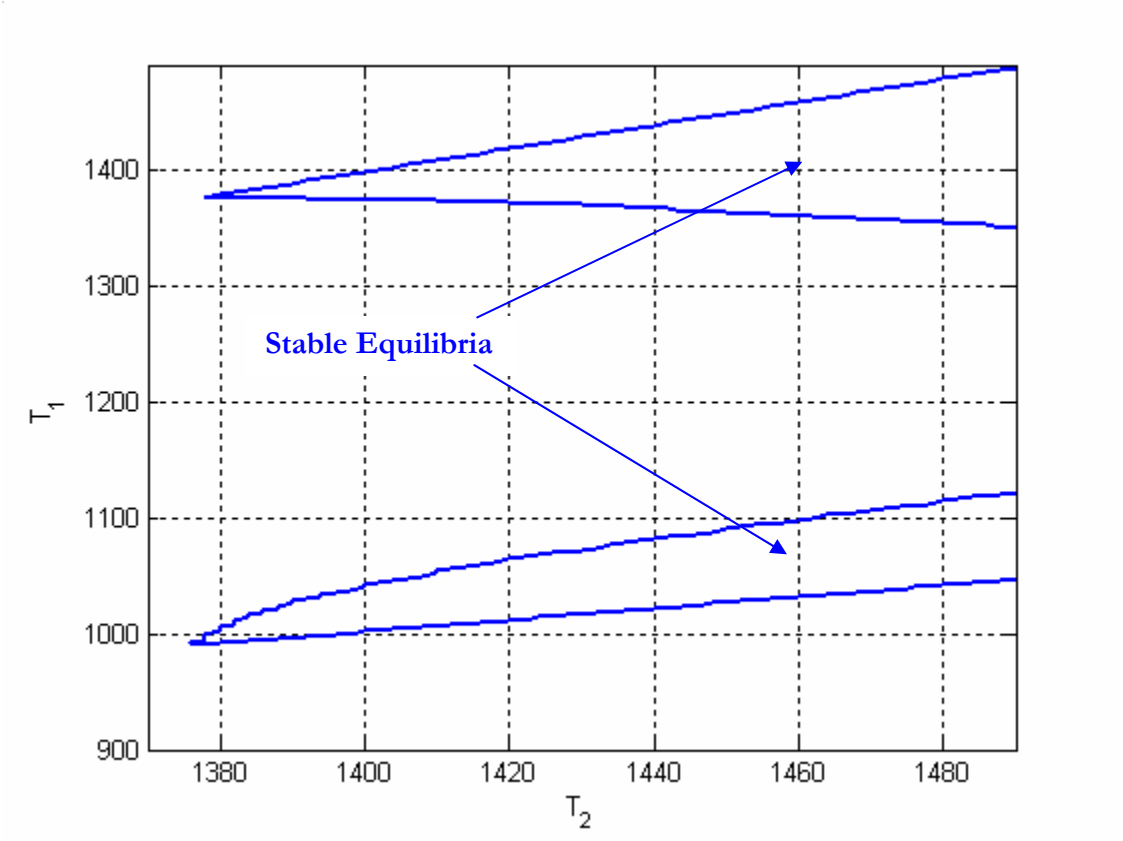

Figure 4.10: Stable equilibrium regions of a two WSR system, α = 30% and Φ = 0.7

When a system is in the lower region, the first reactor acts as a preheat zone, and the main combustion occurs in the second reactor. A system in the upper region represents a system where the major part of the combustion is completed in the first reactor, and its products heat up the second reactor. The stability regions change as a function of recirculation, as shown in Figure 4.11.

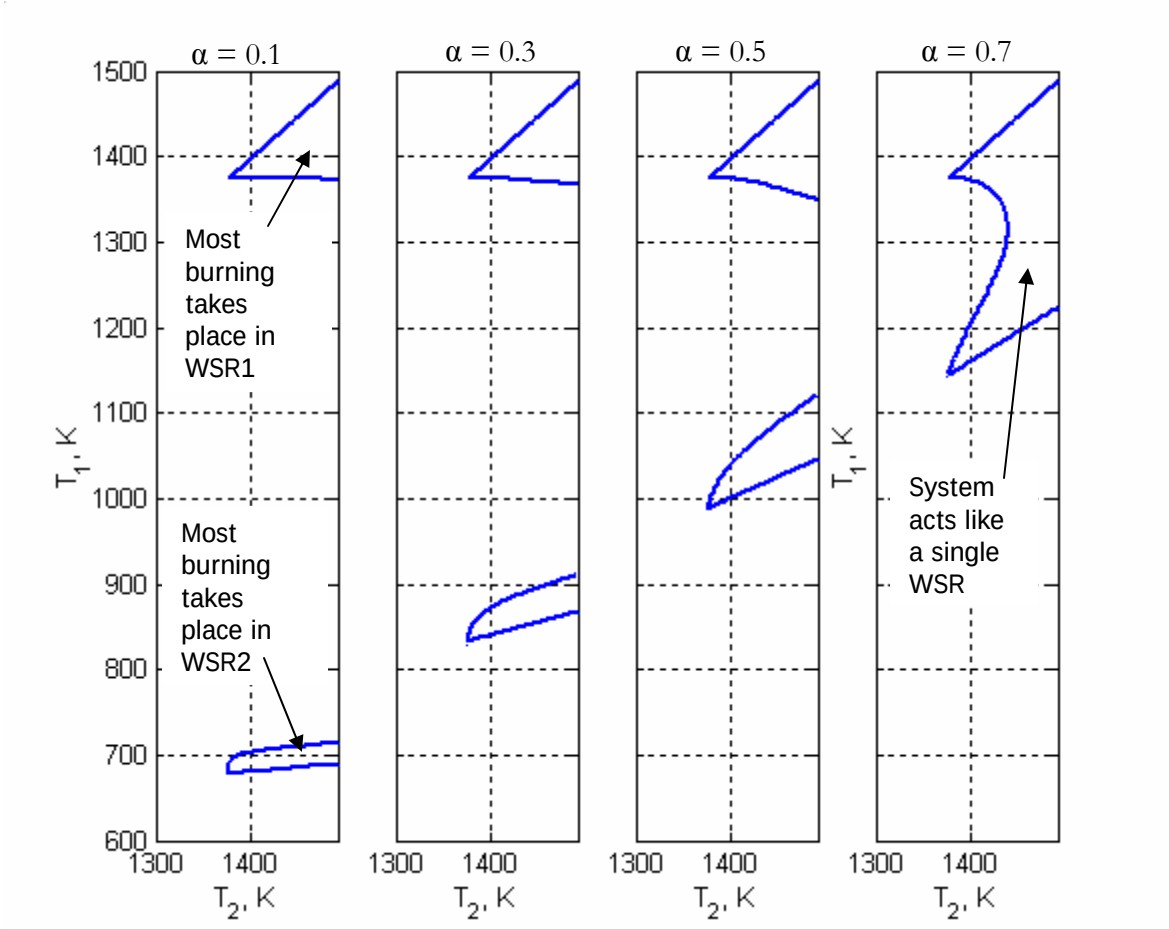

Figure 4.11. The stable equilibrium regions of the two WSR system change with the amount of recirculation.

Increasing the amount of recirculation, increases the mixing of the reactants of the first reactor with the products of the second reactor and the system starts to approximate a single WSR system. This is because of the assumption inherent in a WSR that the mixing of the incoming products is instantaneous and therefore the mixture in the reactor is homogeneous. With so much of the products of the second reactor being re-circulated into the first reactor, the first reactor temperature and mixture approach that of the second reactor, and the whole system functions as a single WSR.

As mentioned before, for cases where there are two stability regions, the system has two possible stable equilibrium points. Since there are an infinite number of equilibria for a given mass flow, fixing the mass flow produces a constant mass flow line

on the stability map. There is an analogous line for constant volume ratio. A given system will have a specified mass flow rate and volume ratio, and therefore the intersection of the constant mass flow line and the constant volume ratio line identifies the possible equilibria for a given system as shown in Figure 4.12.

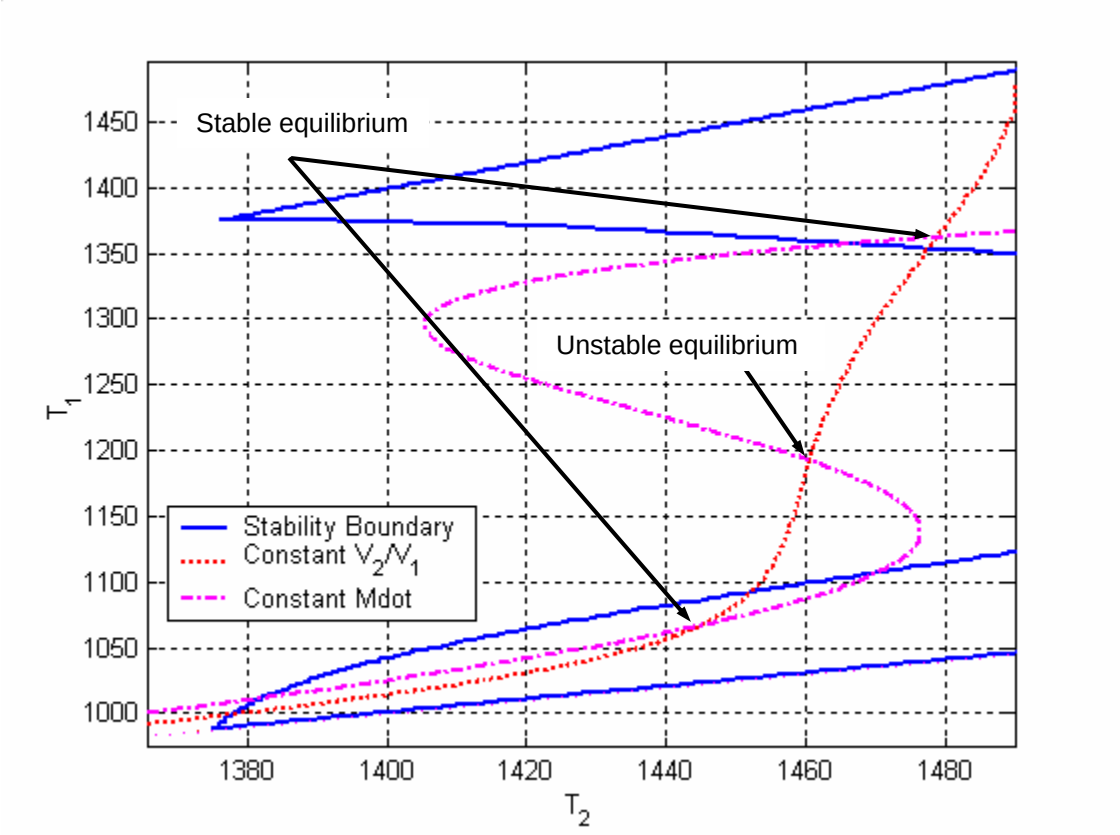

Figure 4.12: Possible equilibrium points of a two-WSR system, α = 50%, Φ = 0.7

The constant volume ratio line is computed by setting the volume ratio and solving for the equilibrium temperature of the first reactor, T_1, given a specified equilibrium temperature for the second reactor, T_2. The constant mass flow line is calculated by making a contour plot of the mass flow data determined while the stability regions were being computed. As you travel along the constant volume ratio line the mass flow increases until the unstable equilibrium point, and then decreases again until it enters the lower stable region. If a system were ignited in one of the two stable regions, for instance, the upper region, as the mass flow was increased, the system would follow the

constant volume ratio line through the upper stable region until it reached the boundary of the stability region and then became unstable. The system would then jump to a point on the constant volume ratio line inside the lower stability region. This point would have the same mass flow rate as the point where the system became unstable. If the mass flow is increased further, the system equilibrium will again follow the line of constant volume ratio down through the nose of the stability region until it finally reaches the border. If the mass flow rate is increased still further, the flame will extinguish, represented here by moving out of the stability region with mass flow and volume conditions which are not present in another stability region.

Another way of viewing this phenomenon is to examine the bifurcation diagram of the system. First an example bifurcation diagram is shown in Figure 4.13. This figure shows the equilibrium temperature of both reactors as a function of mass flow rate.

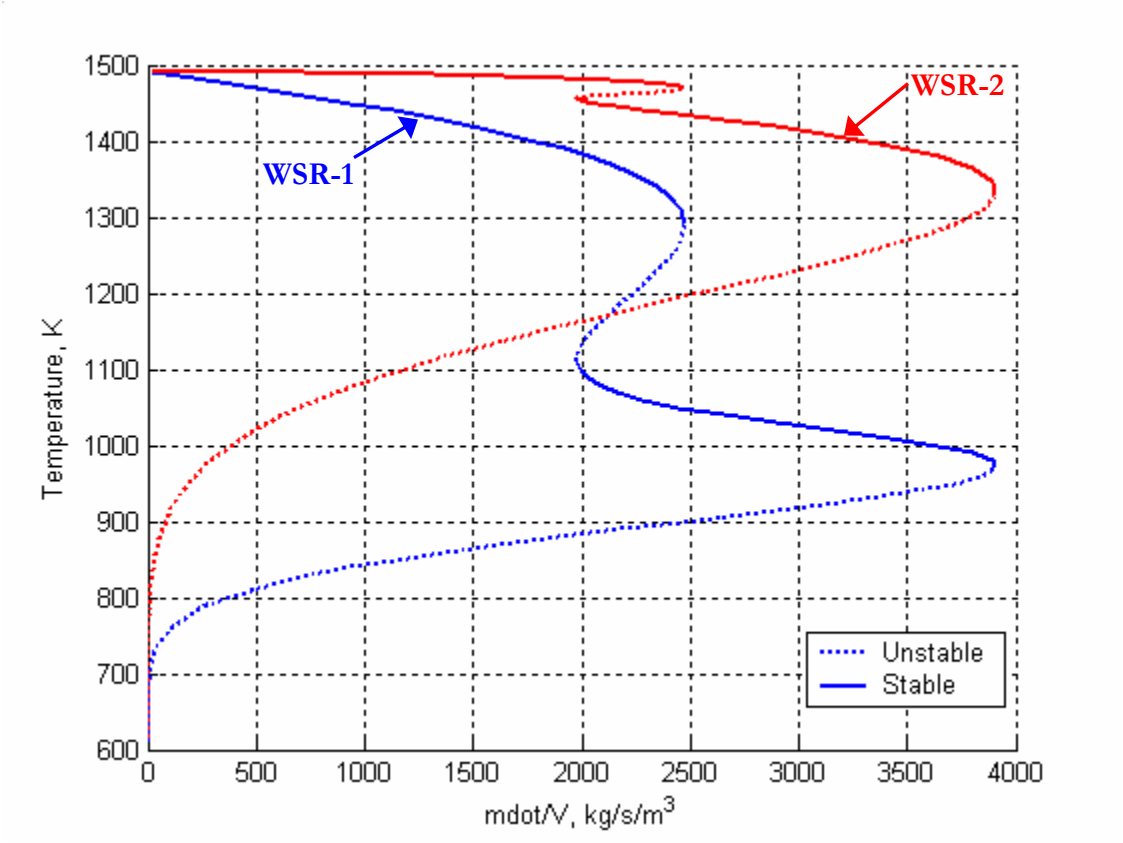

Figure 4.13: Example bifurcation diagram with both equilibrium temperatures shown

Examining the figure, it can be seen that the equilibrium temperature of the second reactor always has a higher value than the first WSR. However, other than that the equilibrium temperature of the second WSR follows the same shape as that of the first WSR. Regions of instability and blowout occur at the same value of mass flow for each of the curves. Therefore, for the remainder of the section, only the equilibrium temperature of the first reactor will be shown in order to simplify the discussion.

A bifurcation diagram for a two WSR system is shown in Figure 4.14. The bifurcation diagram was computed by varying the temperature of the first reactor and solving for the subsequent mass flow and second reactor temperature. The solid lines in the figure represent stable equilibria and the dotted lines represent unstable equilibria. If the system is ignited at point one, with a high temperature in the first reactor and a low mass flow rate, and then the mass flow rate is increased, the equilibrium temperature of the first reactor will follow the curve shown in Figure 4.14. As a reactor's mass flow is ramped up, the system encounters a jump – at point 2 in the figure – from one stability region to another. This jump could be thought of as a relocation of the flame. For the equilibrium points between points 1 and 2, the flame was located in the first reactor and its products resulted in high temperatures in the second reactor. However, after the jump, in the region between points 3 and 4, the flame is located primarily in the second reactor, and the first reactor acts as preheat zone. If the mass flow is further increased, the system will eventually reach point 4 in the figure and blowout. However, if after jumping from point 2 to the lower curve in the figure, the mass flow is decreased, the equilibrium temperature will approach point 3 and eventually jump back up to the upper curve. The existence of this jump phenomenon gives rise to a possible hysteresis loop.

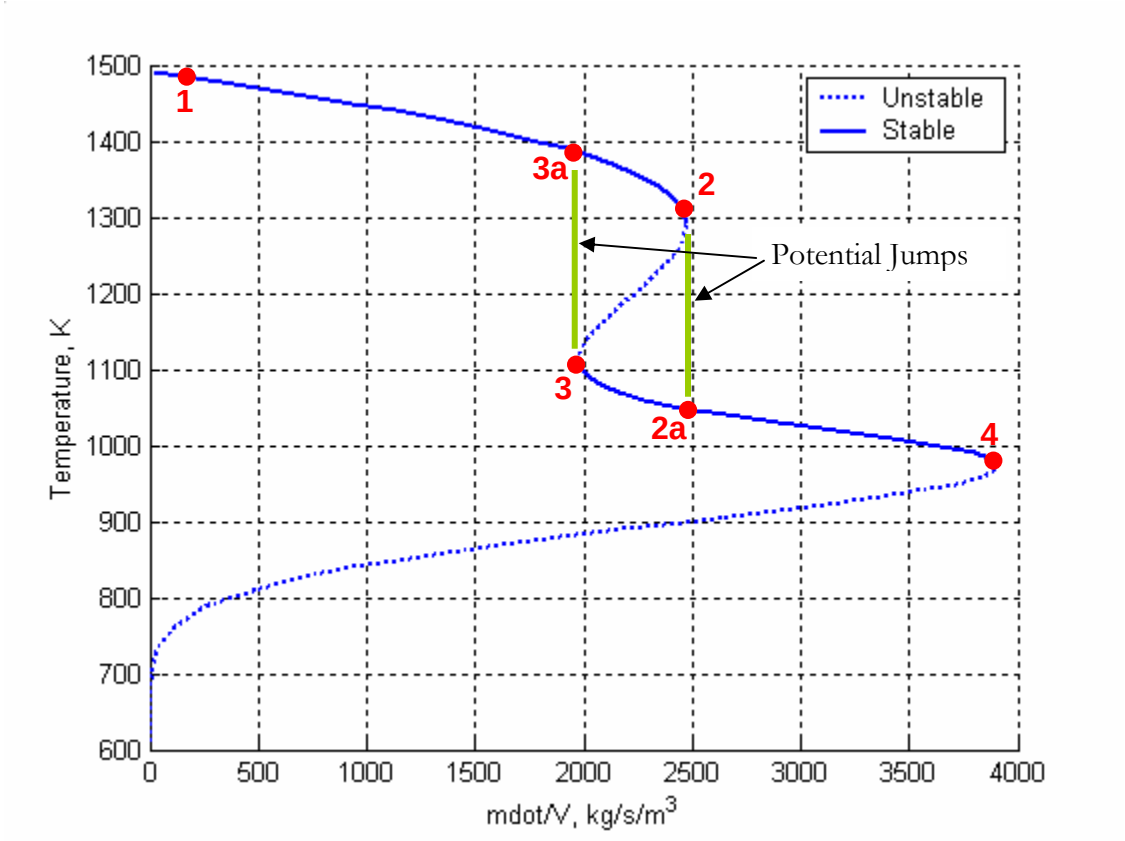

Figure 4.14: Bifurcation diagram showing the possible hysteresis loop in a 2-WSR system, $\alpha = 50\%$, $V_2/V_1 = 2$, $\Phi = 0.7$

If a system operates near the boundary of a stability region, a small perturbation of mass flow (or equivalence ratio) can cause the system to jump from one stability region to another. In certain systems, a small perturbation in mass flow rate can cause the system to jump from one stability region to another repeatedly following a hysteresis loop. This can be seen by examining the bifurcation diagram shown in Figure 4.15. For a sinusoidal perturbation in mass flow as small as 0.2%, the system jumps from one stable equilibrium region to another.

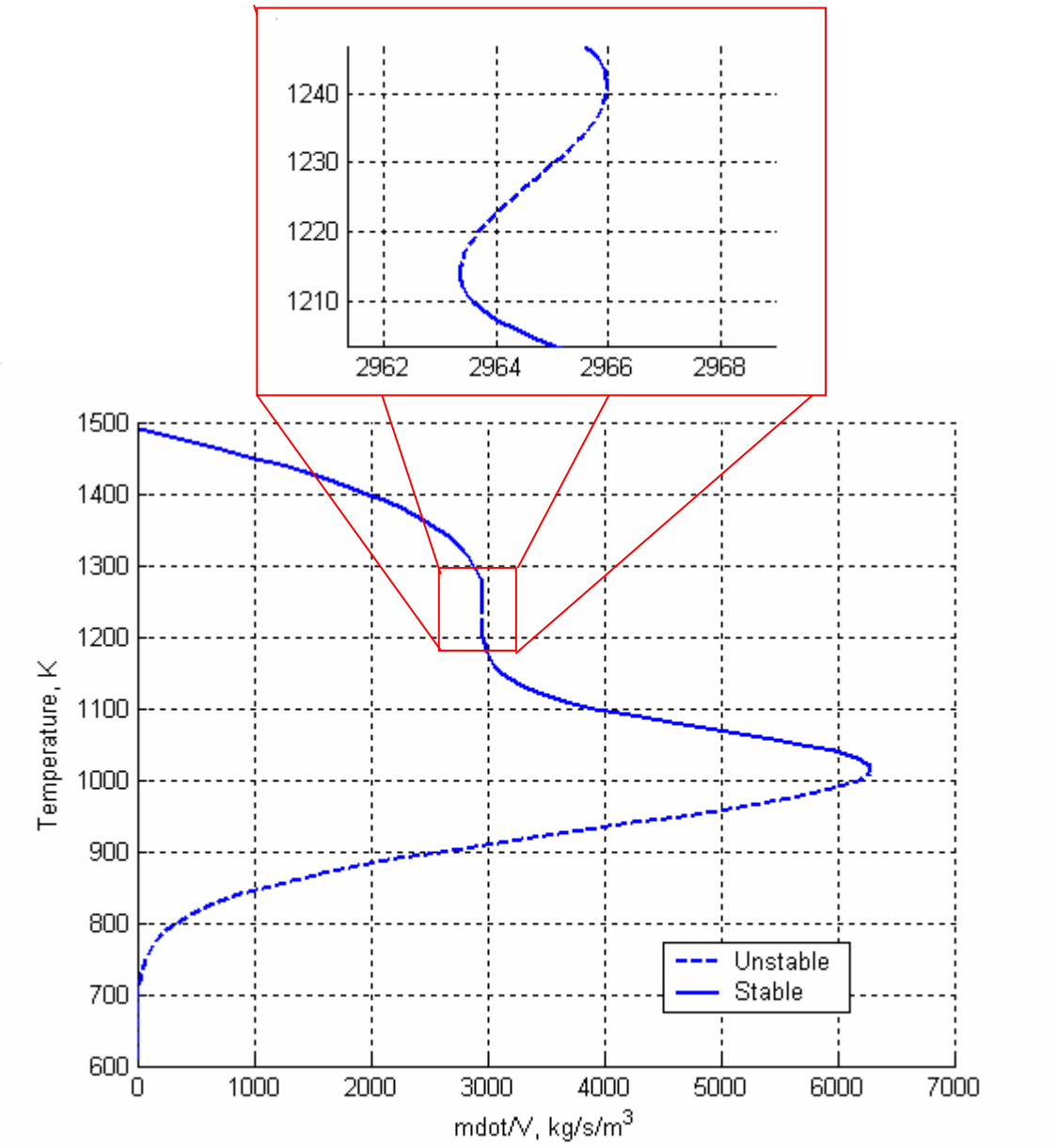

Figure 4.15: Bifurcation diagram of a system with α = 55 %, V_2/V_1 = 3 and Φ = 0.7, inset shows the small region of unstable equilibria

This hysteresis loop can be seen in time simulations of the model by varying the mass flow rate. For two different mean flow rates and a mass flow rate modulation of 0.2%, the input is shown in Figure 4.16; the equilibrium temperatures of the two reactors vary as shown in Figure 4.17. In Figure 4.17, the solid lines represent the system that

corresponds to the input represented by the solid line in Figure 4.16. As can be seen in the figures, if the modulation of the flow remains the same but the mean flow is slightly less (that is, the dotted lines in Figure 4.16 and Figure 4.17), the equilibrium temperatures do not jump from one stability region to another. In Figure 4.17, the jumping of the equilibrium temperatures that occurs (for the system represented by the solid lines) can be thought of as the flame repositioning itself inside the combustor.

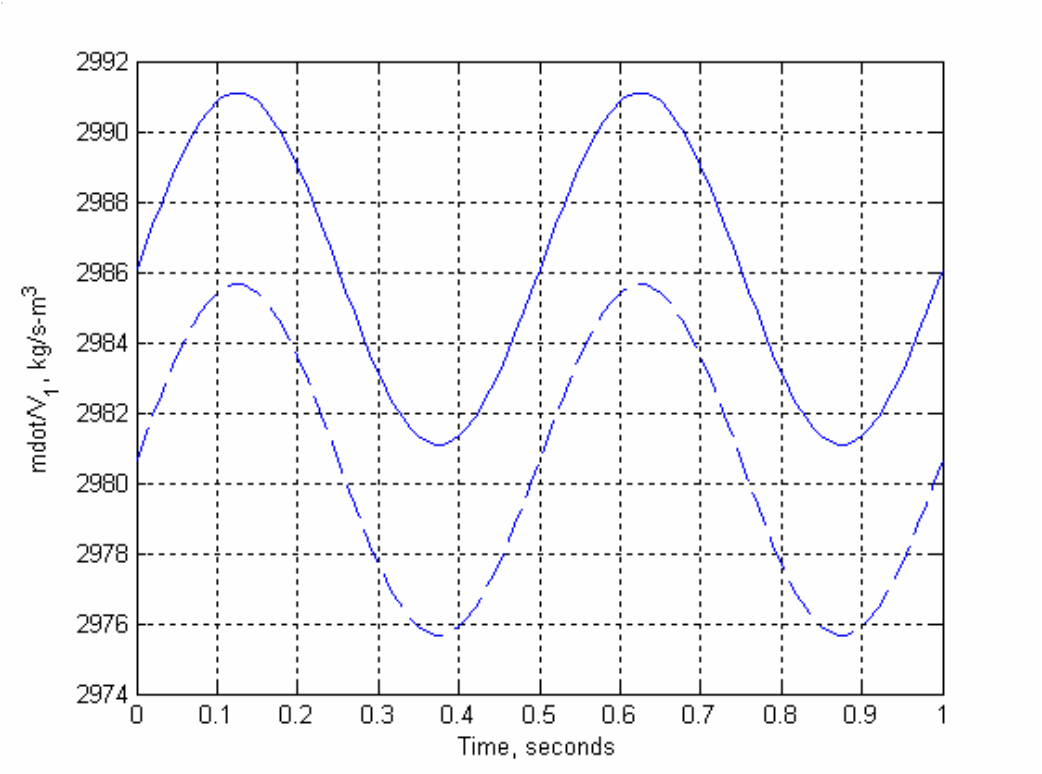

Figure 4.16: Mass flow modulation of 0.2% of the input for time simulation of the two-WSR model.

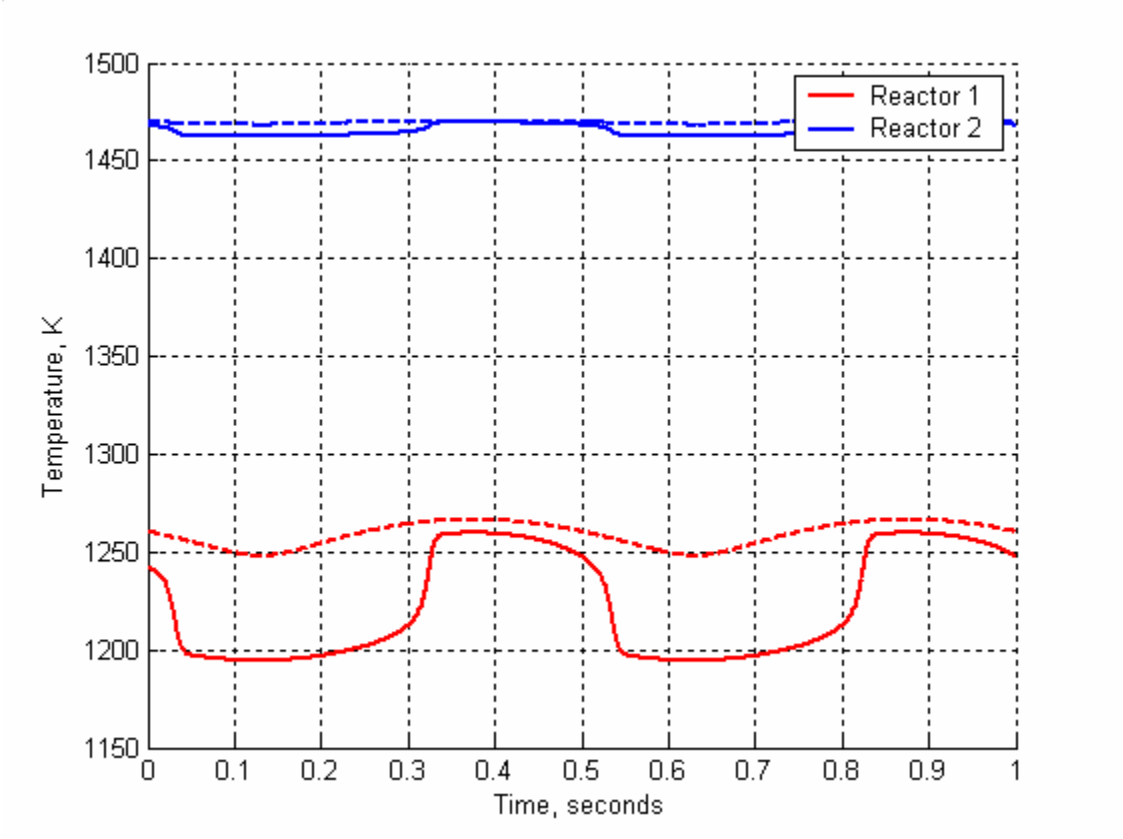

Figure 4.17: Equilibrium temperature response of each of the reactors due to mass flow forcing shown in Figure 4.16.

The bifurcation diagram changes with variations in the amount of recirculation, α, the equivalence ratio, Φ, and the ratio of the volumes of the reactors, V_2/V_1. As the amount of recirculation increases for fixed equivalence ratio and volume ratio, the system behaves like a single WSR, as shown in Figure 4.18.

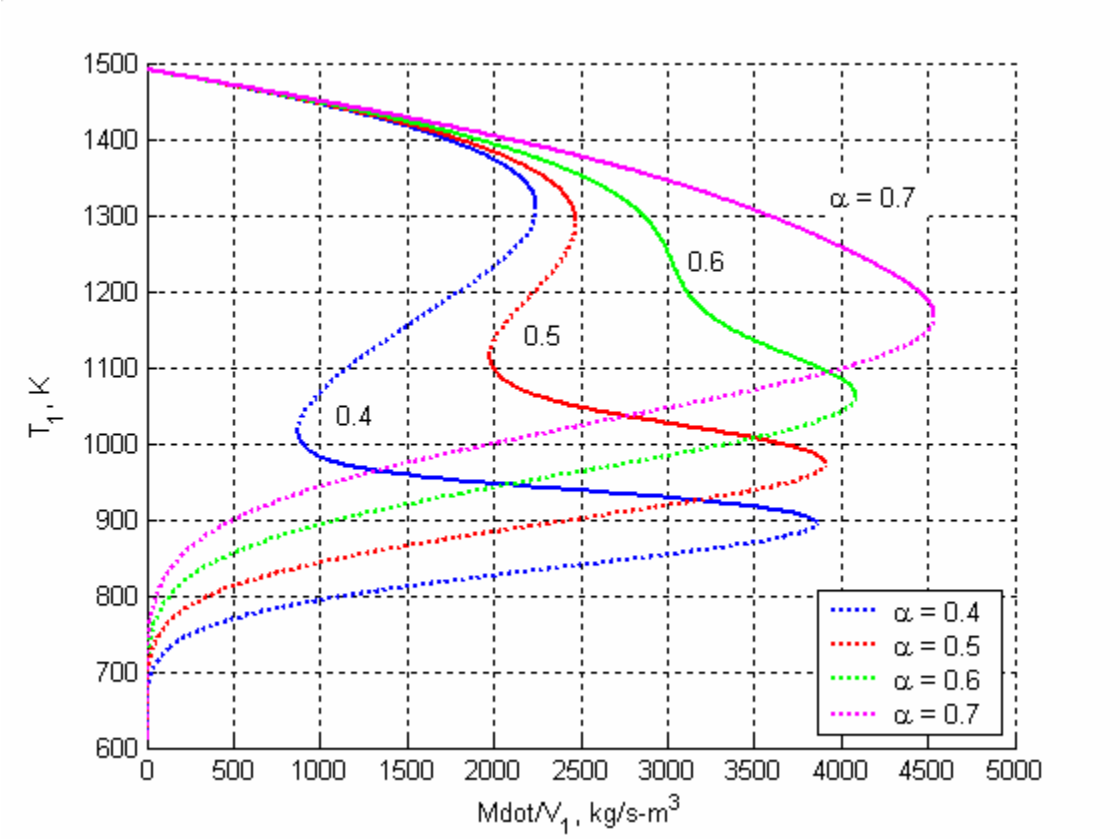

Figure 4.18: Bifurcation diagrams with varying amounts of recirculation, *α*.

The change in the bifurcation diagram as a function of alpha can lead to jumps in the response. Consider a case where there is a steady mass flow of 3000 kg/s-m^3 and the amount of recirculation is 70%. At this operating point, the system behaves like a single WSR. If the amount of recirculation is decreased to 0.5, the system will have to jump down to the lower region of stability in the 0.5 case. This system would then behave like a two WSR system with the first reactor preheating the mixture and the majority of the combustion occurring in the second reactor.

Figure 4.18 also shows that as the amount of recirculation increases, the system bifurcation diagram looks more like the bifurcation diagram for a single WSR reactor case. However, whereas in the single WSR case, a phase shift was observed close to blowout, in the two WSR case, a phase change happens long before blowout. This behavior is shown for $\alpha = 0.7$ as shown in Figure 4.19; the red dot on the graph shows where the phase change occurs.

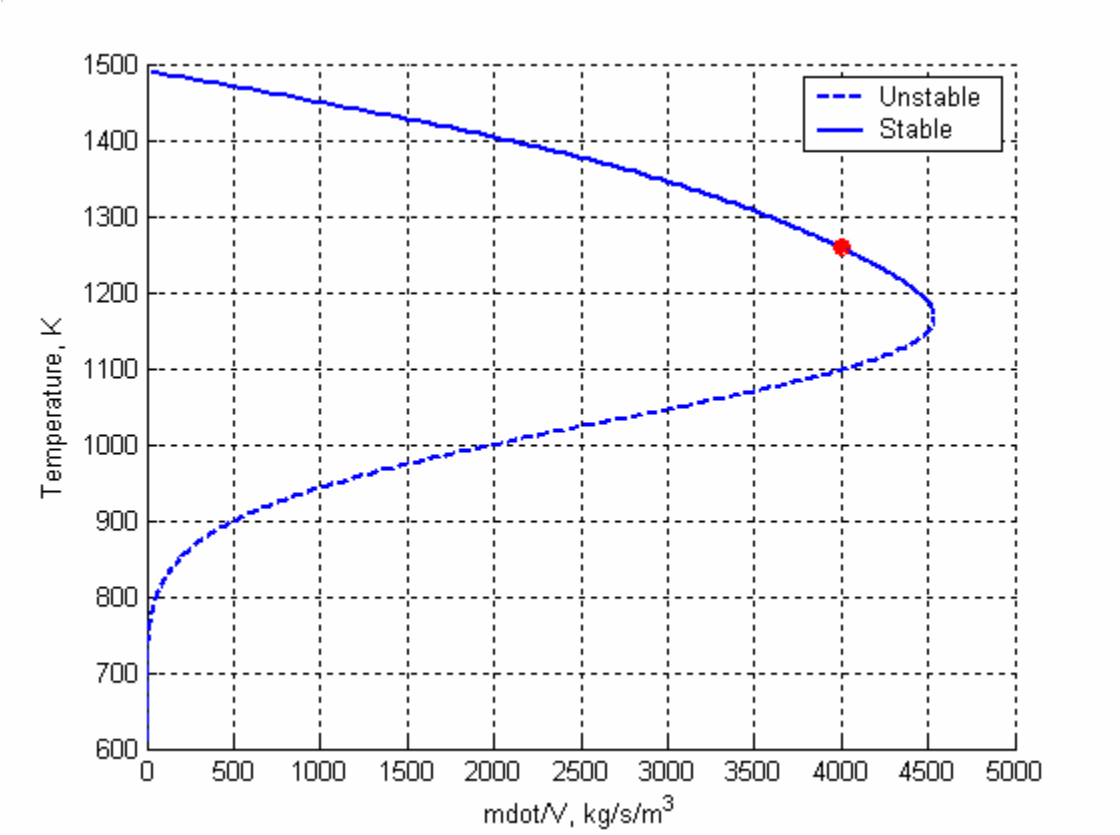

Figure 4.19: Bifurcation diagram for $\alpha = 0.7$ showing an earlier phase transition

Increasing the equivalence ratio extends the graph further down the x-axis ($Mdot/V_1$ axis), as shown in Figure 4.20. A jumping phenomenon similar to the above case can also occur as equivalence ratio is altered. Consider a system in Figure 4.20 at stoichiometric conditions with a mass flow of 10000 kg/s-m^3. If the equivalence ratio is decreased to 0.9, the system will jump from an upper region of stability to a lower region,

changing the system from one where the burning occurred in the first reactor to one in which the burning occurs in the second reactor. If the equivalence ratio is decreased further, eventually the system will blowout.

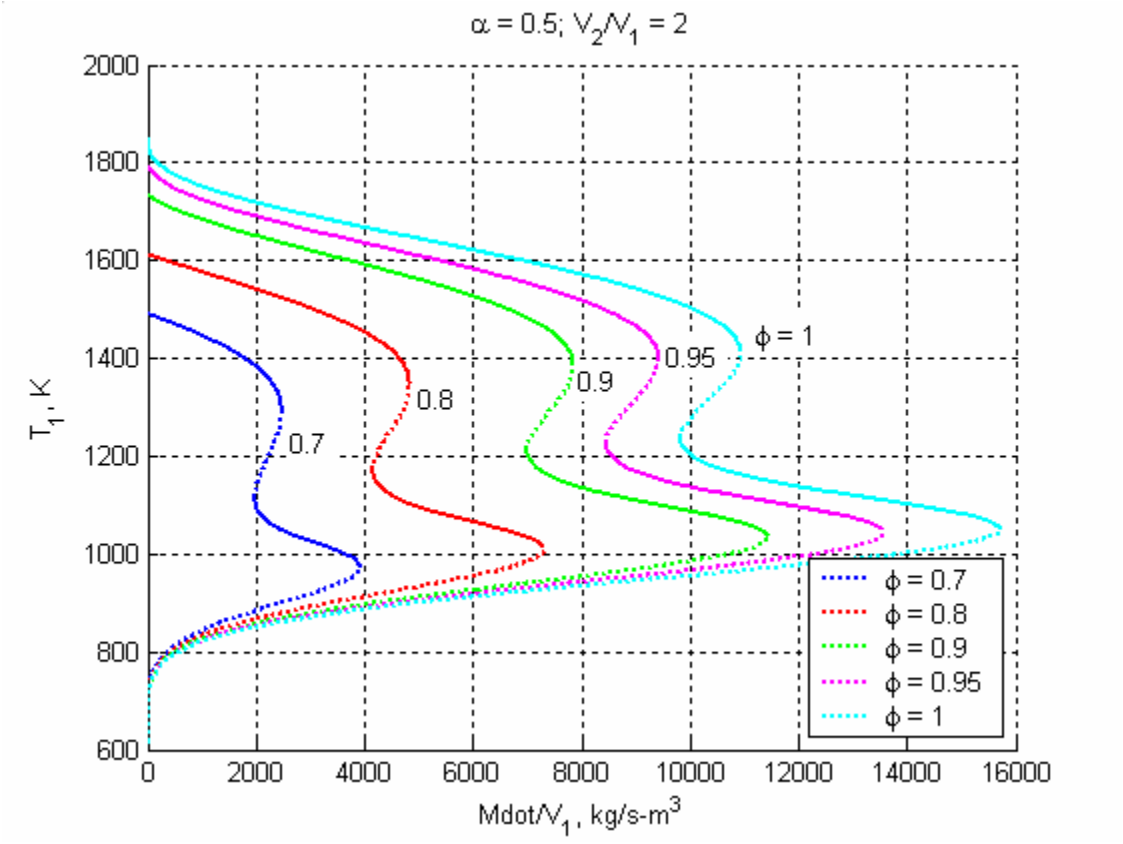

Figure 4.20: Bifurcation diagrams for increasing equivalence ratio, Φ

As the volume ratio, V_2/V_1, decreases the system behaves more like a single WSR, as shown in Figure 4.21. The blowout point of the system decreases with decreasing volume ratio.

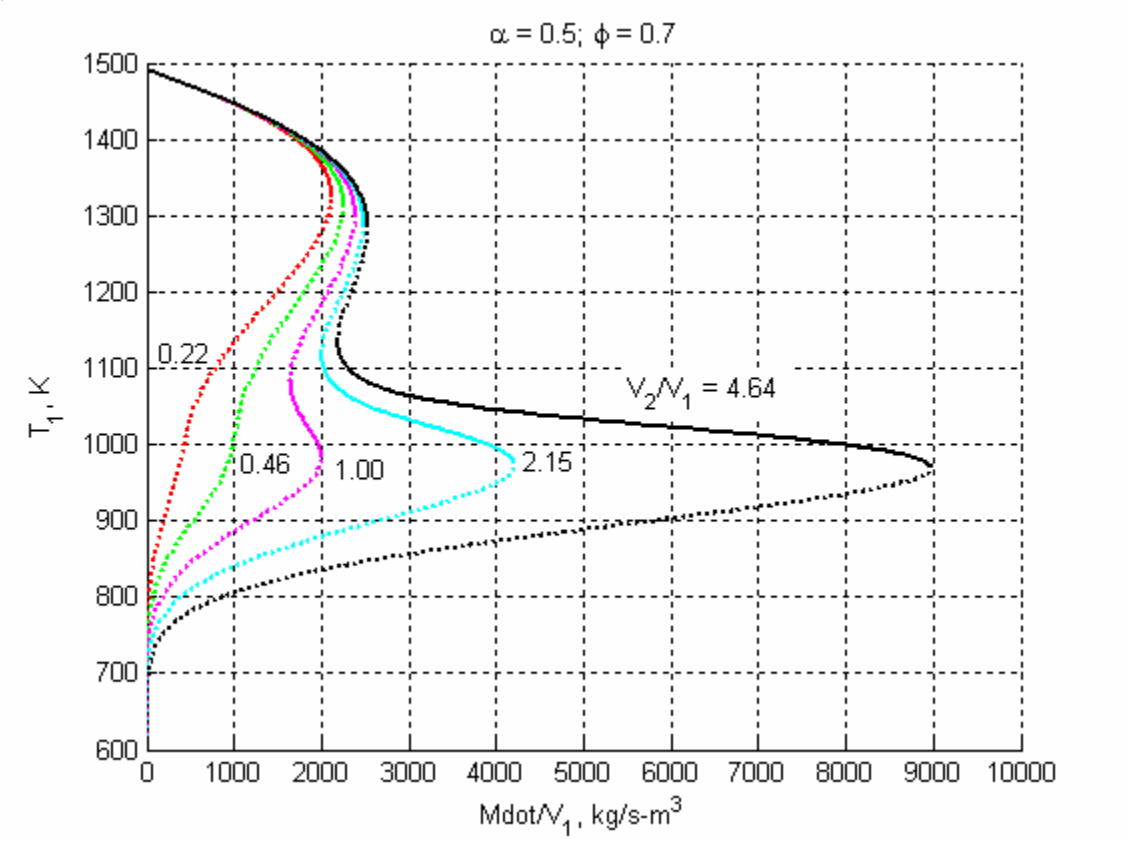

Figure 4.21: Bifurcation diagrams for increasing volume ratio, V_2/V_1

The frequency response plots of the system vary dramatically for different points on the bifurcation diagram. Frequency responses are shown for each of the four points detailed in Figure 4.14. The frequency response of the system at point one is shown in Figure 4.22, and is first order in nature. This response is similar to the response of a single WSR system with no peaking, a gain that falls at -20 dB/decade, and an ultimate phase shift of -90°.

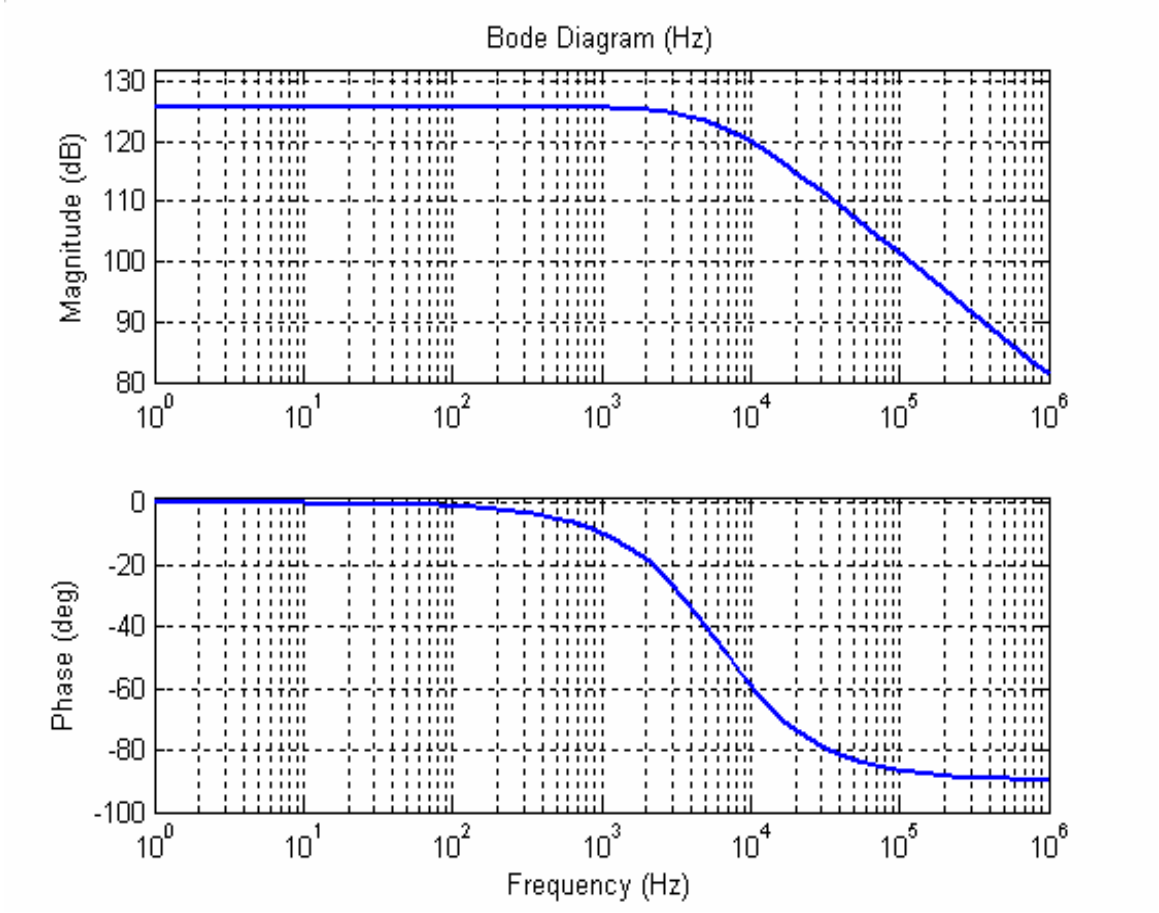

Figure 4.22: Frequency response of system at point 1 in Figure 4.14

The frequency response of the system between points 1 and 2 exhibits this single WSR behavior. However, near point 2, the system frequency response changes dramatically. A portion of the bifurcation diagram is shown in Figure 4.23 showing the section of the diagram near point 2.

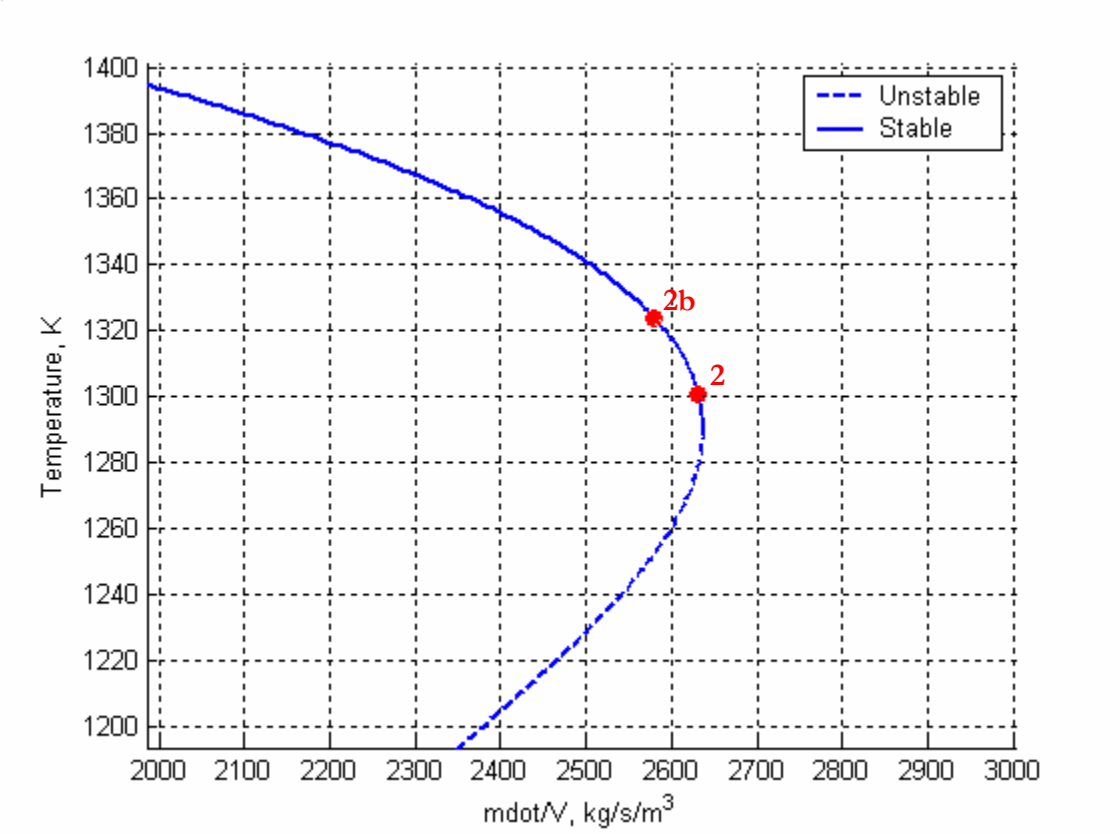

Figure 4.23: Portion of bifurcation diagram shown in Figure 4.14

Near point two, the DC gain begins to decrease, and the system begins to exhibit peaking. A frequency response of the system at point 2b which exhibits this behavior is shown in Figure 4.24. The behavior of the DC gain is similar to the results shown in Park [24]. As the system nears maximum heat release the DC gain begins to decrease as the numerator of the transfer function nears zero. However, in contrast to [24], the system exhibits a peaking phenomenon as the DC gain decreases, which is a result of using multiple WSR's to model the system. As the DC gain transitions from positive to negative, the phase at DC shifts 180 degrees.

It should be noted that while some of the systems shown thus far have exhibited a peaked response, the bandwidths associated with such responses were unrealistically high. This was due to the fundamental WSR assumption of instant mixing. Normally, the entering premixed charge would have to heat up before combusting, however,

because of the instant mixing inside the WSR, the entering reactants instantly mixed and are thus instantly heated up to the equilibrium temperature present in the WSR. This instantaneous elevation in temperature means that the reaction rate of the entering reactants was the hot equilibrium reaction rate, thus the only limiting factor was the reaction rate itself. Eventually, the modulation frequency becomes so high that the system is reaction rate limited and the gain falls off.

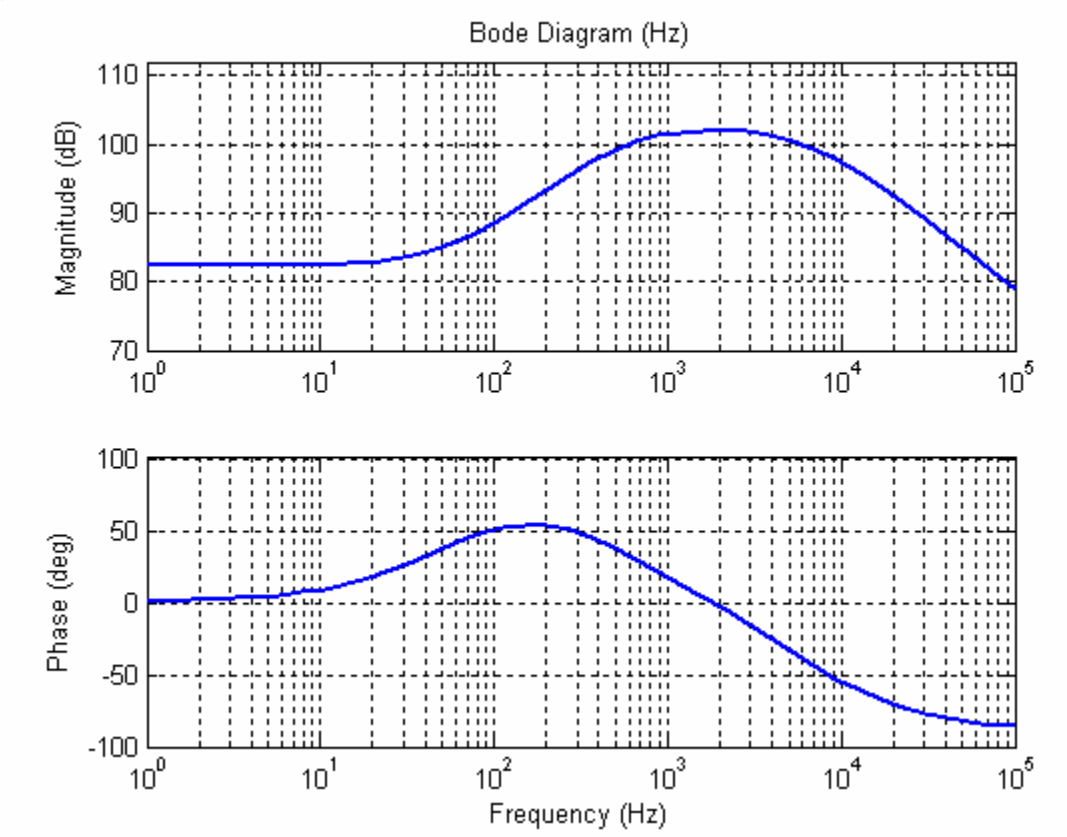

Figure 4.24: Frequency response of 2-WSR system at point 2b from Figure 4.23

The frequency response of the system at point 2 (after the DC gain transition) is shown in Figure 4.25. The system magnitude exhibits a first order response, and the phase starts at 180 degrees and falls to -90 degrees. The extra ninety degrees of phase are due to a zero crossing the axis into the right half plane of the pole-zero map shown in Figure 4.26.

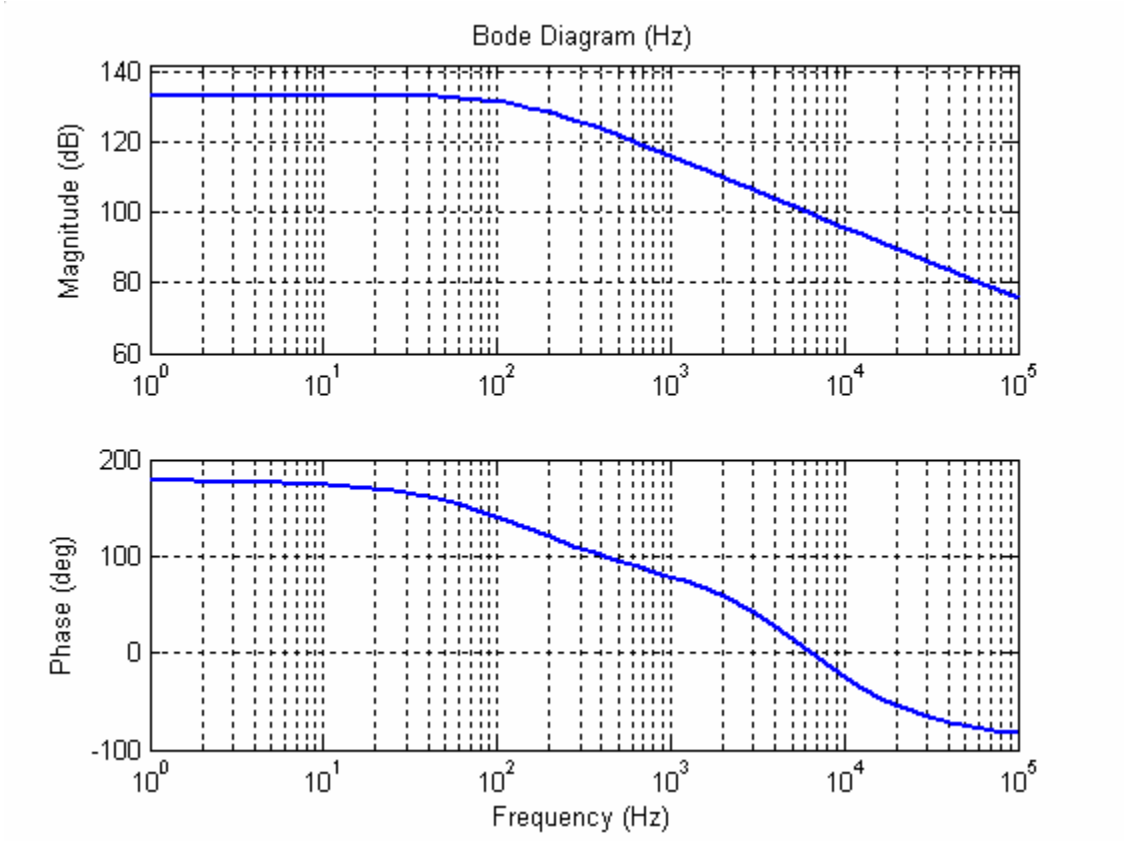

Figure 4.25: Frequency response of system at point 2 in Figure 4.14.

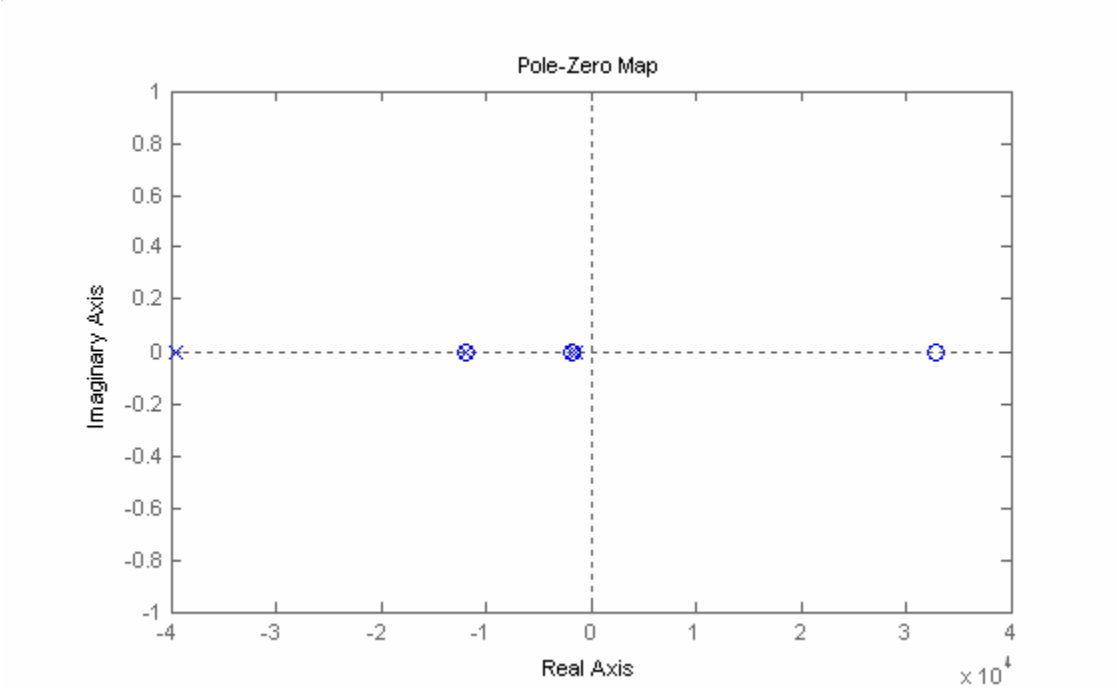

Figure 4.26: Pole-zero map of system at point 2 in Figure 4.14

As considered earlier, if the mass flow rate is increased further from point 2, the system will jump down to point 2a on the lower stability region of the bifurcation diagram. This jump changes the frequency response of the system as well. After the jump the system exhibits a first order response as shown in Figure 4.27. This is frequency response displays the general behavior for the system between points 3 and 4.

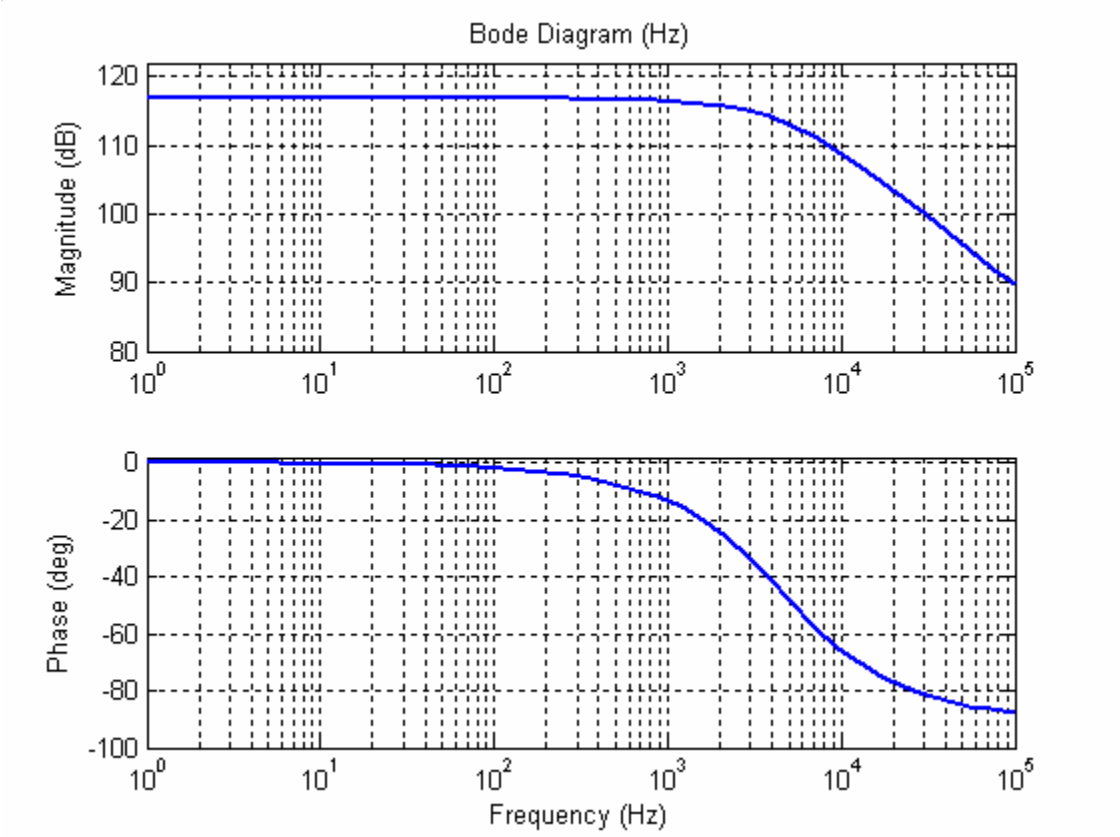

Figure 4.27: Frequency response of system at point 2a in Figure 4.14

Around point 3, the system behaves similar to that of point 2. As the mass flow is decreased towards point 3, the DC gain of the system again decreases until it again changes sign and a 180 degree phase shift is introduced. Also, a zero crosses the axis into the right half plane of the pole-zero map similar to the behavior around point 2. Decreasing the mass flow further from point 3 again results in a jump with dramatic effects. The system jumps to point 3a, which as mentioned before as a first order frequency response as well as being in the upper stability region where the majority of combustion occurs in the first reactor. The frequency response at point 3 does have a few minor differences from point 2 because of the position of the poles and zeros and is shown in Figure 4.28.

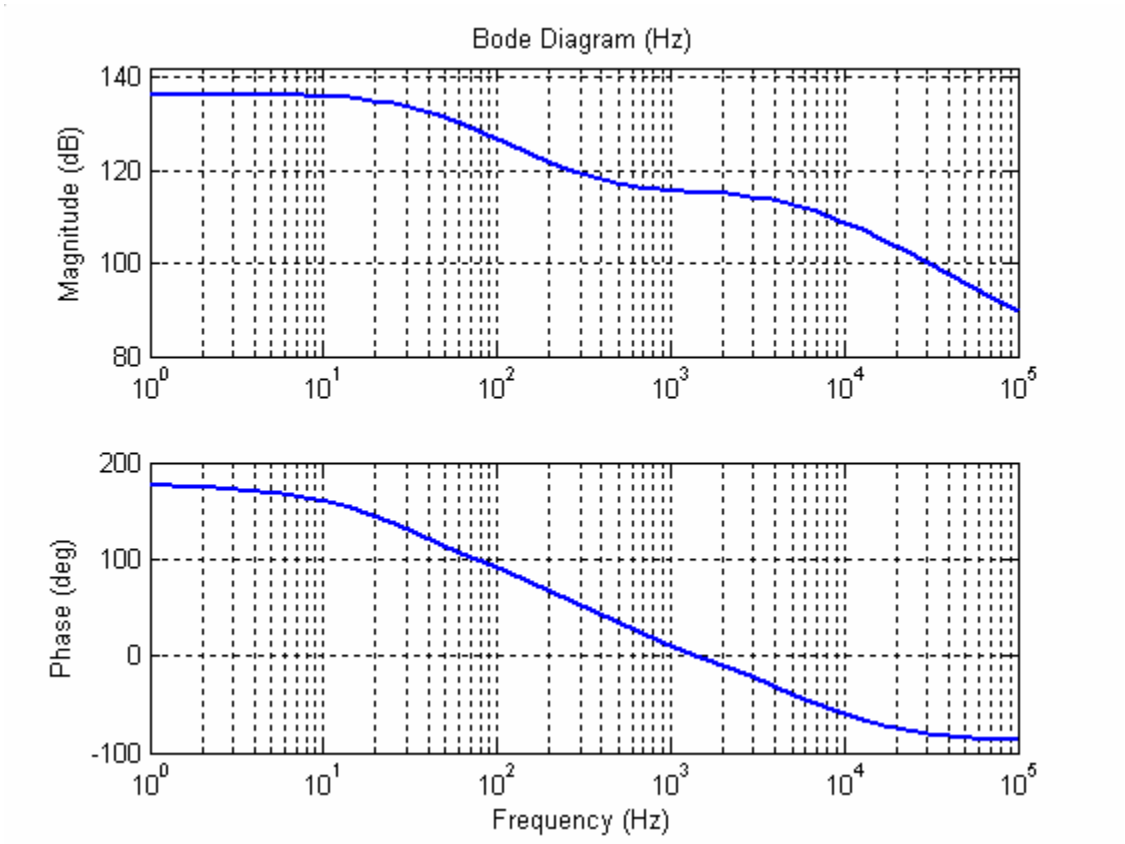

Figure 4.28: Frequency response of system at point 3 in Figure 4.14.

Near point 4, the system exhibits behavior similar to the behavior of points 2 and 3. A portion of the bifurcation diagram near point four is shown in Figure 4.29 for reference.

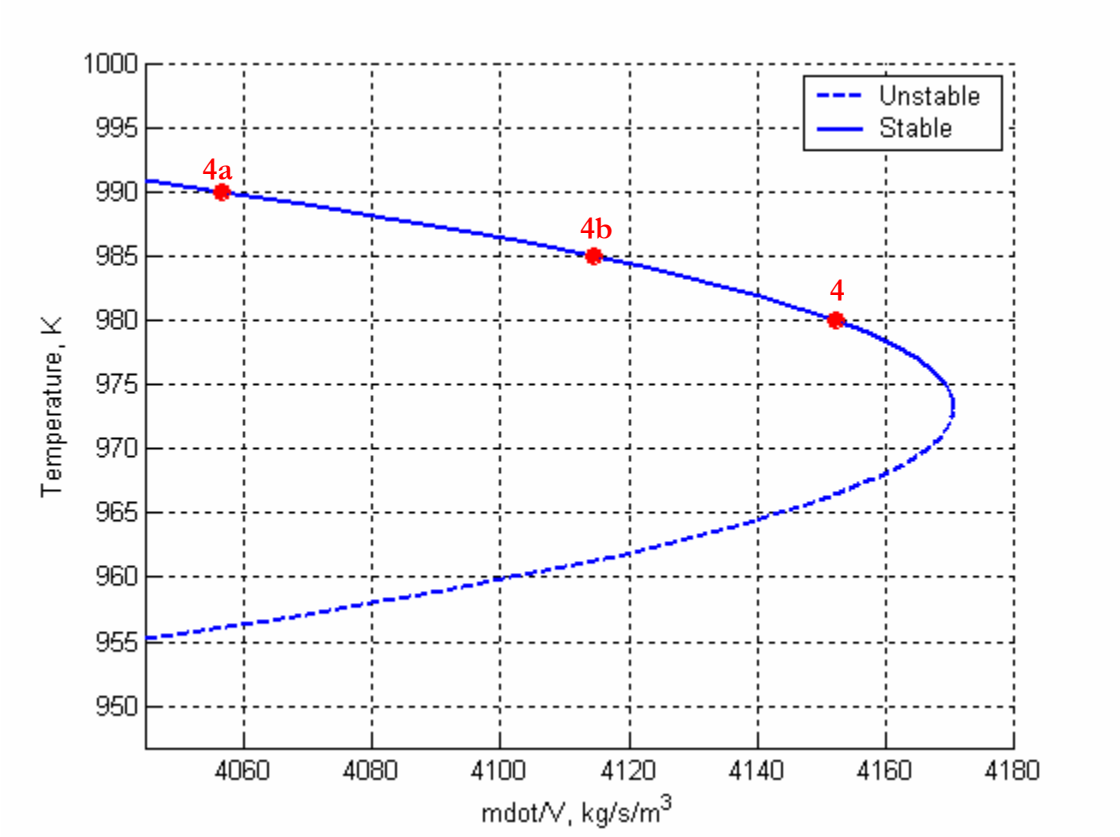

Figure 4.29: Portion of bifurcation diagram shown in Figure 4.14

At point 4a in Figure 4.29, the system frequency response is similar to point 3a; it is a first order response. As the mass flow is increased from point 4a, the system DC gain begins to decrease until it transitions from positive to negative resulting in a 180 degree phase shift. This shift is again accompanied by a zero crossing the axis into the right half plane of the pole zero map. This occurs at point 4b in Figure 4.29. In the region between points 4a and 4b, the system frequency response is similar to that shown in Figure 4.24, with some peaking and a total of 270 degrees of overall phase shift. However, as the mass flow is further increased from point 4b, the zero that moved into the right half plane at 4b wraps around through infinity and reenters the pole-zero map in the left half plane. Near blowout the system exhibits a first order response with just 90 degrees of phase as shown in Figure 4.30. This is similar to the frequency response of a single WSR near blowout and is again similar to the results shown in [24].

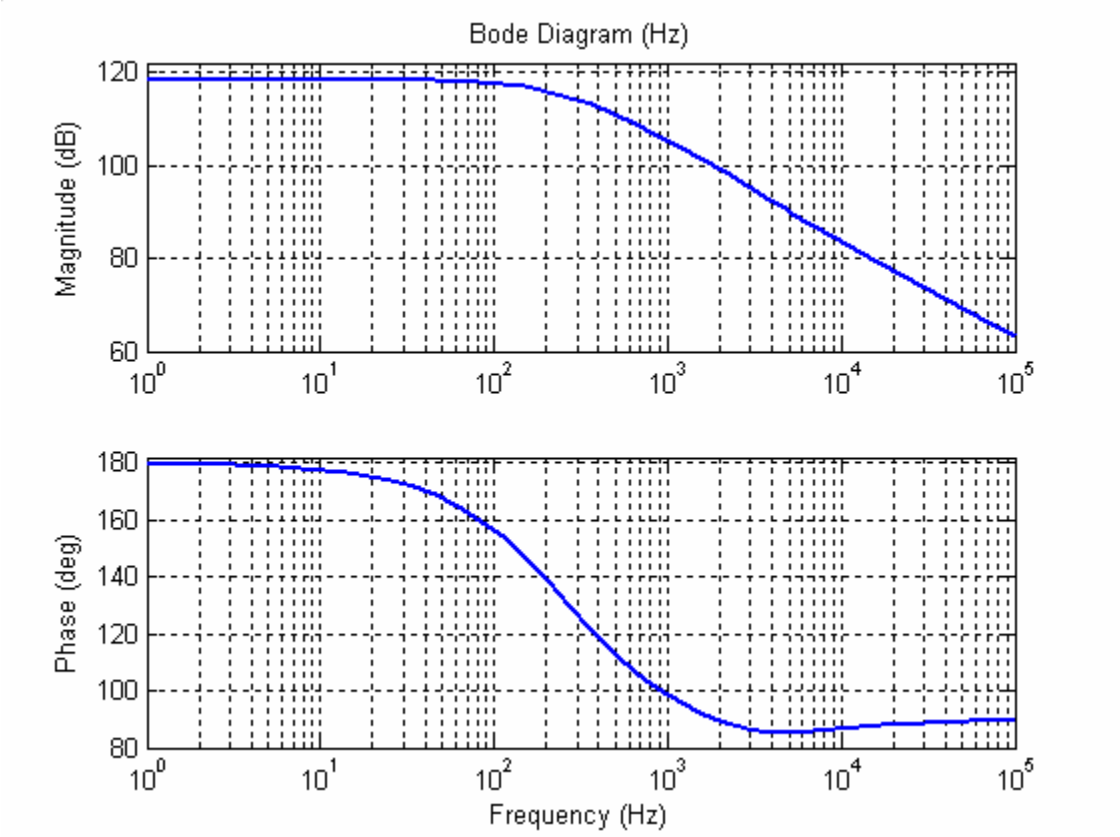

Figure 4.30: Frequency response of system at point 4 in Figure 4.14.

4.4 Three Coupled Well-stirred Reactor System

To determine if adding reactors to the 2-WSR case will produce any new information, three well-stirred reactors were coupled by recirculation as shown in Figure 4.31.

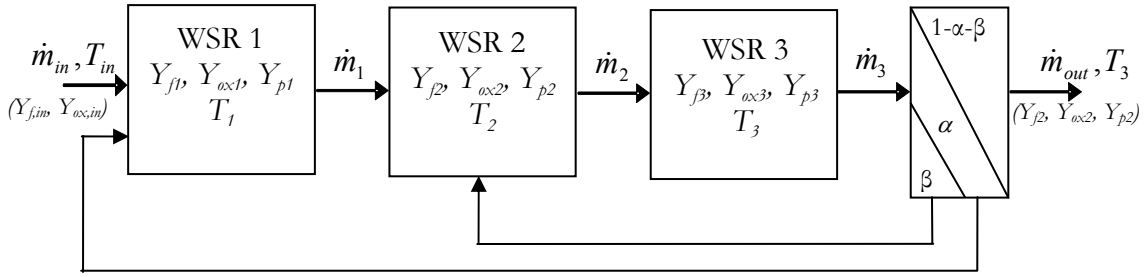

Figure 4.31: Block diagram of three well-stirred reactors coupled by recirculation

4.4.1 Derivation of Equations

The derivation of the linearized equations follows the same procedure applied in Section 4.3. To derive the equations for this system, first note that a mass flow balance requires

$$\dot{m}_1 = \dot{m}_{in} + \alpha \dot{m}_3 \tag{4-60}$$

and that

$$\dot{m}_2 = \dot{m}_1 + \beta \dot{m}_3 = \dot{m}_3 \tag{4-61}$$

In reactor 1, mass conservation of fuel requires that

$$\rho_1 V_1 \dot{Y}_{f1} = \dot{m}_{in} Y_{f,in} + \alpha \dot{m}_3 Y_{f3} - \dot{m}_1 Y_{f1} - \dot{\omega}_{f1} V_1 \tag{4-62}$$

and a similar equation holds for the oxidizer. An energy balance of the first reactor requires that

$$\rho_1 V_1 c_p \dot{T}_1 = \dot{m}_{in} c_p T_{in} + \alpha \dot{m}_3 c_p T_3 - \dot{m}_1 c_p T_1 + \dot{\omega}_{f1} V_1 \Delta h_r \,.$$

(4-63)

Equations derived for the second reactor are similar to the first reactor, with an input consisting of the output of reactor one (Y_{f1}, Y_{ox1}, T_1) and a percentage, β, of the output of reactor three (Y_{f3}, Y_{ox3}, T_3), with a mass flow rate of $\dot{m}_{in}(t)/(1-\alpha-\beta)$. The third reactor has equations with an input consisting of the output of the second reactor, (Y_{f2}, Y_{ox2}, T_2), with a mass flow rate of $\dot{m}_{in}(t)/(1-\alpha-\beta)$. The equations for the entire system are given by

$$\dot{Y}_{f1}(t) = \frac{1}{\rho_1}\left(\frac{\dot{m}_{in}(t)}{V_1}\left(Y_{f,in} + \frac{\alpha}{1-\alpha-\beta}Y_{f3}(t) - \frac{1-\beta}{1-\alpha-\beta}Y_{f1}(t)\right) - \dot{\omega}_{f1}(t)\right)$$

(4-64)

$$\dot{Y}_{ox1}(t) = \frac{1}{\rho_1}\left(\frac{\dot{m}_{in}(t)}{V_1}\left(Y_{ox,in} + \frac{\alpha}{1-\alpha-\beta}Y_{ox2}(t) - \frac{1-\beta}{1-\alpha-\beta}Y_{ox1}(t)\right) - \dot{\omega}_{f1}(t) aMW_{ox}/MW_f\right)$$

(4-65)

$$\dot{T}_1(t) = \frac{1}{\rho_1}\left(\frac{\dot{m}_{in}(t)}{V_1}(T_{in} + \frac{\alpha}{1-\alpha-\beta}T_2(t) - \frac{1-\beta}{1-\alpha-\beta}T_1(t)) + \dot{\omega}_{f1}(t)\frac{\Delta h_r}{c_p}\right)$$

(4-66)

$$\dot{Y}_{f2}(t) = \frac{1}{\rho_2}\left(\frac{\dot{m}_{in}(t)}{V_2(1-\alpha-\beta)}\left((1-\beta)Y_{f1}(t) + \beta Y_{f3}(t) - Y_{f2}(t)\right) - \dot{\omega}_{f2}(t)\right)$$

(4-67)

$$\dot{Y}_{ox2}(t) = \frac{1}{\rho_2}\left(\frac{\dot{m}_{in}(t)}{V_2(1-\alpha-\beta)}\left((1-\beta)Y_{ox1}(t) + \beta Y_{ox3}(t) - Y_{ox2}(t)\right) - \dot{\omega}_{f2}(t) aMW_{ox}/MW_f\right)$$

(4-68)

$$\dot{T}_2(t) = \frac{1}{\rho_2}\left(\frac{\dot{m}_{in}(t)}{V_2(1-\alpha-\beta)}((1-\beta)T_1(t) + \beta T_3(t) - T_2(t)) + \dot{\omega}_{f2}(t)\frac{\Delta h_r}{c_p}\right)$$

(4-69)

$$\dot{Y}_{f3}(t) = \frac{1}{\rho_3}\left(\frac{\dot{m}_{in}(t)}{V_3(1-\alpha-\beta)}\left(Y_{f2}(t) - Y_{f3}(t)\right) - \dot{\omega}_{f3}(t)\right)$$

(4-70)

$$\dot{Y}_{ox3}(t) = \frac{1}{\rho_3}\left(\frac{\dot{m}_{in}(t)}{V_3(1-\alpha-\beta)}\left(Y_{ox2}(t) - Y_{ox3}(t)\right) - \dot{\omega}_{f3}(t) a MW_{ox} / MW_f \right)$$

(4-71)

$$\dot{T}_3(t) = \frac{1}{\rho_3}\left(\frac{\dot{m}_{in}(t)}{V_3(1-\alpha-\beta)}(T_2(t) - T_3(t)) + \dot{\omega}_{f3}(t)\frac{\Delta h_r}{c_p} \right)$$

(4-72)

4.4.2 Reducing the equations

Following the procedure detailed in the first two cases, these equations can be reduced to just three. Again define

$$x_i = [Y_{fi} \quad Y_{oxi} \quad T_i]^T .$$

(4-73)

Then we can write the above equations as

$$\dot{x}_1(t) = \frac{1}{\rho_1}\left(\frac{\dot{m}_{in}(t)}{V_1}\left(x_{in} + \frac{\alpha}{1-\alpha-\beta}x_3(t) - \frac{1-\beta}{1-\alpha-\beta}x_1(t) \right) - \dot{\omega}_{f1}(t)\begin{bmatrix} 1 \\ aMW_{ox}/MW_f \\ -\Delta h_r / c_p \end{bmatrix} \right)$$

(4-74)

$$\dot{x}_2(t) = \frac{1}{\rho_2}\left(\frac{\dot{m}_{in}(t)}{V_2(1-\alpha-\beta)}\left((1-\beta)x_1(t) + \beta x_3(t) - x_2(t)\right) - \dot{\omega}_{f2}(t)\begin{bmatrix} 1 \\ aMW_{ox}/MW_f \\ -\Delta h_r / c_p \end{bmatrix} \right)$$

(4-75)

$$\dot{x}_3(t) = \frac{1}{\rho_3}\left(\frac{\dot{m}_{in}(t)}{V_3(1-\alpha-\beta)}\left(x_2(t) - x_3(t)\right) - \dot{\omega}_{f3}(t)\begin{bmatrix} 1 \\ aMW_{ox}/MW_f \\ -\Delta h_r / c_p \end{bmatrix} \right)$$

(4-76)

Using the same transformation as before gives

$$\dot{z}_1(t) = \frac{1}{\rho_1}\left(\frac{\dot{m}_{in}(t)}{V_1}\left(z_{in} + \frac{\alpha}{1-\alpha-\beta} z_3(t) - \frac{1-\beta}{1-\alpha-\beta} z_1(t) \right) - \dot{\omega}_{f1}(t) \begin{bmatrix} 0 \\ 0 \\ -\Delta h_r / c_p \end{bmatrix} \right)$$

(4-77)

$$\dot{z}_2(t) = \frac{1}{\rho_2}\left(\frac{\dot{m}_{in}(t)}{V_2(1-\alpha-\beta)}\left((1-\beta) z_1(t) + \beta z_3(t) - z_2(t)\right) - \dot{\omega}_{f2}(t) \begin{bmatrix} 0 \\ 0 \\ -\Delta h_r / c_p \end{bmatrix} \right)$$

(4-78)

$$\dot{z}_3(t) = \frac{1}{\rho_3}\left(\frac{\dot{m}_{in}(t)}{V_3(1-\alpha-\beta)}\left(z_2(t) - z_3(t)\right) - \dot{\omega}_{f3}(t) \begin{bmatrix} 0 \\ 0 \\ -\Delta h_r / c_p \end{bmatrix} \right)$$

(4-79)

It can be seen that the first two components in each of the above equations evolve independently of the third components, although as before the first and second components of each equation are linked to one another. As before the equations for the first and second components are asymptotically stable and converge to the equilibrium point

$$\begin{bmatrix} z_{11}(t) \\ z_{21}(t) \\ z_{31}(t) \end{bmatrix} = \begin{bmatrix} z_{in,1} \\ z_{in,1} \\ z_{in,1} \end{bmatrix}$$

(4-80)

Considering both sets of equations, the components $z_{11}, z_{21}, z_{31}, z_{12}, z_{32}$ converge to an equilibrium point and, in terms of the original variables, the following algebraic relationships result:

$$\begin{bmatrix} -(aMW_{ox}/MW_f)Y_{f1}+Y_{ox1} \\ (\Delta h_r/c_p)Y_{f1}+T_1 \\ -(aMW_{ox}/MW_f)Y_{f2}+Y_{ox2} \\ (\Delta h_r/c_p)Y_{f2}+T_2 \\ -(aMW_{ox}/MW_f)Y_{f3}+Y_{ox3} \\ (\Delta h_r/c_p)Y_{f3}+T \end{bmatrix} = \begin{bmatrix} -(aMW_{ox}/MW_f)Y_{f,in}+Y_{ox,in} \\ (\Delta h_r/c_p)Y_{f,in}+T_{in} \\ -(aMW_{ox}/MW_f)Y_{f,in}+Y_{ox,in} \\ (\Delta h_r/c_p)Y_{f,in}+T_{in} \\ -(aMW_{ox}/MW_f)Y_{f,in}+Y_{ox,in} \\ (\Delta h_r/c_p)Y_{f,in}+T_{in} \end{bmatrix} \tag{4-81}$$

The remaining dynamic equations are given by

$$\dot{T}_1(t) = \frac{1}{\rho_1}\left(\frac{\dot{m}_{in}(t)}{V_1}(T_{in} + \frac{\alpha}{1-\alpha-\beta}T_2(t) - \frac{1-\beta}{1-\alpha-\beta}T_1(t)) + \dot{\omega}_{f1}(t)\frac{\Delta h_r}{c_p}\right) \tag{4-82}$$

$$\dot{T}_2(t) = \frac{1}{\rho_2}\left(\frac{\dot{m}_{in}(t)}{V_2(1-\alpha-\beta)}((1-\beta)T_1(t) + \beta T_3(t) - T_2(t)) + \dot{\omega}_{f2}(t)\frac{\Delta h_r}{c_p}\right) \tag{4-83}$$

$$\dot{T}_3(t) = \frac{1}{\rho_3}\left(\frac{\dot{m}_{in}(t)}{V_3(1-\alpha-\beta)}(T_2(t) - T_3(t)) + \dot{\omega}_{f3}(t)\frac{\Delta h_r}{c_p}\right) \tag{4-84}$$

with the total heat release rate given by

$$\dot{Q}_r = \Delta h_r(\dot{\omega}_{f1} + \dot{\omega}_{f2} + \dot{\omega}_{f3}) \tag{4-85}$$

4.4.3 Linearization of Nonlinear Equations

To find the possible equilibrium points of the system it is easiest to pick values for T_1, T_2, and T_3 then solve for the required values of $\dot{m}(t)/V_1$ and the volume ratios V_2/V_1 and V_3/V_1. This approach will produce all possible equilibrium points for this

configuration of WSR's. The linearization of the above equations about an equilibrium point proceeds analogously to the single WSR case and results in

$$\dot{T}_1' = \frac{1}{\rho_1}\left(\begin{array}{l} \dfrac{\dot{m}_{eq}}{V_1(1-\alpha-\beta)}\left(\alpha T_3'(t) - (1-\beta)T_1'(t)\right) + \nabla\dot{\omega}_{f1,eq}\begin{bmatrix} -1 \\ \dfrac{-aMW_{ox}}{MW_f} \\ \Delta h_r / c_p \end{bmatrix} T_1'(t) \\ \\ + \dfrac{\dot{m}'(t)}{V_1}\left(T_{in} + \dfrac{\alpha}{1-\alpha-\beta}T_{3,eq} - \dfrac{1-\beta}{1-\alpha-\beta}T_{1,eq} \right) \end{array} \right) \tag{4-86}$$

$$\dot{T}_2' = \frac{1}{\rho_2}\left(\begin{array}{l} \dfrac{\dot{m}_{eq}}{V_2(1-\alpha-\beta)}\left((1-\beta)T_1'(t) + \beta T_3'(t) - T_2'(t)\right) + \nabla\dot{\omega}_{f2,eq}\begin{bmatrix} -1 \\ \dfrac{-aMW_{ox}}{MW_f} \\ \Delta h_r / c_p \end{bmatrix} T_2'(t) \\ \\ + \dfrac{\dot{m}'(t)}{V_2(1-\alpha-\beta)}\left((1-\beta)T_{1,eq} + \beta T_{3,eq} - T_{2,eq}\right) \end{array} \right) \tag{4-87}$$

$$\dot{T}_3' = \frac{1}{\rho_3}\left(\begin{array}{l} \dfrac{\dot{m}_{eq}}{V_3(1-\alpha-\beta)}\left(T_2'(t) - T_3'(t)\right) + \nabla\dot{\omega}_{f3,eq}\begin{bmatrix} -1 \\ \dfrac{-aMW_{ox}}{MW_f} \\ \Delta h_r / c_p \end{bmatrix} T_3'(t) \\ \\ + \dfrac{\dot{m}'(t)}{V_3(1-\alpha-\beta)}\left(T_{2,eq} - T_{3,eq}\right) \end{array} \right) \tag{4-88}$$

The linearization of the output equation is

$$\dot{Q}_r' = \nabla\dot{\omega}_{f1,eq}\begin{bmatrix} -c_p \\ \dfrac{-ac_pMW_{ox}}{MW_f} \\ \Delta h_r \end{bmatrix} T_1'(t) + \nabla\dot{\omega}_{f2,eq}\begin{bmatrix} -c_p \\ \dfrac{-ac_pMW_{ox}}{MW_f} \\ \Delta h_r \end{bmatrix} T_2'(t) + \nabla\dot{\omega}_{f3,eq}\begin{bmatrix} -c_p \\ \dfrac{-ac_pMW_{ox}}{MW_f} \\ \Delta h_r \end{bmatrix} T_3'(t) \tag{4-89}$$

4.4.4 Results

A map of the stability regions (analogous to the stability map for the 2-WSR case shown in Figure 4.10) is shown in Figure 4.32. As in the 2-WSR case, as the amount of recirculation if increased, the stability regions of the stability map begin to mesh together as shown in the series of figures: Figure 4.32, Figure 4.33 and Figure 4.34.

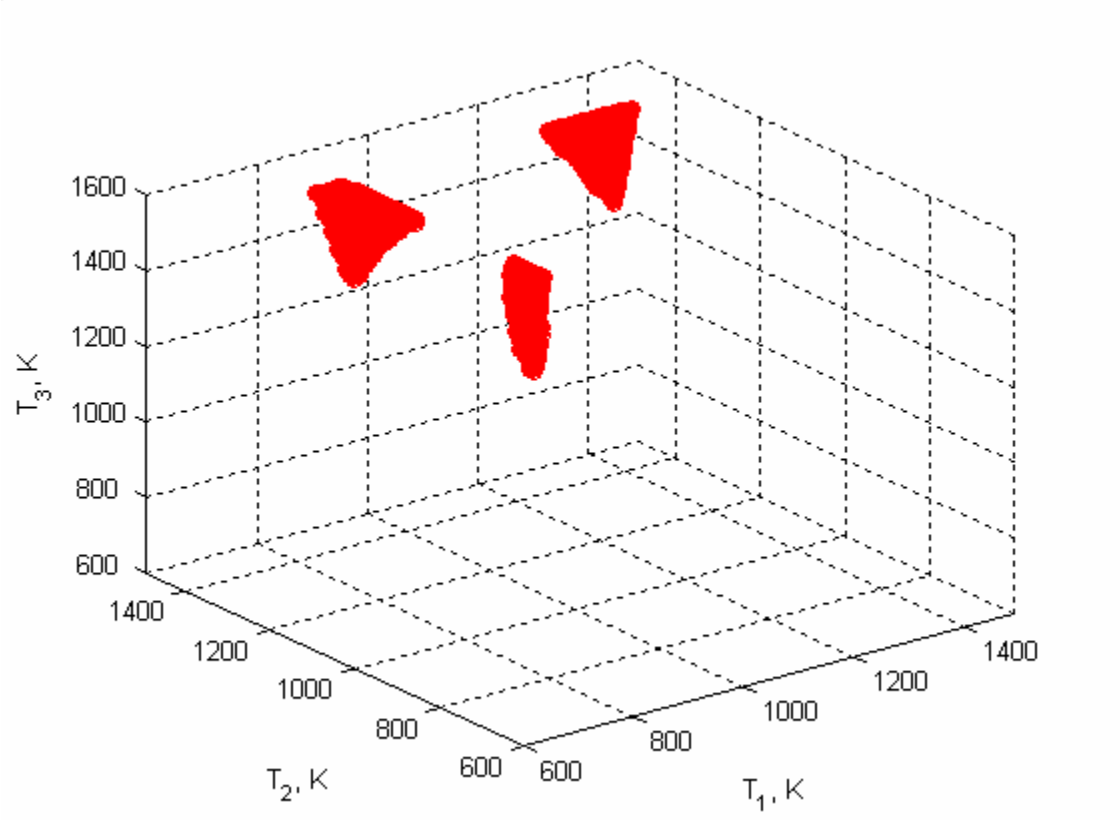

Figure 4.32: Stability map of a coupled 3-WSR system; Φ = 0.7, α = 30 %, β = 10 %

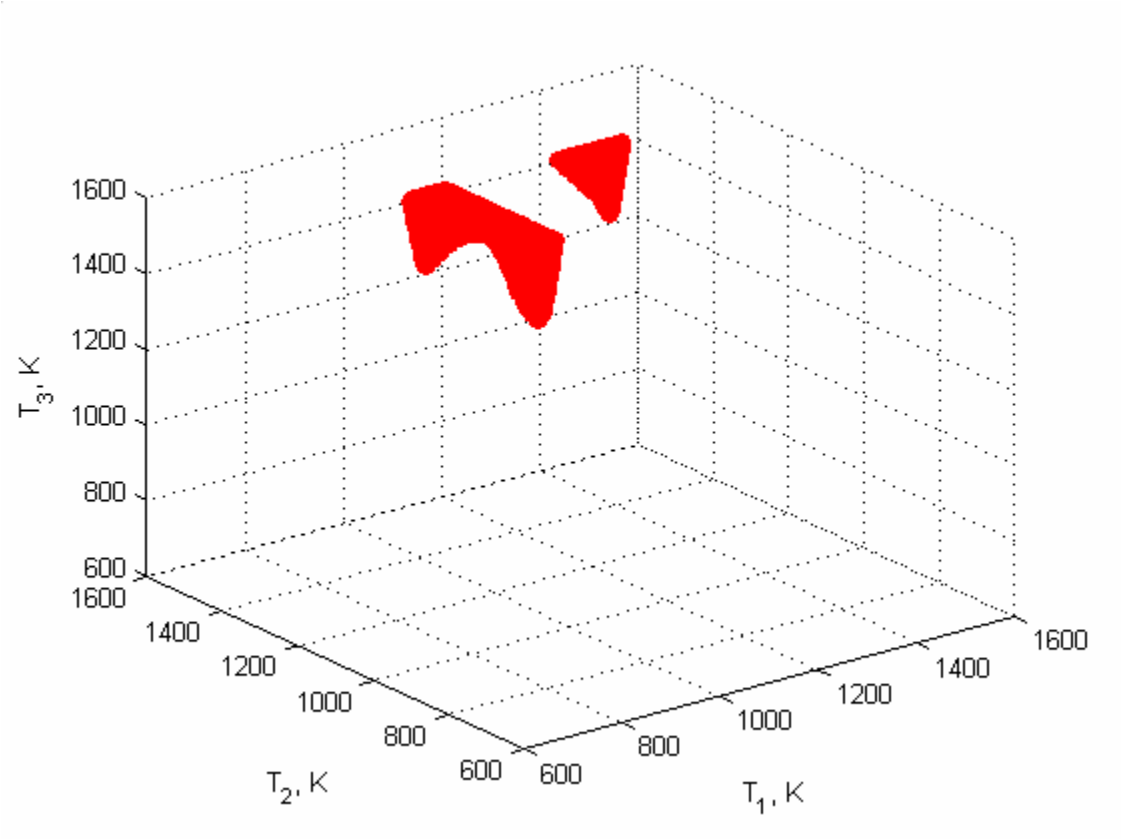

Figure 4.33: Stability map of a coupled 3-WSR system; Φ = 0.7, α = 40 %, β = 20 %

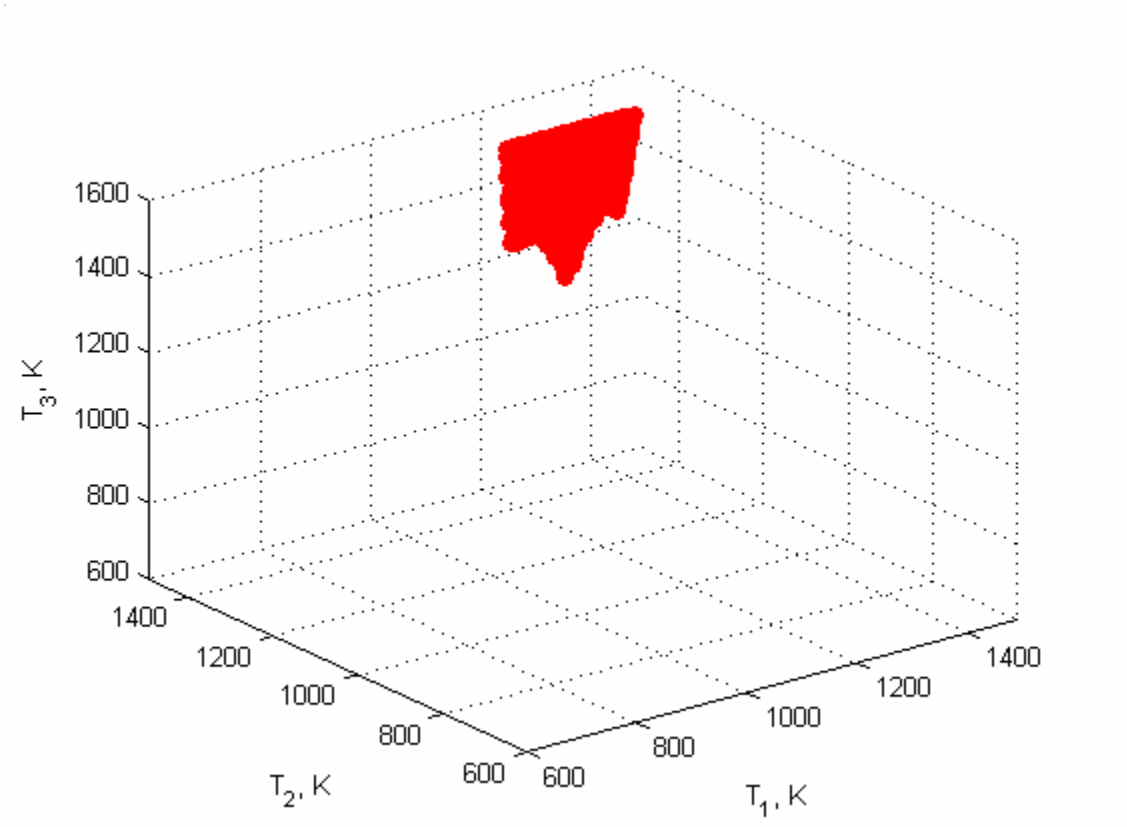

Figure 4.34: Stability map of a coupled 3-WSR system; Φ = 0.7, α = 50 %, β = 30 %

The bifurcation diagram for a coupled 3-WSR system can take on three different shapes. The first resembles that of a single WSR and is shown in Figure 4.35. In this case no jumps or hysteresis are possible. The dynamics of the system also resemble that of the single WSR case. The system exhibits a first order response for all the equilibria represented on the diagram; a representative frequency response would take the qualitative shape shown in Figure 4.6. Similarly to the single WSR case, a phase change occurs just prior to blowout, at the point 2 shown in the bifurcation diagram of Figure 4.35. The frequency response at this point resembles the frequency response of the single WSR shown in Figure 4.7.

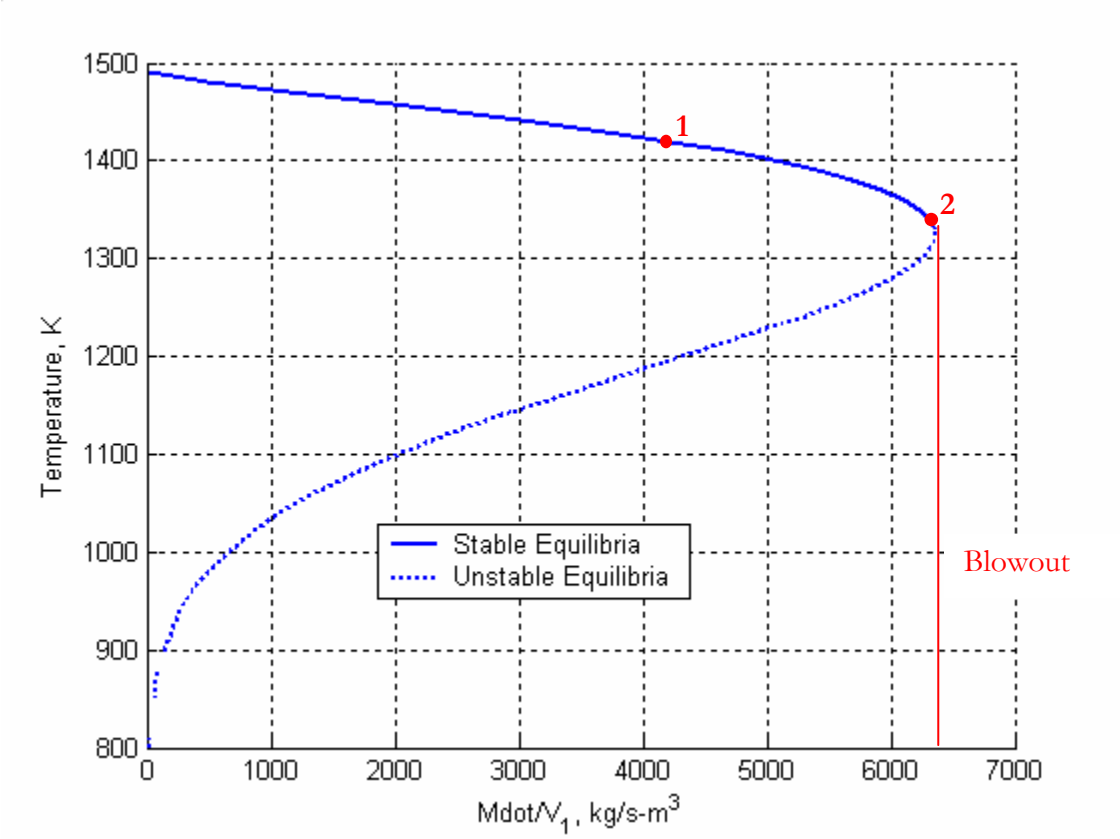

Figure 4.35: Bifurcation diagram of a 3-WSR system which resembles the bifurcation diagram of a single WSR; $\Phi = 0.7$, $\alpha = 50\%$, $\beta = 49\%$, $V_2/V_1 = 2$, $V_3/V_1 = 0.1$

The coupled 3-WSR system can also exhibit a bifurcation diagram which resembles that of the bifurcation diagram shown for the 2-WSR system shown in Figure 4.14; an example of this type of bifurcation diagram is shown in Figure 4.36.

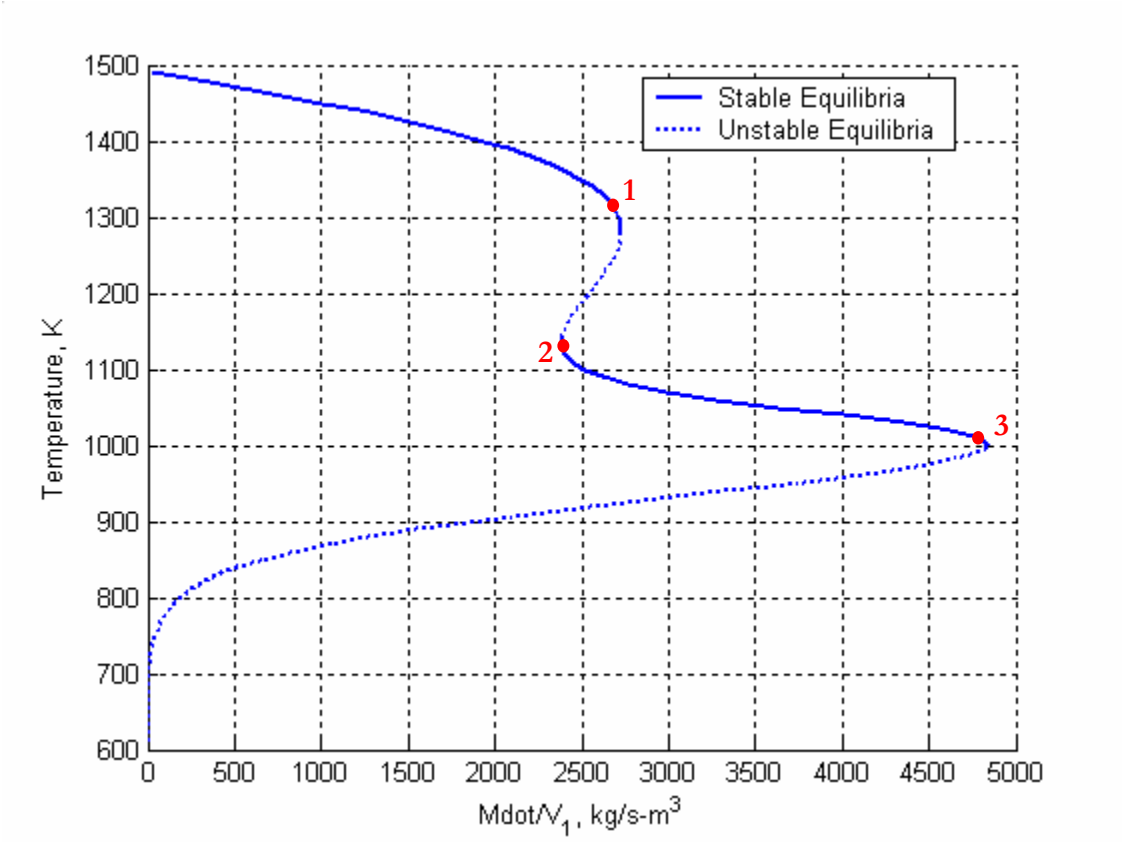

Figure 4.36: Bifurcation diagram of 3-WSR system which resembles that of a 2-WSR system; $\Phi = 0.7$, $\alpha = 40\%$, $\beta = 20\%$, $V_2/V_1 = 2$, $V_3/V_1 = 0.5$

The system frequency response at various points on the bifurcation diagram also resembles that of the 2-WSR system. For increasing mass flow rate, as the mass flow nears the point 1, the system exhibits a phase change similar to that of the 2-WSR case. The frequency response at point 1 is similar to that of the response of the 2-WSR system shown in Figure 4.25. The frequency response at point 2 is similar to that of the 2-WSR system shown in Figure 4.28. The frequency responses prior to blowout (point 3) are also similar to those of the 2-WSR case and their description resembles the description surrounding Figure 4.29.

The coupled 3-WSR system has another type of bifurcation diagram, an example of which is shown in Figure 4.37. This bifurcation diagram has three tiers of stability corresponding to where each of three WSR's act as the primary combustor. These three tiers are separated by two portions where unstable equilibria exist, similar to the way the bifurcation diagram of a 2-WSR diagram is broken up by a portion of unstable equilibria.

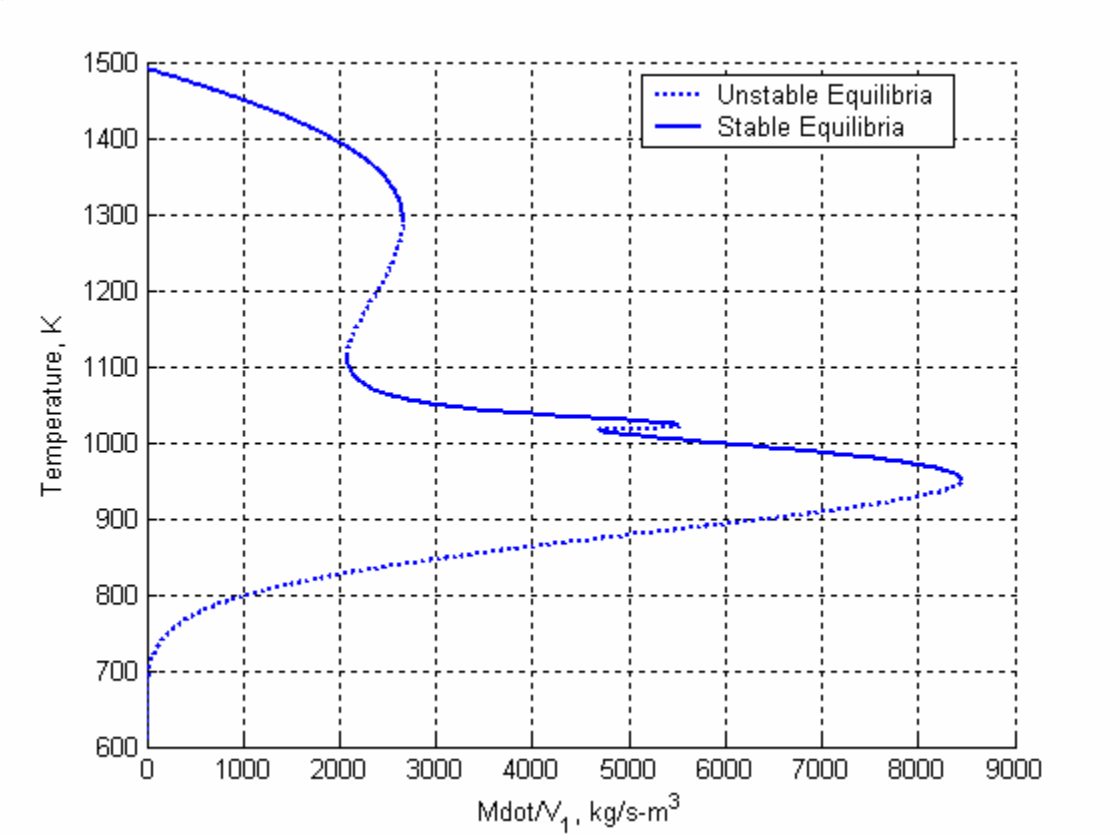

Figure 4.37: Bifurcation diagram of a coupled 3-WSR system;

$\Phi = 0.7$, $\alpha = 45\%$, $\beta = 5\%$, $V_2/V_1 = 2$, $V_3/V_1 = 4$

The frequency responses along the bifurcation diagram in Figure 4.37 are again similar to those of the 2-WSR case. As the mass flow approaches a region of unstable equilibria, the phase jumps as shown in the preceding figures.

The various bifurcations change as parameters vary, as in the 2-WSR case. As in the 2-WSR case, increasing the equivalence ratio, Φ, elongates the bifurcation diagram along the x-axis ($Mdot/V_1$) as was shown in Figure 4.20. Increasing the recirculation

percentage, either α or β, results in the bifurcation appearing more like the bifurcation diagram of a single WSR, as was shown for the 2-WSR case in Figure 4.18.

5 Conclusions and Future Work

5.1 Conclusions

The primary objective of the first part of this research was to accurately predict the mass flow rate, the equivalence ratio and the frequency at which instability will occur in a Rijke tube combustor. It was first shown that the pressure oscillations are forced by both the chemical heat release rate as well as by convection within this laminar flat flame. This was shown by using an experimentally validated model of a laminar flat flame capable of calculating the exact acoustic forcing. It was then shown that modeling the acoustic forcing by the summation of chemical heat release term and the convection term accurately modeled the forcing function calculated in the laminar flat flame model. Using this new model of the acoustic forcing, the flame dynamics and acoustic dynamics could be coupled in a new model to predict instability. This model was capable of predicting the mass flow rate, equivalence ratio and the frequency at which instability would occur. However, given an unstable point at a particular frequency, the model could not predict at what equivalence ratio or what mass flow rate the system would become stable. This is due to the inability of the PREMIX code to reach a solution at lower equivalence ratios or mass flow rates. However, the data trend does suggest that a mass flow or equivalence ratio that is low enough will stabilize the system.

The primary objective of the second half of this research was to model qualitative features of turbulent combustion with dynamic well-stirred reactors (WSR) or networks of such reactors. First, a single dynamic WSR was used. This model was unable to model the dynamic features of a real combustor because it was inherently first order in nature and therefore could never exhibit the peaking seen in the real combustor. A network of two WSR's was constructed by coupling the two reactors together with recirculation. This network could exhibit peaking; however, it could not exhibit peaking while exhibiting a realistic bandwidth for the system. However, the network did model blowout as well as exhibit a bifurcation diagram within which it was possible for the equilibrium temperatures to jump. This jumping phenomenon could be explained as flame repositioning within the reactor. These jumps also gave rise to possible hysteresis

loops. The effect of varying several of the model's parameters was examined. This portion of the study showed that it was possible to cause the system to jump by varying the equivalence ratio or the mass flow rate, as well as the recirculation parameters. These results are encouraging since similar behavior has been observed in real combustors. Finally, a network of three WSR's was constructed using recirculation. The 3-WSR network demonstrated the same qualitative behavior as the 2-WSR system. It had three sections of equilibria solutions in its bifurcation diagram, allowing for more jumping and possible hysteresis loops. The 3-WSR network could also exhibit a qualitatively peaked response but it too was accompanied by an unrealistically large bandwidth. As mentioned before, the unrealistic bandwidths can be attributed to the WSR assumption of instantaneous mixing.

5.2 Future Work

The major work that needs to be completed to finish up the first portion of this research is to show that the model can accurately predict where the system will go stable. Toward this goal it is suggested a variable Nusselt number used to model the heat transfer due to convection within the model be investigated. It also may be necessary to port the code to a format that is capable of running on a shared processor platform that will be able to run the code with smaller time steps and not be so computationally expensive.

There are many ways to improve upon the WSR models developed during this research. Many of those paths involve making the models more complicated but are necessary since the simpler models are not capable of accurately modeling turbulent combustion. First, the WSR model needs to be adjusted so that it can store mass, and thus allow for a variable density. This most likely will necessitate the model being coupled with acoustics. The WSR networks could also be constructed with different topologies, that is, they do not have to be combined in a straight line format. Improvements could also be made to the modeling of the chemical reactions within the reactor. The current model uses an over-simplified global reaction mechanism and perhaps a multi-step combustion mechanism is warranted. As noted within this work, time delay will be required to accurately model the phase of the experimental flame

transfer function. It is noted that most, if not all, of these future work suggestions will complicate the model and most likely increase its order, which is not desired; however, the simple model does not accurately model the desired phenomena.

Appendix A: Combustion Model Validation

Table A 1: Honeycomb surface temperature comparison

Flow rate	Equivalence Ratio	Top Surface Temperature Experimental (K)	Top Surface Temperature Model (K)	Bottom Surface Temperature Experimental (K)	Bottom Surface Temperature Model (K)
145	0.50	641	552	328	307
145	0.55	799	742	340	313
145	0.60	903	849	348	316
145	0.65	958	921	354	318
145	0.75	1064	1035	366	321
200	0.60	1025	877	330	306
200	0.75	1161	1119	276	309

The following figures, A1 – A8, show that in the combustion model CHR dynamically correlates to OH*. This correlation allows a comparison between experiment and the model. The subsequent figures, A9 – A13, show the comparison between experimental OH* measurements and OH* calculations obtained from the modified PREMIX program.

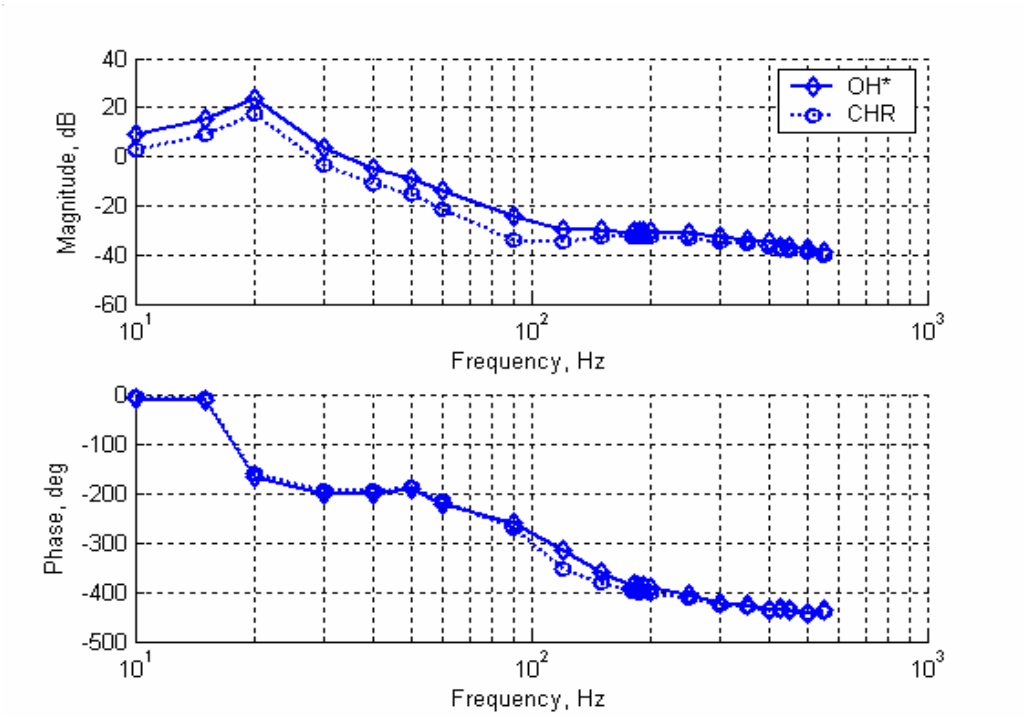

Figure A 1: Dynamic comparison of OH* and CHR for Q = 145 cc/sec, Φ = 0.50

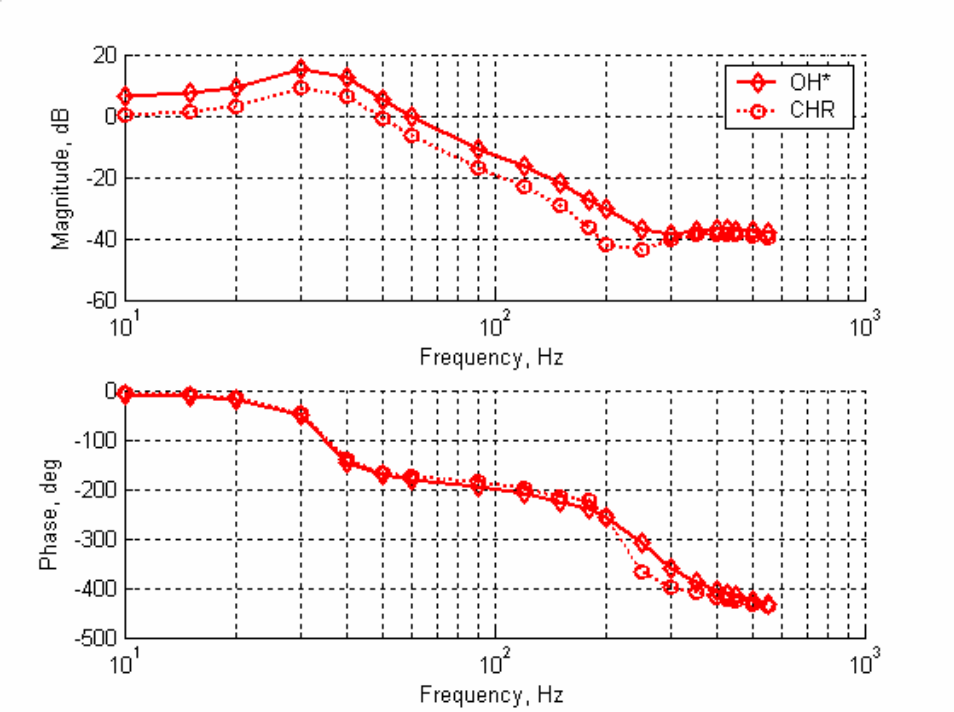

Figure A 2: Dynamic comparison of OH* and CHR for Q = 145 cc/sec, Φ = 0.52

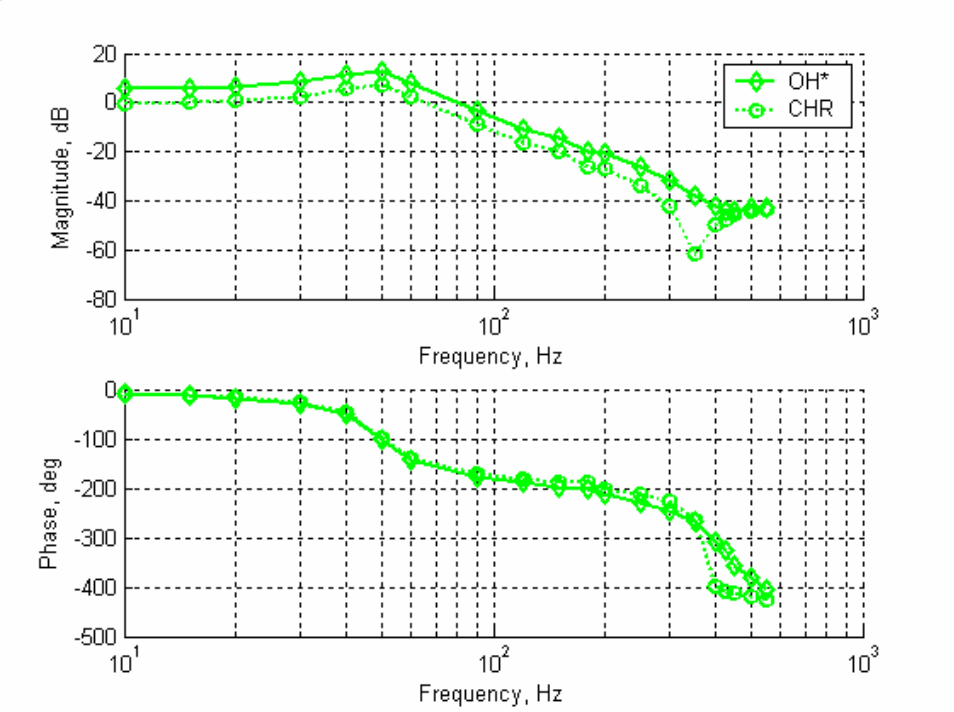

Figure A 3: Dynamic comparison of OH* and CHR for Q = 145 cc/sec, Φ = 0.55

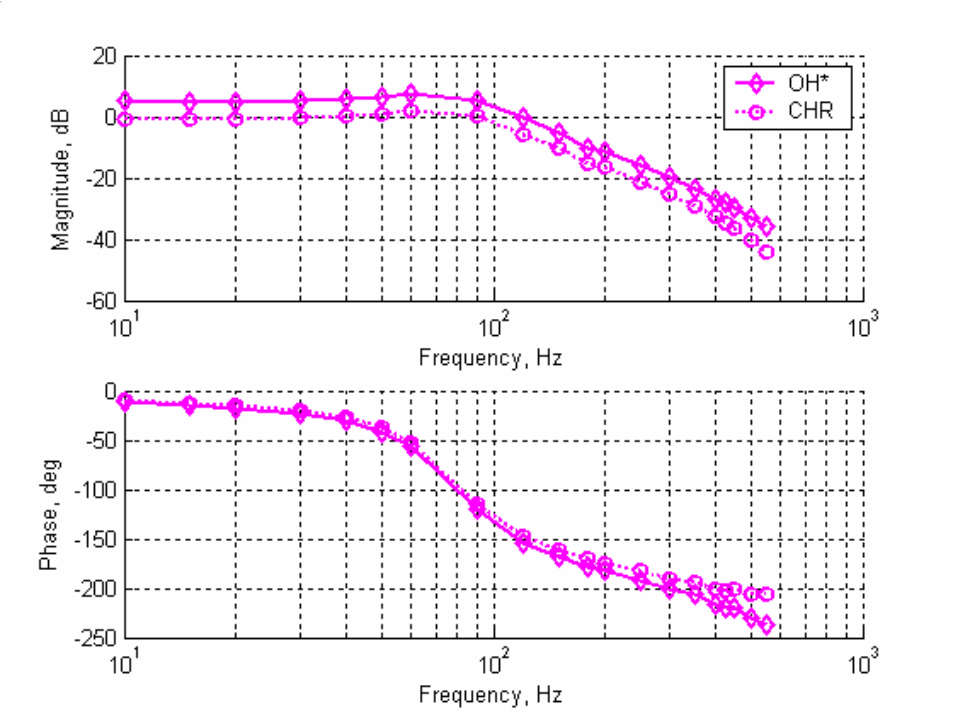

Figure A 4: Dynamic comparison of OH* and CHR for Q = 145 cc/sec, Φ = 0.60

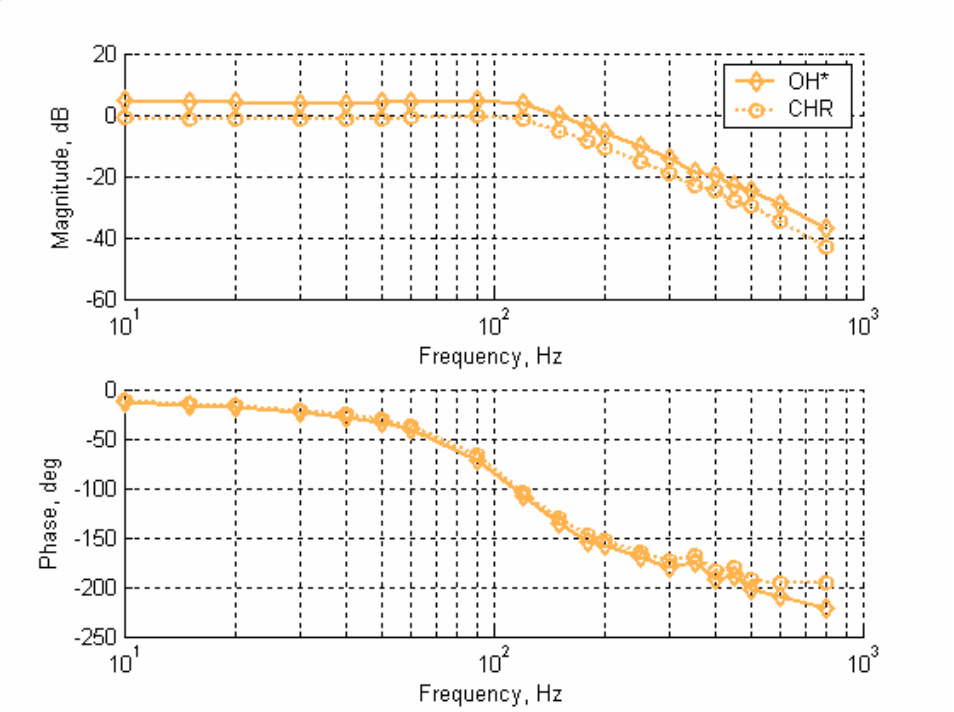

Figure A 5: Dynamic comparison of OH* and CHR for Q = 145 cc/sec, Φ = 0.65

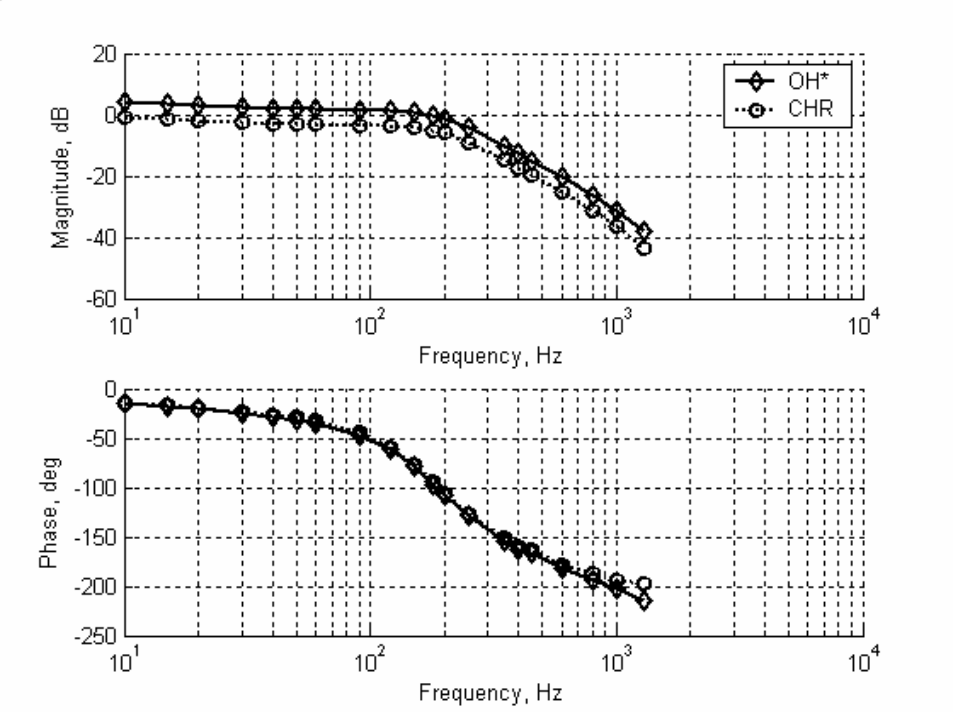

Figure A 6: Dynamic comparison of OH* and CHR for Q = 145 cc/sec, Φ = 0.75

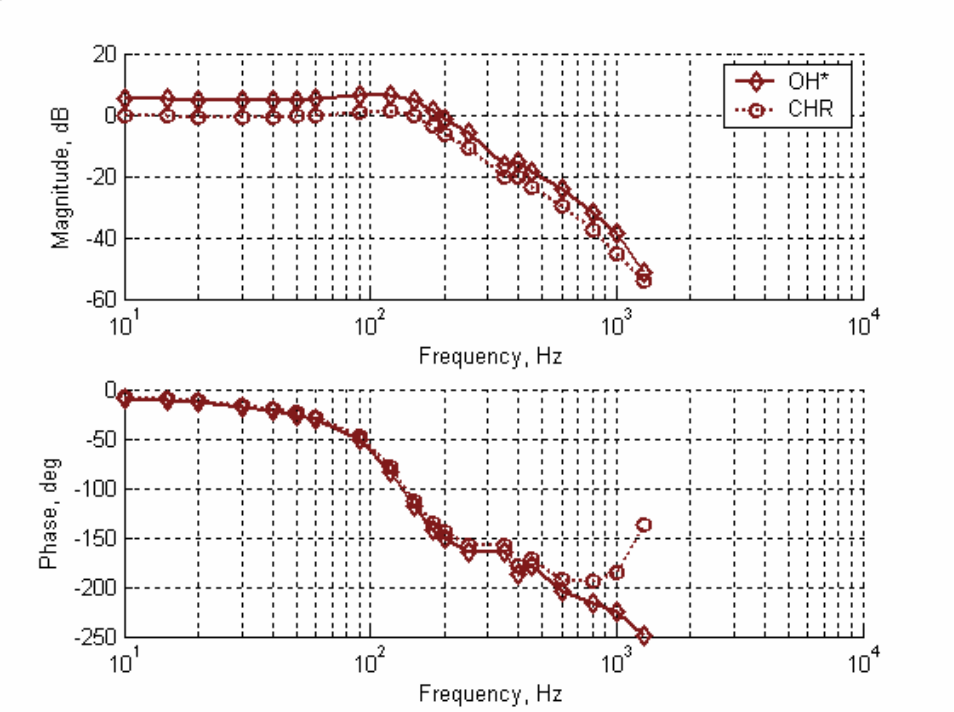

Figure A 7: Dynamic comparison of OH* and CHR for Q = 200 cc/sec, Φ = 0.60

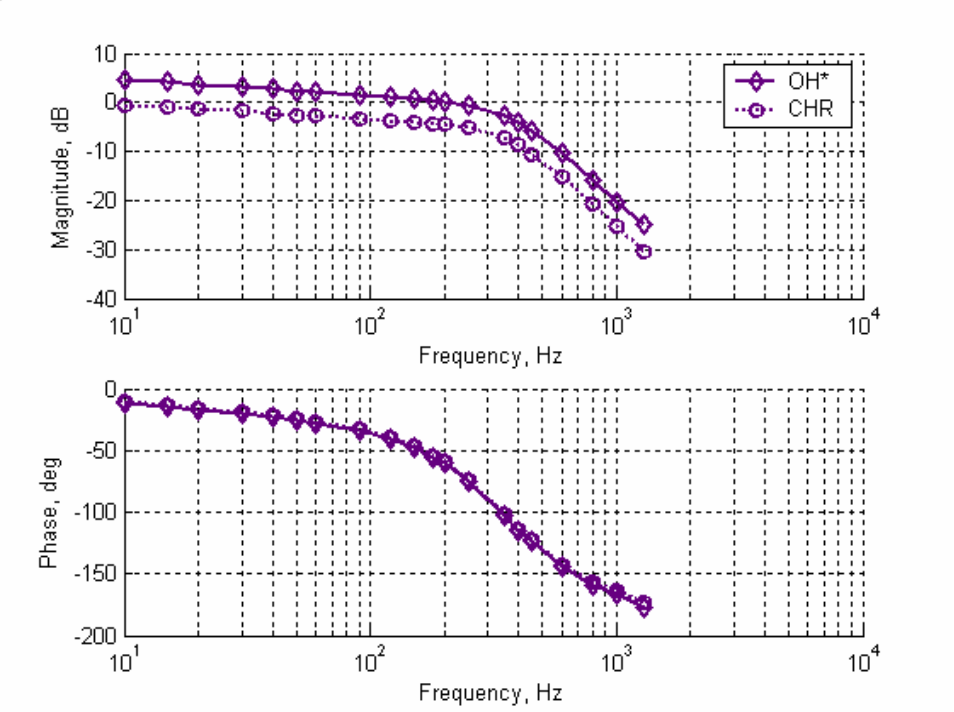

Figure A 8: Dynamic comparison of OH* and CHR for Q = 200 cc/sec, Φ = 0.75

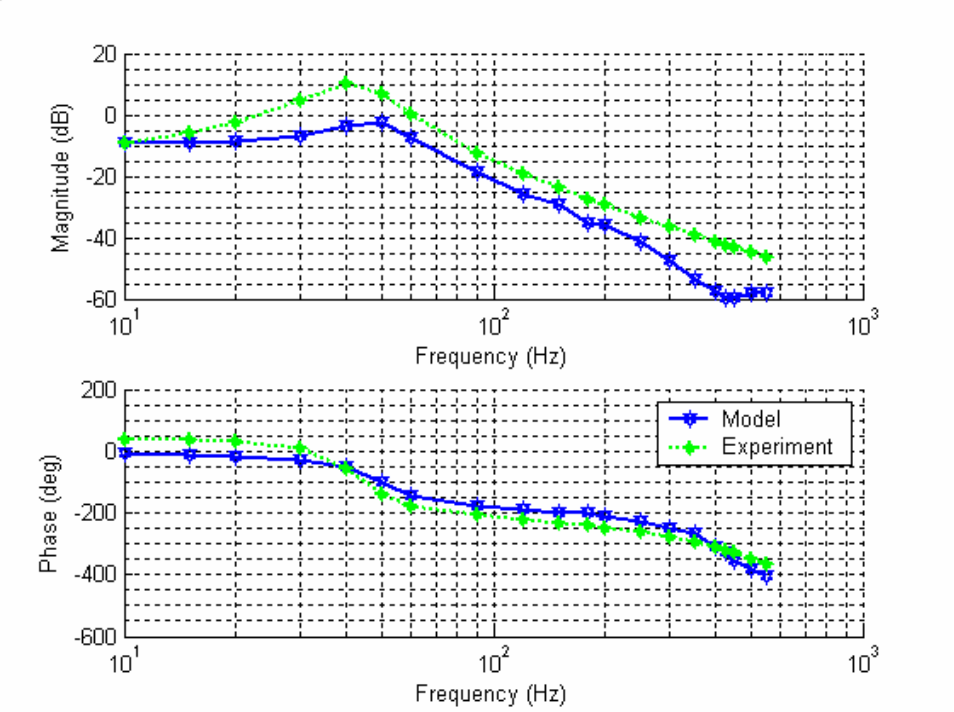

Figure A 9: Comparison between model and experimental OH* measurements, Q = 145 cc/sec, Φ = 0.55

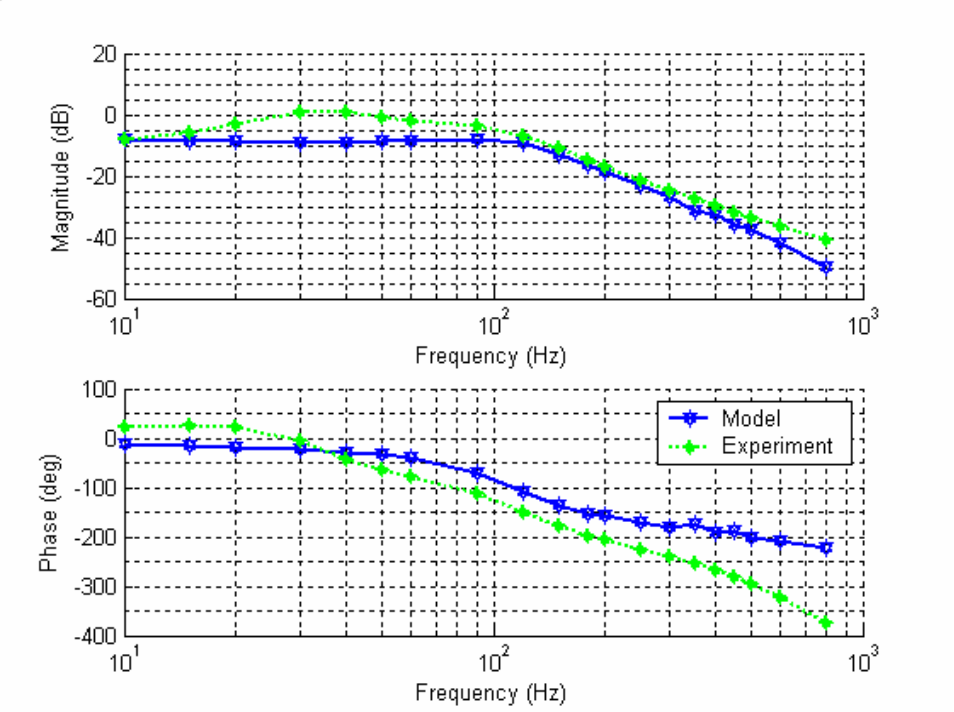

Figure A 10: Comparison between model and experimental OH* measurements, Q = 145 cc/sec, Φ = 0.65

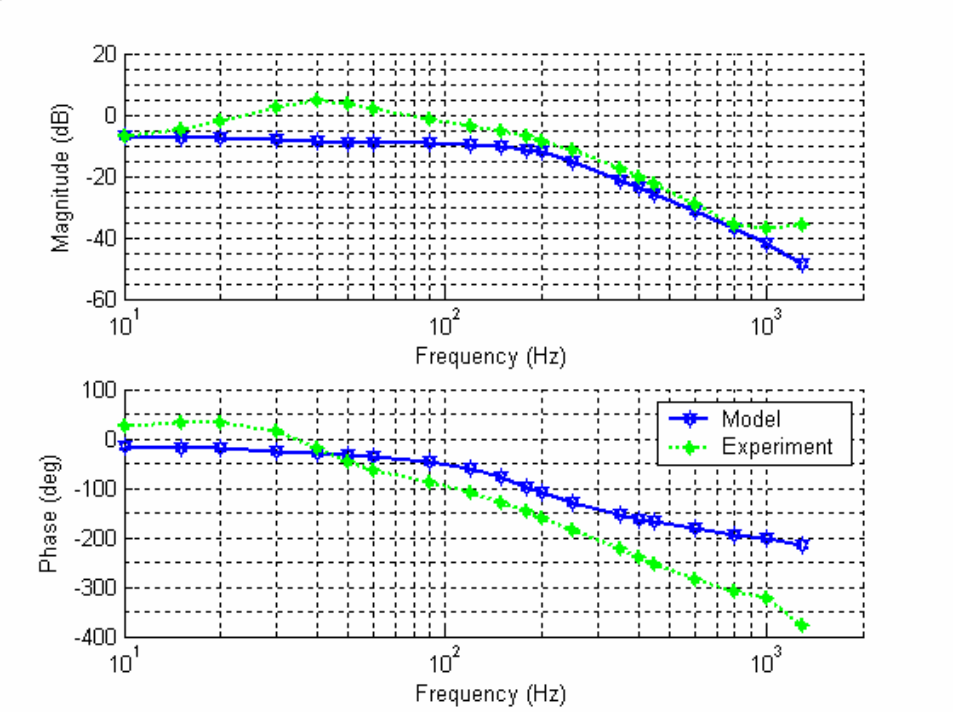

Figure A 11: Comparison between model and experimental OH* measurements, Q = 145 cc/sec, Φ = 0.75

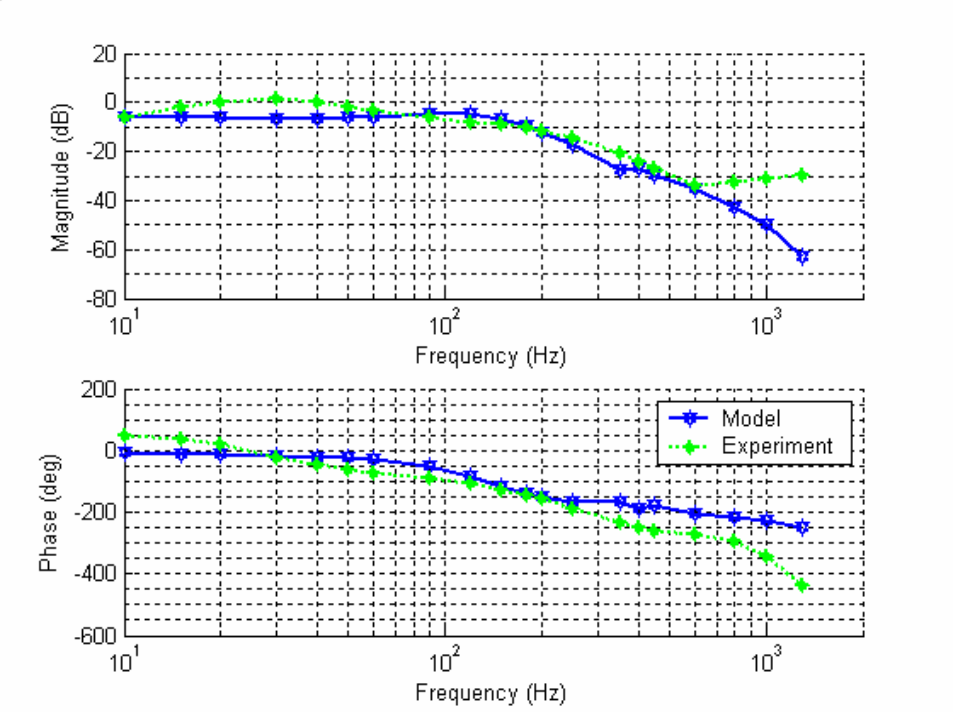

Figure A 12: Comparison between model and experimental OH* measurements, Q = 200 cc/sec, Φ = 0.60

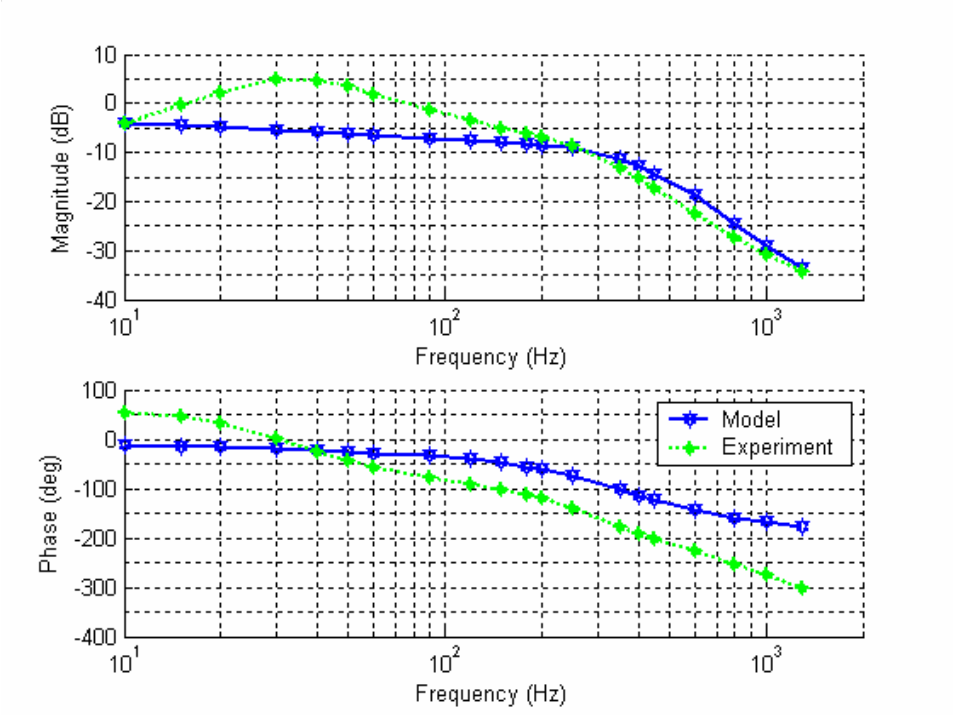

Figure A 13: Comparison between model and experimental OH* measurements, Q = 200 cc/sec, Φ = 0.75

Appendix B: Importance of convection in dynamic acoustic forcing term

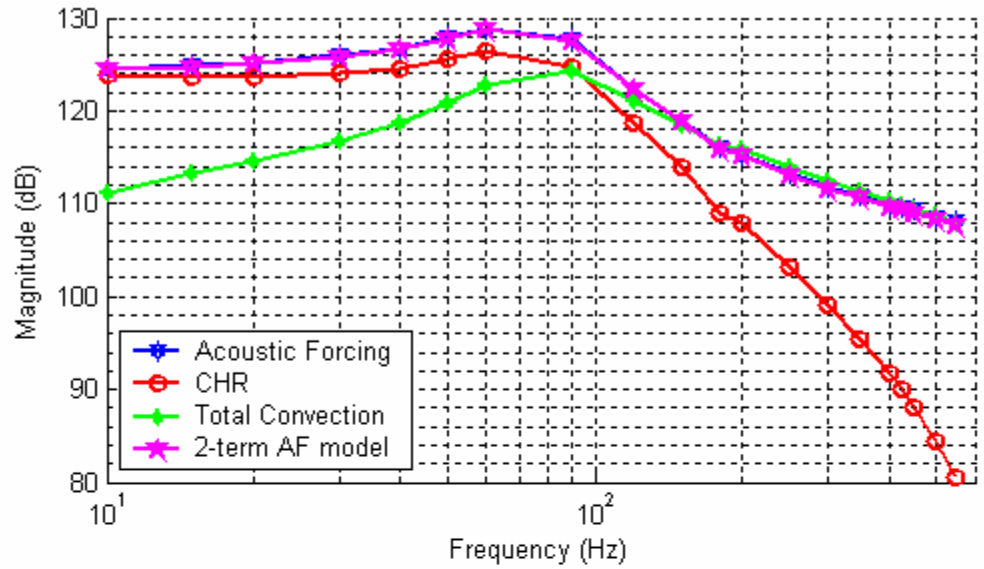

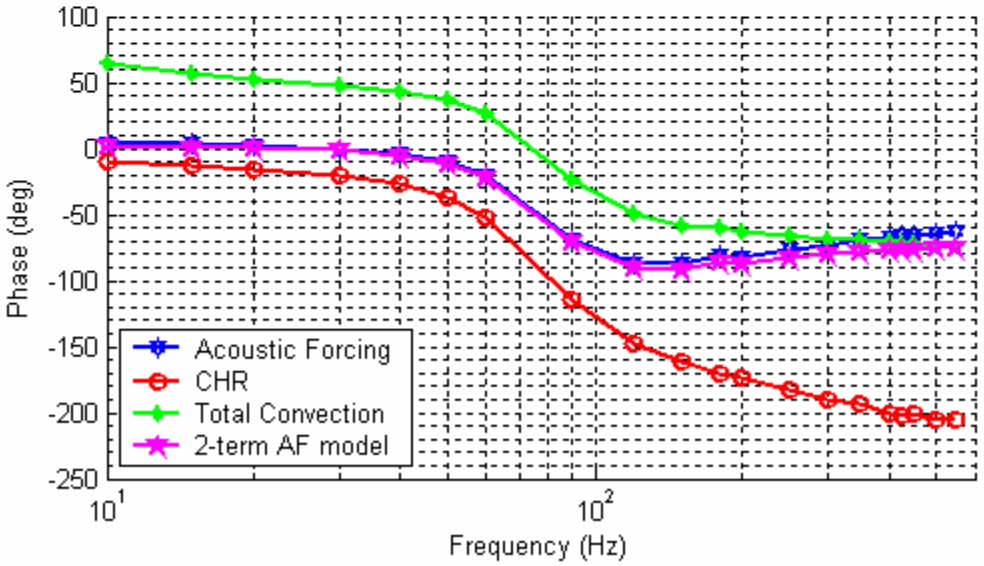

Figure B 1: Frequency response for Q = 145 cc/sec, Φ=0.60

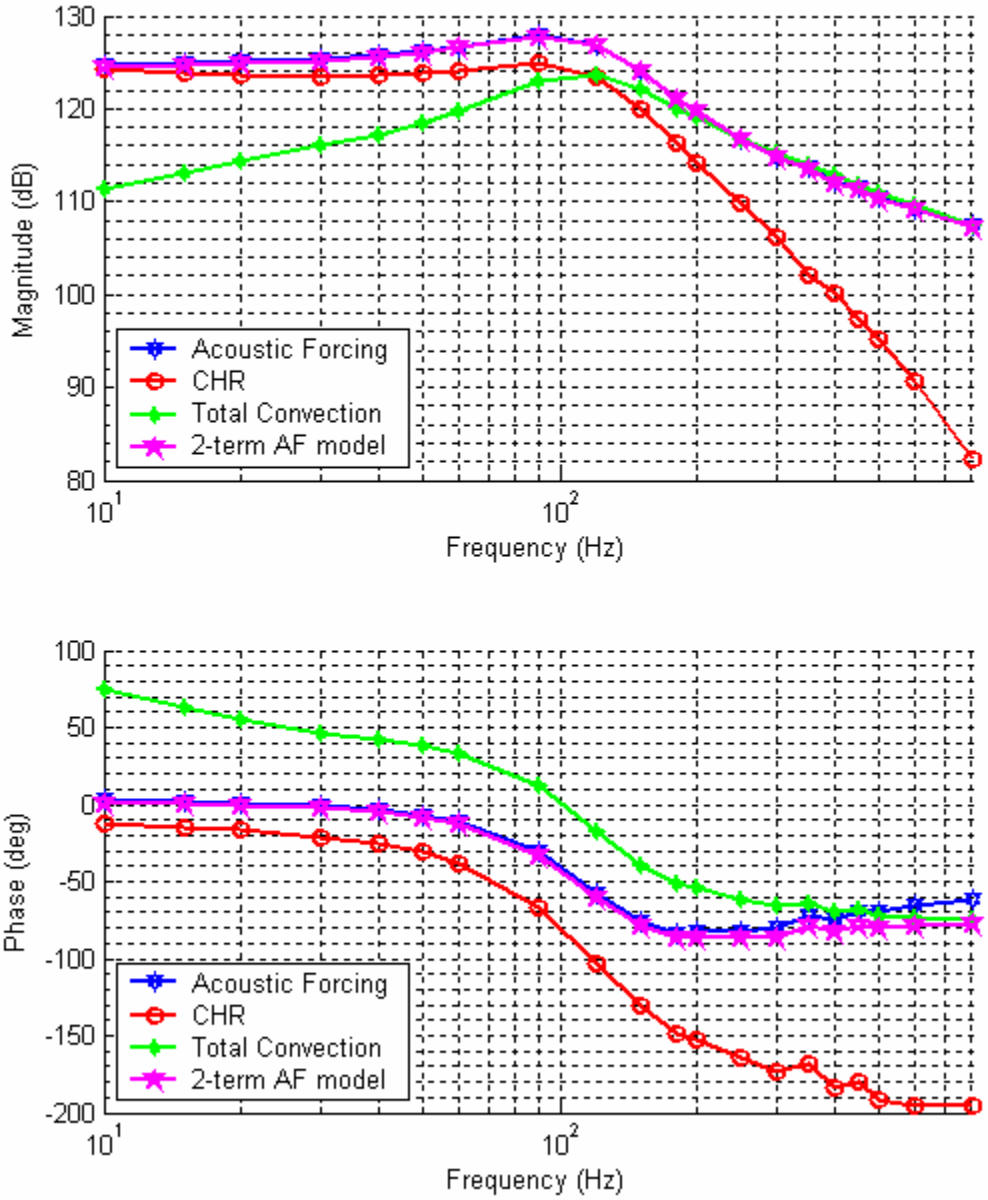

Figure B 2: Frequency response for Q = 145 cc/sec, Φ = 0.65

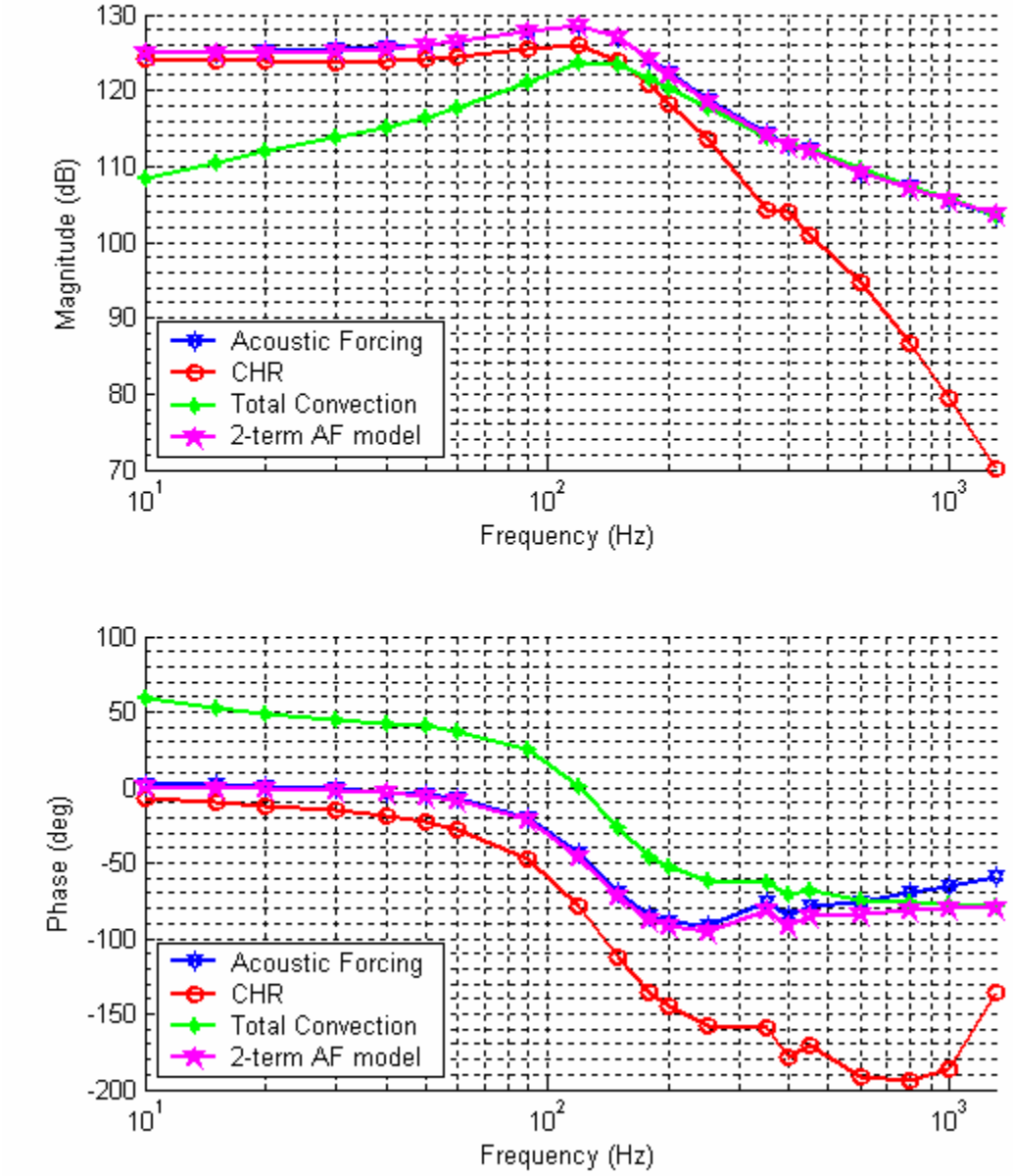

Figure B 3: Frequency response for Q = 200 cc/sec, Φ = 0.60

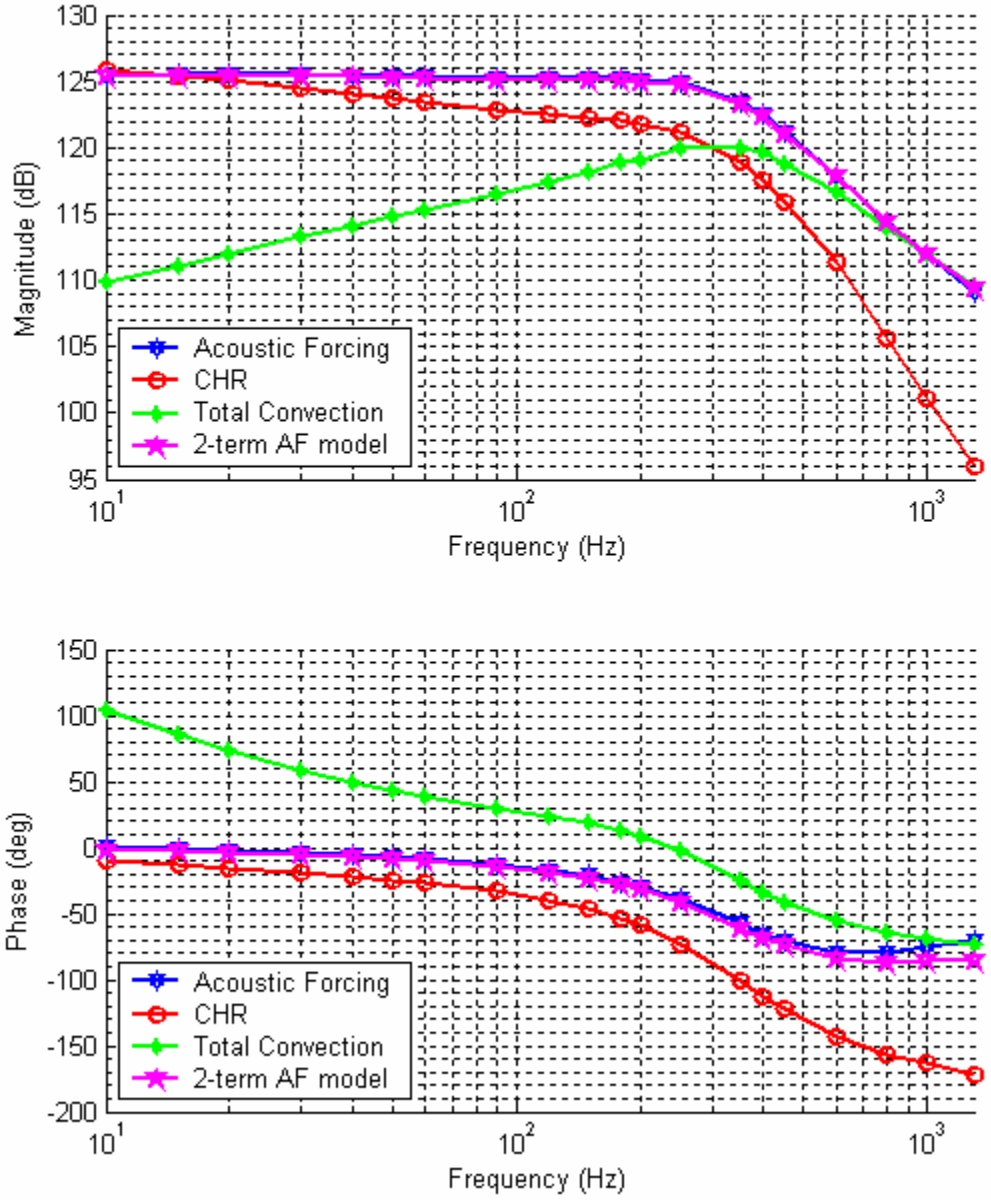

Figure B 4: Frequency response for Q = 200 cc/sec, Φ = 0.75

Appendix C: Simulink Models for WSR Modeling

The Simulink models used in this research are provided here in the appendix.

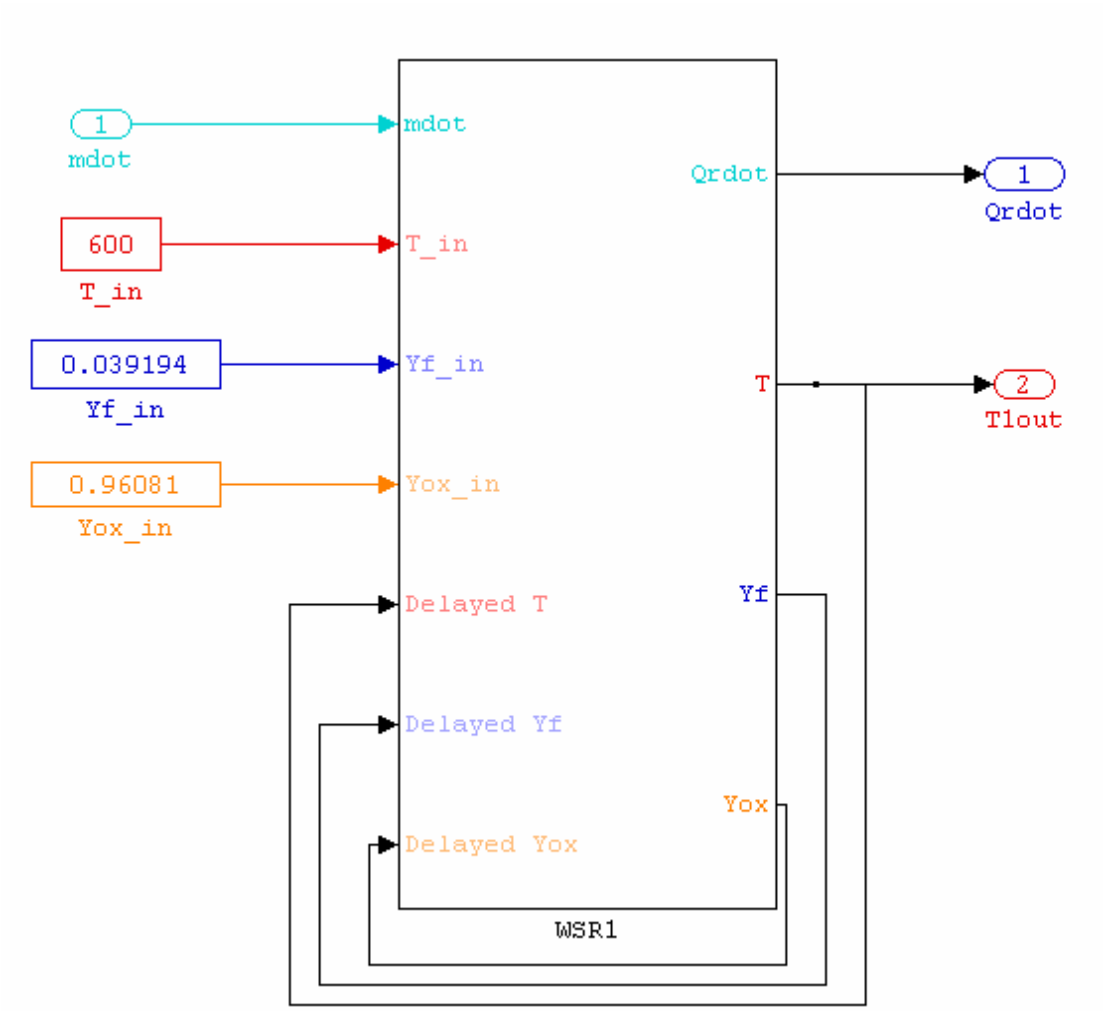

Figure C 1: Block diagram of single WSR Model

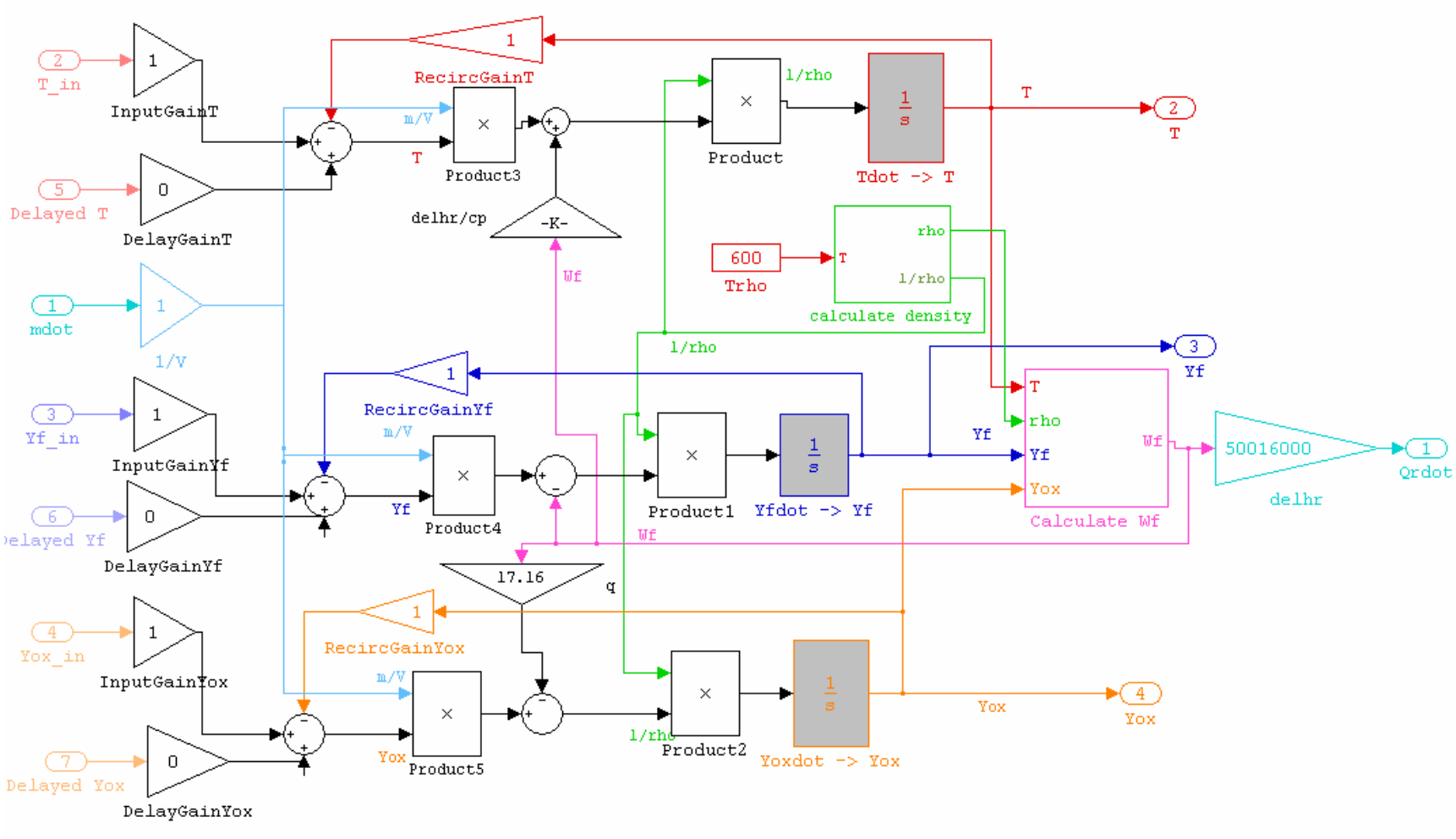

Figure C 2: : Block diagram of masked subsystem, WSR1, shown in Figure C 1

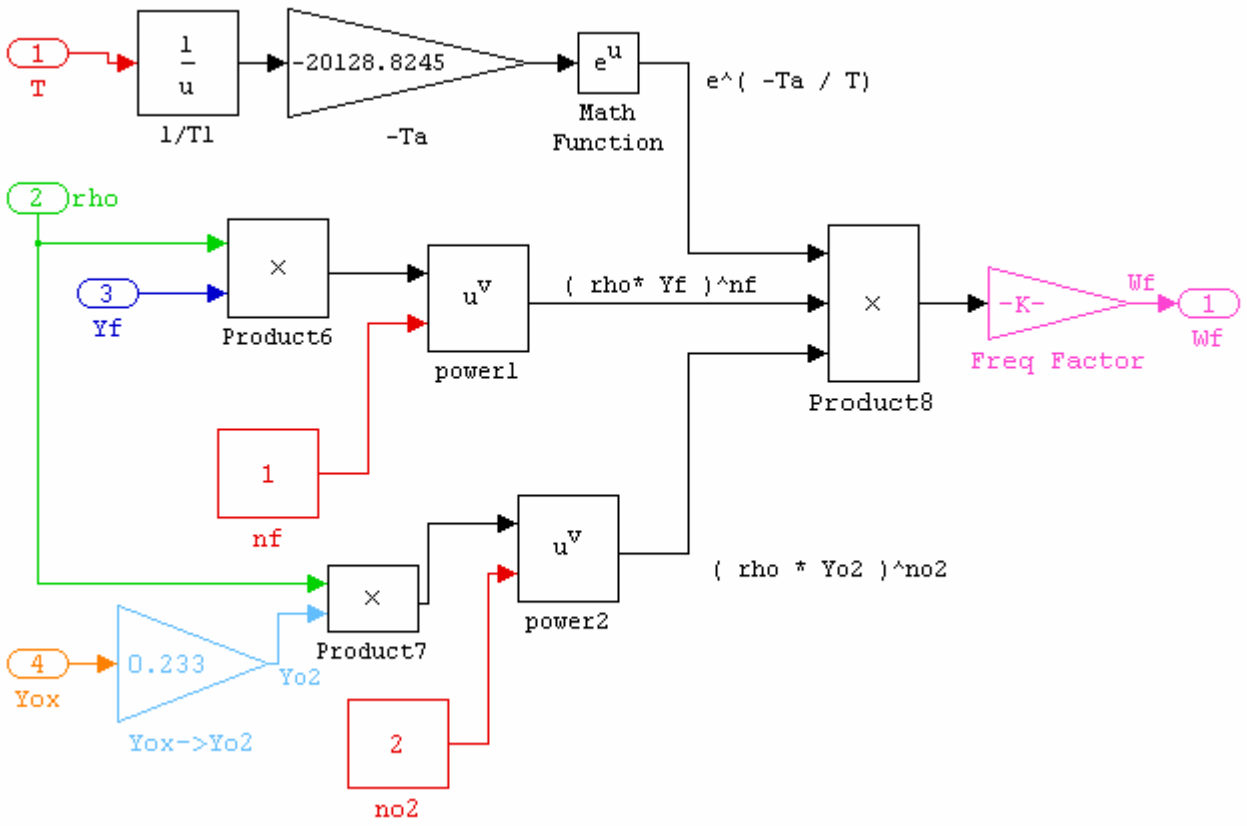

Figure C 3: Simulink block diagram of the masked subsystem, Calculate Wf, shown in Figure C 2

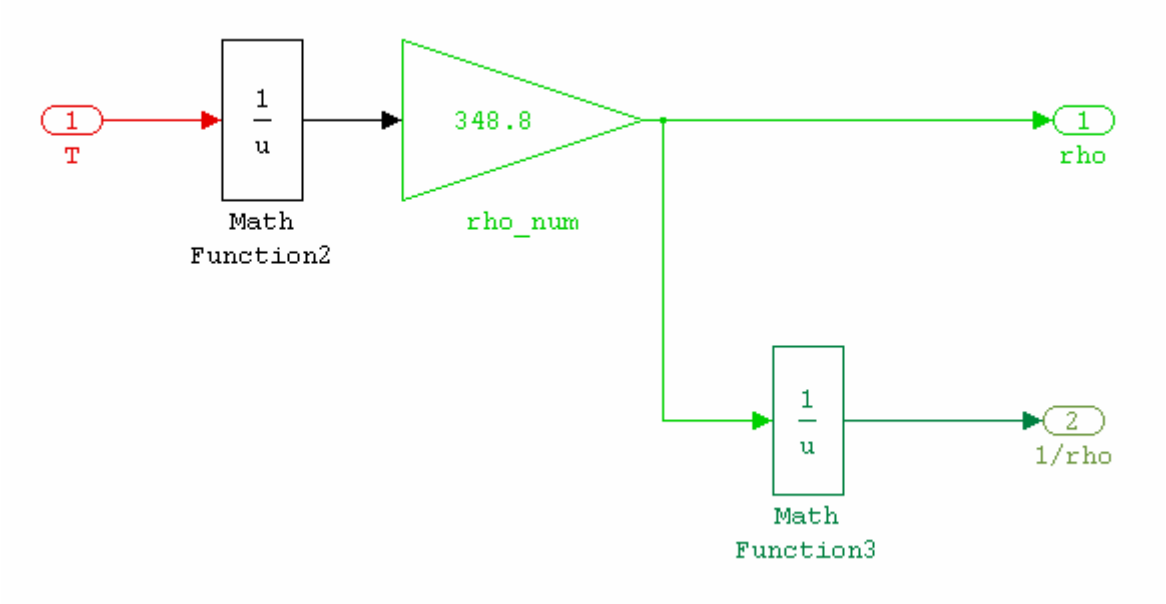

Figure C 4: Simulink block diagram of masked subsystem, calculate density, shown in Figure C 2

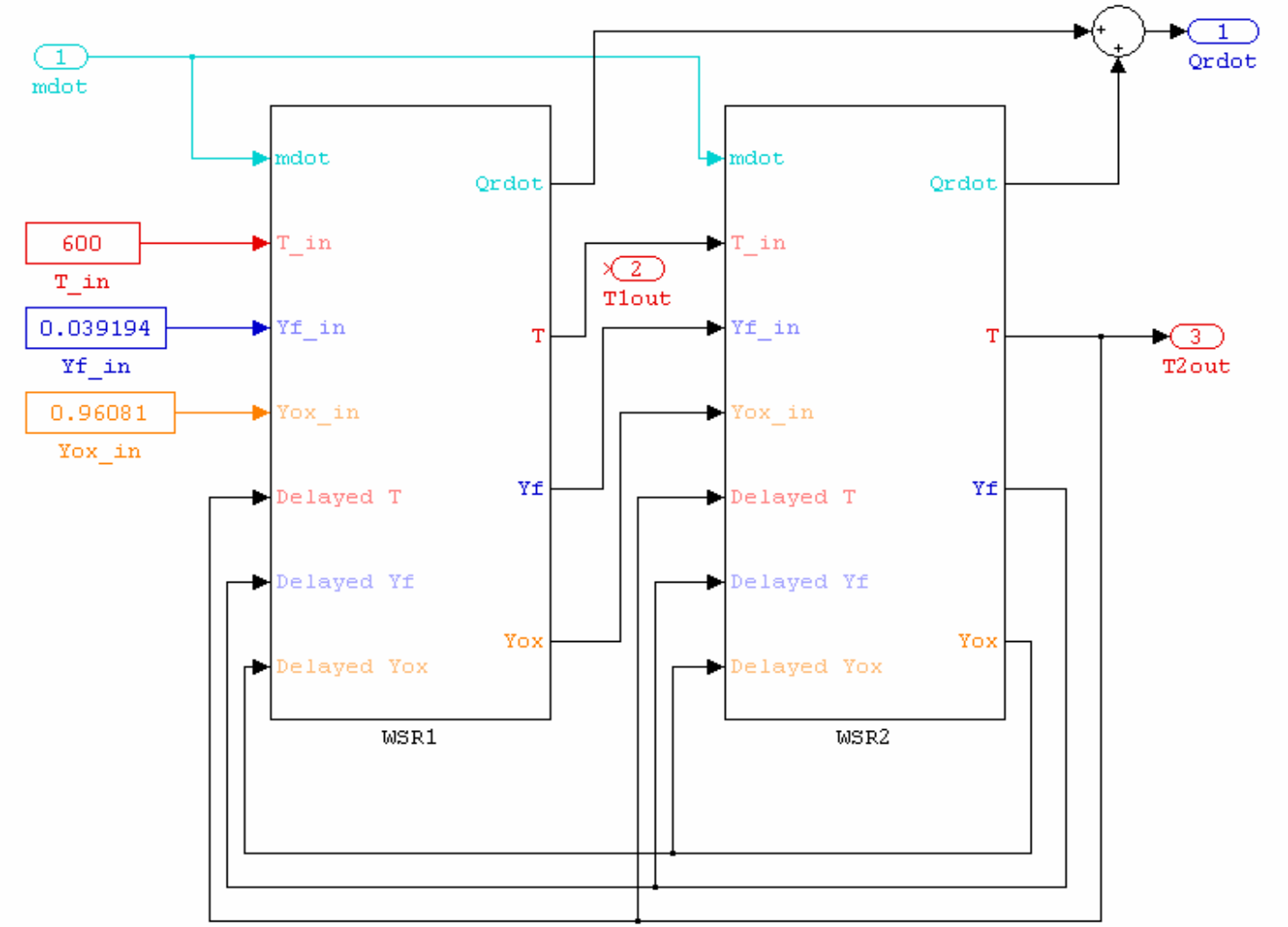

Figure C 5: Simulink block diagram of coupled 2-WSR network. The masked subsystems WSR1 and WSR2 are identical to that shown in Figure C 2

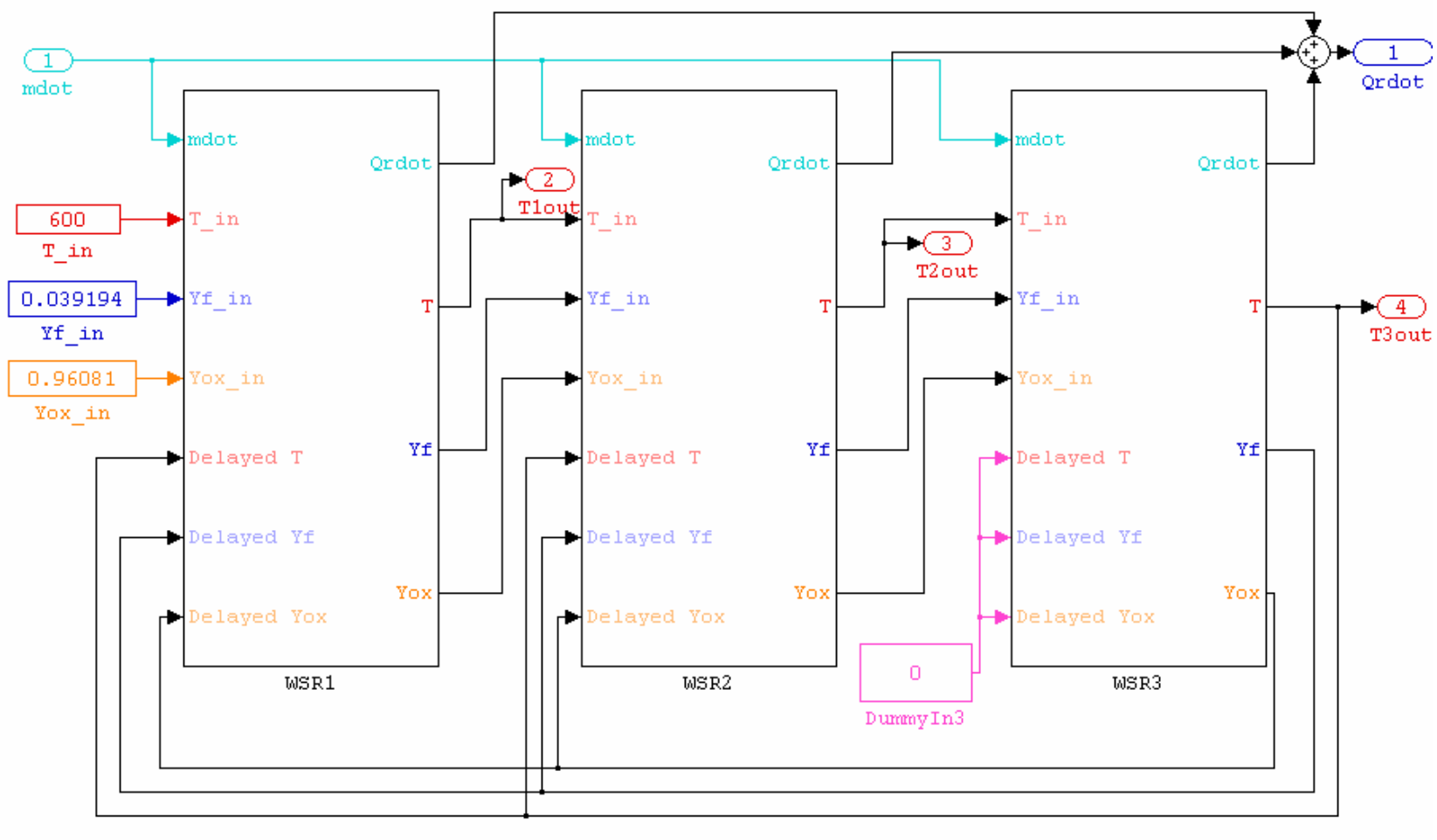

Figure C 6: Simulink block diagram of coupled 3-WSR network. The masked subsystems WSR1, WSR2 and WSR3 are identical to that shown in Figure C 2

Appendix D: MatLab Code

The MatLab functions provided here are but a small part of the code written for this endeavor. The individual functions are separated by a solid line divider.

```
function [ MWox, MWo2, MWpr, MWfuel, Ta, Ru, A, cp, delhr, T_in, m, n, mol_AFs ]
= wsr_parameters( fuel )
% WSR_PARAMETERS returns fuel specific parameters required for evaluation of
%    WSR problems.
%
%    [ MWOX, MWO2, MWPR, MWFUEL, TA, RU, A, CP, DELHR, T_IN, M, N,
MOL_AFS ] = WSR_PARAMETERS( FUEL )
%         returns the parameters for a specific fuel, FUEL.
%         Current acceptable values of fuel are 'ethane' or 'methane'
%         The values returned are the molecular weight of the oxidizer, MWOX, the
molecular weight of oxygen,
%         MWO2, the molecular weight of the products, MWPR, the molecular weight of
the fuel, MWFUEL, the activation
%         temperature, TA, the gas constant, RU, the preexponential factor, A, the specific
heat, CP,
%         the enthalpy of reaction, DELHR, the exponents for the fuel and oxygen, M and
N, and the molar ratio of
%         air to fuel, MOL_AFS.  T_IN is no longer used.
%
%    Values taken from Intro to Combustion, 2nd ed. by S. Turns, and
%    Doctoral thesis of Xinming Huang.
%
% Written by Losh.
% Version 1.3, 4/20/2004 10:53PM.
%

% Universal parameters.
MWox = (32+28*3.76)/4.76  ;    % kg/kmol
T_in = [] ;   % K
Ru = 8314 ;    % J/kg-K - Universal Gas Constant.
MWo2 = 32 ;    % kg/kmol - Molecular weight of O2
MWpr = 28 ;    % kg/kmol

% Fuel dependent parameters.
switch upper( fuel )
    case 'ETHANE'
```

```
        MWfuel = 30 ;
        m = 0.1 ;
        n = 1.65 ;
        Ta = 15098 ;  % K
        A = 6.19e9 ;  %
        cp = 1.25e3 ;    % J/kg-K
        delhr = 4.75e7 ; % J/kg
        mol_AFs = 3.5 ;    % Stoichometric Air-Fuel ratio.

    case 'METHANE'
        MWfuel = 16 ; % kg/kmol
        Ru_cal = 1.9872e-3; %kcal/gmol-K

        % Select which global mechanism to use via data_source: prateep, turns, or
xinming.
        data_source = 'xinming'  ;

        switch data_source
            case 'turns'
                m = -0.3 ;
                n = 1.3 ;
                A = 8.3e5 * (1e3)^(1-m-n) ;
                Ta = 15098 ;
            case 'xinming'
                m = 1 ;
                n = 2 ;
                A = 2.0e22 * (1e3)^(1-m-n) ;
                Ea = 40 ;      %kcal/gmol
                Ta = Ea / Ru_cal ;
            case 'prateep'
%               Data taken from FLUENT program, via prateep.
                m = 0.2 ;
                n = 1.3 ;
                A_prateep = 2.119e+11 ; % already in kmol/m^3 system.
                A = A_prateep ;
                Ea = 2.027e+08 ; % J/kmol
                Ta = Ea / Ru ;
            otherwise
                error('Data not available for data source specified.') ;
        end

        cp = 2200 ;         % J/kg-K
        delhr = 50016e3 ;   % J/kg - Actually LHV in Turns, pg 649, Appendix B, Table
B.1
```

```
        mol_AFs = 2 ;       % molar Air-Fuel ratio at stoichometric mixture. also, a = x+y/4
in turns.
    otherwise
        error('No information available for fuel specified.') ;
end
```

```
function [ Yf_in, Yox_in, MWfuel, FA, rho_num, varargout ] = initial_mass_fract( phi,
fuel, printing, varargin )
% INITIAL_MASS_FRACT calculates the stoichometric entering mass fractions
% of the fuel and oxidizer for a given fuel and equivalence ratio entering a WSR.
%
%    [ YF_IN, YOX_IN, MWFUEL, FA, RHO_NUM ] = INITIAL_MASS_FRACT(
PHI, FUEL )
%    [ YF_IN, YOX_IN, MWFUEL, FA, RHO_NUM, PHI ] =
INITIAL_MASS_FRACT( [Yf1, Yox1], FUEL )
%        returns the inlet mass fractions of fuel, YF_IN, and oxidizer, YOX_IN, the
molecular
%        weight of the fuel, MWFUEL, the fuel-air ratio, FA, the RHO_NUM, and the
equivalence
%        ratio, PHI.
%
%
% See also: wsr_parameters.m
%
% Written by Losh.
% Version 1.4, 4/20/2004 10:59PM.
%

if nargin < 3
    printing = 0 ;
end

if nargin > 3
    Patms = varargin{ 1 } ;
else
    Patms = 1 ;
end

% Function call to wsr_parameters.m
[ MWox, MWo2, MWpr, MWfuel, Ta, Ru, A, cp, delhr, T_in, m, n, a ] =
wsr_parameters( fuel );

% Molecular weight of Nitrogen, N2.
MWn2 = 28 ;    % kg/kmol

% Calculate stoichometric F/A (fuel-air) ratio.
FAstoic = 1 * MWfuel / ( a * MWo2 + a * 3.76 * MWn2 );
```

```
if length( phi ) == 1

    % Calculate actual F/A ratio based on equivalence ratio, phi.
    FA = FAstoic * phi ;

    % Calculate the mass fraction of fuel.
    Yf_in = FA / ( 1 + FA ) ;

    % Calculate the mass fraction of the oxydizer.
    Yox_in = 1 - Yf_in;

else
    % Retrieve variables.
    Yf_in = phi( 1 ) ;
    Yox_in = phi( 2 ) ;

    % Calculate F/A ratio based on the inlet mass fraction of fuel, Yf.
    FA = Yf_in / ( 1 - Yf_in )  ;
end

% Calculate the Molecular weight of the mixture.
MWmix = ( Yf_in/MWfuel + Yox_in/MWox )^-1 ;

% Calculate the rho number to calculate density later on.
rho_num = 101325 * Patms * MWmix / Ru ;

% Calculate the equivalence ratio of the incoming mixture.
phi = FA / FAstoic ;

% Set Output values.
varargout = { phi } ;


if printing == 1
    fprintf('\nFuel Mass Fraction input: %4.9f\n', Yf_in ) ;
    fprintf('Oxidizer Mass Fraction input: %4.9f\n', Yox_in ) ;
    fprintf('Rho number: %4.9f\n\n', rho_num ) ;
end
```

```
function [Tmax, Yf, Yo2, mdot_over_V, rho, solved] = solve_equilib_T( T, phi, fuel,
T_in, printing )
% SOLVE_EQUILIB_T solves the equilibrium of a WSR.
%
%    [TMAX, YF, YO2, MDOT_OVER_V] = SOLVE_EQUILIB_T( T, PHI, FUEL,
T_IN, PRINTING )
```

```
%       returns the maximum equilibrium temperature, the equilibirum values of the
%       fuel mass fraction, YF, and the oxygen mass fraction, YO2, and the equilibrium
%       mass flux, MDOT_OVER_V, given the equilibrium temperature T, the
equivalence ratio
%       PHI, the fuel, either 'methane' or 'ethane', and the inlet temperature, T_IN.
%
%   See also: wsr_parameters.m, initial_mass_fract.m
%
% Written by Losh.
% Version 1.5, 4/20/2004 10:40PM.
%


if nargin < 5
    printing = 0 ;
end

solved = 1 ;

% Parameter Definitions.
[ MWox, MWo2, MWpr, MWfuel, Ta, Ru, A, cp, delhr, Tin, m, n, AFs ] =
wsr_parameters( fuel ) ;

if length( phi ) > 1
    Yfin = phi( 1 ) ;
    Yoxin = phi( 2 ) ;
    rho_num = 101325 * (( Yfin/MWfuel + 0.233*Yoxin/MWo2 + 0.767*Yoxin/28 )^-1 )
/ 8314 ;
else
    % Calculate initial mass fractions of oxidzier and fuel.
    [ Yfin, Yoxin, MWfuel, MWmix, rho_num ] = initial_mass_fract( phi, fuel ) ;
end

Tmax = T_in + Yfin * delhr / cp ;


%fprintf( 'Tmax = %4.0f K \n', Tmax ) ;
if printing == 1
        fprintf('Tmax = %5.4f\n', Tmax ) ;
end

if T > Tmax
    solved = 0 ;
    if printing == 1
        fprintf('\n\nMAX TEMP = %5.0f\n\n', Tmax ) ;
    end
```

```
    T = 0 ; Yf = 0 ; Yo2 = 0 ; mdot_over_V = 0 ; rho = 0 ;
    return
end

% Solve for Yf based on given temperature, T.
Yf = ( cp / delhr ) * ( T_in - T ) + Yfin ;

% Solve for Yo2 based on Yf.
q = 0.23310023310023 ;
Yox = Yoxin + 4.76 * ( MWox / MWfuel ) * AFs * ( Yf - Yfin ) ;
Yo2 = q * Yox ;

% Calculate the density of the mixture.
rho = 348.8 / Tin ;

% Calculate the pre-exponential frequency factor, Af.
Af = A * MWfuel / (MWfuel^m * MWo2^n) ;


% Calculate RR of fuel.
omegaF = A * exp( -Ta / T ) * ((rho*Yf/MWfuel)^m) * ((rho*Yo2/MWo2)^n);

Wf = Af * (rho * Yf )^m * (rho * Yo2 )^n * exp( -Ta / T );
Qrdot_b = delhr * Wf ;

% Check to make sure the equilibrium solution does not rely on imaginary numbers.
if isreal([omegaF Yf rho])~=1
    if printing == 1
    fprintf('COMPLEX VALUE!\n') ;
    end
    T=0; Yf=0; Yo2=0; mdot_over_V=0; rho=0;
    solved = 0 ;
    return
end

% Calculate heat release rate.
Qrdot =  Wf * delhr ;

% Solve for mdot/V, using conservation of species, fuel.
mdot_over_V = omegaF * MWfuel  / ( Yfin - Yf ) ;
mdot_over_V1 =  Qrdot / cp  / ( T - T_in ) ;

if (mdot_over_V-mdot_over_V1)>1e-7
    fprintf('MDOT MISMATCH\n') ;
end
```

```
if printing == 1
    fprintf( 'Mass fraction of fuel: %4.9f\n', Yf ) ;
    fprintf( 'Mass fraction of O2: %4.9f\n', Yo2 ) ;
    fprintf( 'Mass fraction of Oxidizer: %4.9f\n', Yo2/0.233 ) ;
    fprintf( 'Mdot/V: %4.9f\n', mdot_over_V ) ;
    fprintf( 'Wf: %4.9f\n', Wf ) ;
    fprintf( 'Qrdot : %1.4e\n', Qrdot ) ;
end
```

```
function [ mag, ph, w, mV, bw, sys_stab, varargout ] = wsr11_sim_linearz( model, T,
phi, fuel, T_in, alpha, time_delay,printing, fig )
% WSR11_SIM_LINEARZ linearizes a simulink model of a single WSR system.
%
%   [ MAG, PH, W, MV, BW, SYS_STAB, TMAX, SYS ] = WSR11_SIM_LINEARZ(
MODEL, T, PHI, FUEL, T_IN, ALPHA, TIME_DELAY,PRINTING, FIG )
%       attempts to linearize model MODEL at equilibrium temperature T1 and
equivalence ratio PHI,
%       and fuel FUEL, with an inlet temperature of T_IN, recirculation percent ALPHA,
%       and a time delay of TIME_DELAY.
%       PRINTING is a flag (0 or 1) that determines if output is printed to the command
window.
%       FIG specifies which figure number is used when graphing is performed.
%
%   WSR22_SIM_LINEARIZ returns the a vector of magnitudes in MAG and the
associated phases PH from a FRF,
%   performed at frequencies, W. It also returns a vecotr of mdot/V's in mV, the
bandwidth in hertz, BW,
%   a system stability flag, SYS_STAB, (0 for unstable, 1 for stable), the maximum
temperature of the system
%   at the given parameters, TMAX, the actual system, SYS.
%
% See also: initial_mass_fract.m, wsr_parameters.m, solve_equilib_T.m,
set_wsr_sim_param.m, and
%           linmod.m

% Written by Losh, Febuary, 2004.
% Version 1.2, 3/17/2004 12:16PM.
%



V = 1 ;

% For simplified inputs, set flags and parameters. ------------------------
if nargin < 9
```

```
% If not inputed, specify the range of the frequency response to be plotted.
    printing = 0 ;
end
% ------------------------------------------------------------------------

if nargin ~= 10
    fig = 21 ;
end


% Initialize system stability flag to stable,ie,1.
sys_stab = 1 ;

% Function call to initial_mass_fract.m to compute initial mass fraction of species.
[ Yf_in, Yox_in, MWfuel, FA, rho_num1 ] = initial_mass_fract( phi, fuel, printing );

% Function call to wsr_parameters.m to retrieve parameters of WSR's.
[ MWox, MWo2, MWpr, MWfuel, Ta, Ru, A, cp, delhr, Tin, nf, no2, a ] =
wsr_parameters( fuel );

% Compute frequency factor for reaction rate of fuel.
Af = MWfuel * A / ( MWfuel^nf * MWo2^no2 ) ;

% Function call to solve_equilib_T.m which returns mdot/V value for 1st reactor.
[ Tmax, Yf, Yo2, mV, rho, solved ] = solve_equilib_T( T, phi, fuel, T_in, printing ) ;

% If equilibrium could not be solved, set values to zero and return out of function.
if solved == 0
    mag = 0 ;
    ph = 0 ;
    w = 0 ;
    mV = 0 ;
    bw = 0 ;
    sys_stab = 0 ;
    varargout = { Tmax, 0, 0 } ;
    return ;

end

rho_num1 = rho_num1(1) ;
mdot = mV * V ;

Yox = Yo2 / 0.233 ;
g = alpha ;
Trho = T_in ;
```

```
% Create structure, S, which contains all current variables. ----------------------
W = whos ;

% Create initial string.
e_str = [ 'S = struct(W(',num2str(1),').name,eval([W(',num2str(1),').name])' ];

% Loop that adds on additional strings for the several variables.
for i = 2: length( W )
    e_str = strcat(e_str,',W(',num2str(i),').name,eval([W(',num2str(i),').name])') ;
end

% Ending string.
e_str = strcat( e_str, ');' ) ;

% Evaluate the string, which creates the structure.
eval( e_str ) ;


% Set the parameters of the WSR.
[ success ] = set_wsr_sim_param1( S, 1 ) ;


if success == 0
        fprintf('SET_WSR_SIM_PARAM FAILED\n') ;
        mag = 0 ;
        ph = 0 ;
        w = 0 ;
        mV = 0 ;
        bw = 0 ;
        sys_stab = 0 ;
        varargout = { Tmax, 0, 0 } ;
        return
end



% ------------------------------------------------------------------------------
% Simulate the system at the equilibrium point.
%model = model
%T = T
%Yf = Yf
%Yox = Yox
%
[ A, B, C, D ] = linmod( model, [ T Yf Yox ], mdot ) ; %T2 Yf( 2 ) Yox( 2 )

% Create system from obtained matrices.
```

```
sys = ss( A, B, C, D ) ;

% If model has extra outputs, force into SISO.
sys = sys( 1, 1 ) ;

if issiso( sys)
    % Compute bandwidth of system.
    bw = bandwidth( sys ) / 2 / pi ;
else
    bw = 0 ;
    if printing == 1
    fprintf('Bandwidth not available, because system is not SISO.\n') ;
    end
end

% Calculate the poles of the system.
poles = eig( A ) ;

% Calculate zeros of system.
zs = zero( sys ) ;

% Find pole-zero cancellations.
delta = 1 ; % How close to a pole and zero have to be to cancel.
[ zuc, puc, zc, pc ] = pz_cancel( poles, zs, delta ) ;
% ------------------------------------------------------------------------------

% Determine if any of the poles have positive real parts, ie, are unstable poles.
for i = 1 : length( poles )
    if real(poles(i)) > 0
        sys_stab = 0 ;
        if printing == 1
            fprintf('\n#### UNSTABLE SYSTEM #### .\n\n') ;
        end
        mag = 0 ; ph = 0 ; w = 0 ; bw = 0 ; varargout = { Tmax, 0 } ;
    end
end


% ------------------------------------------------------------------------------------------
% ---------------------------------- PLOTTING ----------------------------------------

    w1 = 1e0 ; w2 = 1e5 ;

if nargout ~= 0
    [ mag, ph, w ] = bode( sys, { w1, w2 } ) ;
    mag = squeeze( mag ) ;
```

```
    ph = squeeze( ph ) ;

else
    W = logspace(0,6,500) ;

    h2 = figure( fig  ) ; clf;
    name_figure( h2, [model,': T = ', num2str(T)] ) ;
    bode( sys, {w1, w2} ) ; grid on

    figure( fig +1 )
    pzmap( sys )
    grid on


end
% ------------------------------------------------------------------------------


% ------------------------------------------------------------------------------
% Printing Option.
if printing == 1

    Uncancelled_zeros = zuc.'
    Uncancelled_poles = puc.'

    fprintf('\n\n----------------------------------\n');
    fprintf( 'Mdot = %4.4f\n', mdot ) ;
    if bw > 1e6
        fprintf('BANDWIDTH = %1.6e Hz\n', bw ) ;
    else
        fprintf('BANDWIDTH = %1.f Hz\n', bw ) ;
    end

    fprintf('Number of poles: %2.0f\n', length( poles ) ) ;
    fprintf('Number of zeros: %2.0f\n', length( zs ) ) ;
    fprintf('----------------------------------\n\n') ;
end
% ------------------------------------------------------------------------------



% Assign variable output variables.
varargout = { Tmax, sys } ;
```

---

function [Tmax, Yf, Yox, Yo2, mV, rho, solved, varargout] = solve_equilib_T22(T1, T2, phi, fuel, T_in, alpha,beta, Patms, printing)

```
% SOLVE_EQUILIB_T2 solves the equilibrium of a coupled 2-WSR system.
%
%    [ TMAX, YF, YOX, YO2, MV, RHO, SOLVED ] =  SOLVE_EQUILIB_T2( T1,
T2, PHI, FUEL, T_IN, ALPHA, PRINTING )
%        returns the maximum equilibrium temperature, TMAX, a vector of equilibrium
mass fuel mass
%        fractions, YF and oxygen mass fractions, YO2, the equilibrium mass fluxes, MV,
the density
%        of the system, RHO, and a flag indicating whether or not a solution was found,
SOLVED
%        given the equilibirum temperatures of the WSR's, T1 and T2, the equivalence
ratio, PHI,
%        the fuel, either 'methane' or 'ethane', the inlet temperature, T_IN, and the amount
of
%        recirculation, ALPHA.
%
%    See Also: solve_equilib_T.m, initial_mass_fract.m, wsr_parameters.m
%
% Written by Losh.
% Version 1.12, 4/20/2004 10:45PM.
%

% If no printing preference specified, assume no printing.
if nargin < 8
    printing = 0 ;
end


% Initialize solved flag.
solved = 1 ;

% Function call to wsr_parameters.m to retrieve the parameter definitions.
[ MWox, MWo2, MWpr, MWfuel, Ta, Ru, A, cp, delhr, Tin, m, n, a ] = wsr_parameters(
fuel ) ;

% Calculate initial mass fractions of oxidzier and fuel by function call to
initial_mass_fract.m
[ Yf_in, Yox_in, MWfuel, MWmix, rho_num ] = initial_mass_fract( phi, fuel, 0, Patms )
;
Yo2_in = 0.233 * Yox_in;

% Calculate the maximum equilibrium temperature for given case of fuel and
equivalence ratio.
T1max = T_in + Yf_in * delhr / cp ;
```

```
% Calculate equilibrium values. - - - - - - - - - - - - - - - - - - -

% Calculate fuel mass fraction, Yf1, from T1.
Yf1 = (cp/delhr) *(T_in - T1) + Yf_in ;

% Calculate T2max.
T2max = T1 + Yf1 * delhr / cp ;

% Check to see that the desired equilibrium temperatures are less than the maximum
allowed Temp.
if (T1 > T1max) | (T2 > T1max) | (T2 > T2max)
    solved = 0 ;
    if printing == 1
        fprintf('\n\nMAX TEMP1 = %5.0f\n\n', T1max ) ;
        fprintf('\n\nMAX TEMP2 = %5.0f\n\n', T2max ) ;
    end

    % Set outputs to zero to signify no solution found.
    Yf = 0 ;
    Yo2 = 0 ;
    Yox = 0 ;
    mV = 0 ;
    rho = 0 ;
    solved = 0 ;
    Tmax = [ T1max T2max ] ;
    varargout = {0,0,0,0,0,0 } ;
    return
end
% Calculate fuel mass fraction, Yf2, from Yf1, and T1, T2.
Yf2 = (cp/delhr) *(T1 - T2) + Yf1 ;

% Calculate oxidizer mass fraction, Yox1, from Yf1.
Yox1 = Yox_in -  4.76 * ( MWox / MWfuel ) * a *  ( Yf_in - Yf1 );

% Calculate oxidizer mass fraction, Yox2, from Yox1 and Yf1,Yf2.
Yox2 = Yox1 - 4.76 * ( MWox / MWfuel ) * a *  ( Yf1 - Yf2 );

% Calculate oxygen mass fractions.
Yo21 = Yox1 * 0.233 ;
Yo22 = Yox2 * 0.233 ;



%- - - - - - - - - - - - - - - - - - - - - - - - - - - - - - - - - - - -
```

```
% Calculate the rho_num for the systems.
[ fubar, fubar, fubar, fubar, rho_num1, phi1 ] = initial_mass_fract( [ Yf_in ; Yox_in ],
fuel ) ;
[ fubar, fubar, fubar, fubar, rho_num2, phi2 ] = initial_mass_fract( [ Yf1 ; Yox1 ], fuel ) ;

% Calculate the density of the mixture.
Trho = T_in ;
rho1 = rho_num / Trho;
rho2 = rho_num / Trho;

% Calculate the pre-exponential frequency factor, Af.
Af = A * MWfuel / ( MWfuel^m * MWo2^n ) ;

% Calculate mass RR of fuel.
WF1 = Af * exp( -Ta / T1 ) * ( ( rho1 * Yf1 )^m ) * ( ( rho1 * Yo21 )^n ) ;
WF2 = Af * exp( -Ta / T2 ) * ( ( rho2 * Yf2 )^m ) * ( ( rho2 * Yo22 )^n ) ;
WF = [ WF1  WF2 ] ;
Qrdot = delhr .* WF ;

% Solve for both mdot/V 's: mV1 and mV2.
%mV1 = WF1 / ( Yf_in + ( alpha / ( 1 - alpha ) ) * Yf2 - (1/(1-alpha))*Yf1 ) ;
%mV2 = WF2 / ( ( Yf1 - Yf2 ) / ( 1 - alpha ) ) ;
mV1 = (delhr/cp) * WF1 * (alpha+beta-1)/((T1*(beta-1) + alpha*T2 + T_in*(1-alpha-
beta))) ;
mV2 = -(delhr/cp) * WF2 * (alpha+beta-1)/((beta-1)*(T1-T2)) ;

% Assign values to output variables.
Yf = [ Yf1  Yf2 ] ;
Yox = [ Yox1  Yox2 ] ;
Yo2 = [Yo21  Yo22 ] ;
mV = [ mV1  mV2 ] ;
rho = [ rho1  rho2 ] ;
rho_num = [ rho_num1 rho_num2 ] ;
phi = [ phi1 phi2 ]  ;
Tmax = [ T1max T2max ] ;

% If either of the mdot/V values are negative, then the solution is incorrect.
if mV1 < 0 | mV2 < 0
    solved = 0 ;
end

% Calculate Tdot, which should be zero.
Tdot1 = ( 1 / rho1 ) *( mV1 * (T_in + (alpha/(1-alpha))*T2 - (1/(1-alpha))*T1 ) +
(delhr/cp)*WF1 ) ;
Tdot2 = ( 1 / rho2 ) *( mV2 * ( 1 / ( 1 - alpha ) ) * ( T1 - T2 ) + ( delhr / cp ) * WF2 ) ;
Tdot = [ Tdot1 Tdot2 ] ;
```

```
% Print data to command window if desired.
if printing == 1
    if solved == 1
        fprintf('A Solution was found:\n');
    else
        fprintf('ERROR: The solution found used unrealistic values:\n');
    end
    fprintf( '----- First Reactor Volume ----- \n') ;
    fprintf( 'Equivalence ratio of 1st Reactor: %4.4f\n', phi1 ) ;
    fprintf( 'Equilibrium Temperature, T1: %4.9f\n', T1 ) ;
    fprintf( 'Mass fraction of fuel, Yf1: %4.9f\n', Yf1 ) ;
    fprintf( 'Mass fraction of O2, Yo2,1: %4.9f\n', Yo21 ) ;
    fprintf( 'Mass fraction of Oxidizer, Yox1: %4.9f\n', Yox1 ) ;
    fprintf( 'Density, rho1: %4.9f\n', rho1 ) ;
    fprintf( 'Mdot/V1: %4.9f\n', mV1 ) ;
    fprintf( 'Wf1: %4.9f\n', WF1 ) ;
    fprintf( 'Qrdot1: %1.9e\n', Qrdot(1) ) ;
    fprintf( 'Tdot1 check: %1.2e\n', Tdot1 ) ;
    fprintf( '-------------------------------- \n\n\n' ) ;

    fprintf( '----- Second Reactor Volume ----- \n') ;
    fprintf( 'Equivalence ratio of 2nd Reactor: %4.4f\n', phi2 ) ;
    fprintf( 'Equilibrium Temperature, T2: %4.9f\n', T2 ) ;
    fprintf( 'Mass fraction of fuel, Yf2: %4.9f\n', Yf2 ) ;
    fprintf( 'Mass fraction of O2, Yo2,2: %4.9f\n', Yo22 ) ;
    fprintf( 'Mass fraction of Oxidizer, Yox2: %4.9f\n', Yox2 ) ;
    fprintf( 'Density, rho2: %4.9f\n', rho2 ) ;
    fprintf( 'Mdot/V2: %4.9f\n', mV2 ) ;
    fprintf( 'Wf2: %4.9f\n', WF2 ) ;
    fprintf( 'Qrdot2: %1.9e\n', Qrdot(2) ) ;
    fprintf( 'Tdot2 check: %1.2e\n', Tdot2 ) ;
    fprintf( '-------------------------------- \n' ) ;

end

varargout = { rho_num, phi, Tdot,WF, Qrdot, Trho };
```

```
function [ mag, ph, w, mV, bw, sys_stab, varargout ] = wsr22_sim_lineariz( model,
T1,T2, phi, fuel, T_in, alpha,beta,Patms, time_delay,printing, fig )
% WSR22_SIM_LINEARIZ linearizes a simulink model of a coupled 2 WSR system.
%
%    [ MAG, PH, W, MV, BW, SYS_STAB, TMAX, SYS, VRATIO ] =
WSR22_SIM_LINEARIZ( MODEL, T1,T2, PHI, FUEL, T_IN, ALPHA,BETA,
TIME_DELAY,PRINTING, FIG )
```

```
%       attempts to linearize model MODEL at equilibrium temperatures T1 and T2 and
equivalence ratio PHI,
%       and fuel FUEL, with an inlet temperature of T_IN, recirculation percent ALPHA,
recirculation, BETA,
%       and a time delay of TIME_DELAY.
%       PRINTING is a flag (0 or 1) that determines if output is printed to the command
window.
%       FIG specifies which figure number is used when graphing is performed.
%
%   WSR22_SIM_LINEARIZ returns the a vector of magnitudes in MAG and the
associated phases PH from a FRF,
%   performed at frequencies, W. It also returns a vecotr of mdot/V's in mV, the
bandwidth in hertz, BW,
%   a system stability flag, SYS_STAB, (0 for unstable, 1 for stable), the maximum
temperature of the system
%   at the given parameters, TMAX, the actual system, SYS, and the ratio of volumes,
V2/V1, VRATIO.
%
% See also: initial_mass_fract.m, wsr_parameters.m, solve_equilib_T2.m,
set_wsr_sim_param22.m, and
%           linmod.m
%
%   Written by Losh.
%   Version 1.0 11/24/2003 3:04PM
%

% Check number of inputs.
error( nargchk( 10, 12, nargin ) ) ;


% Specify volume of first reactor.
V1 = 1 ;


% For simplified inputs, set flags and parameters. ------------------------
if nargin < 11
% If not inputed, specify the range of the frequency response to be plotted.
    printing = 0 ;
end
% ------------------------------------------------------------------------

if nargin ~= 12
    fig = 21 ;
end
```

```
% Initialize system stability flag to stable,ie,1.
sys_stab = 1 ;

% Function call to initial_mass_fract.m to compute initial mass fraction of species.
[ Yf_in, Yox_in, MWfuel, FA, rho_num ] = initial_mass_fract( phi, fuel, printing );

% Function call to wsr_parameters.m to retrieve parameters of WSR's.
[ MWox, MWo2, MWpr, MWfuel, Ta, Ru, A, cp, delhr, Tin, nf, no2, a ] =
wsr_parameters( fuel );

% Compute frequency factor for reaction rate of fuel.
Af = MWfuel * A / ( MWfuel^nf * MWo2^no2 ) ;

% Function call to solve_equilib_T.m which returns mdot/V value for 1st reactor.
[ Tmax, Yf, Yox, Yo2, mV, rho, solved, rho_num, phi, Tdot,WF, Qrdot, Trho ] =
solve_equilib_T22( T1, T2, phi, fuel, T_in, alpha,beta, Patms, printing ) ;

% If equilibrium could not be solved, set values to zero and return out of function.
if solved == 0
    mag = 0 ;
    ph = 0 ;
    w = 0 ;
    mV = 0 ;
    bw = 0 ;
    sys_stab = 0 ;
    varargout = { Tmax, 0, 0 } ;
    return ;

end

% Define rho_num variables for setting the parameters later in set_wsr_sim_param.m
rho_num = rho_num( 1 ) ;

% Compute ratio of volumes, Vratio = V2/V1.
Vratio = mV(1) / mV(2) ;

% Compute mdot based on mdot/V and volume 1 specified earlier.
mdot = mV( 1 ) * V1 ;

% Compute volume of second reactor segment, V2.
V2 = mdot * mV( 2 ) ^ -1 ;

% Set volume string for output.
if V2 < V1
    vol_str = 'Volume: V2 < V1' ;
else
```

```
    vol_str = 'Volume: V1 < V2' ;
end



V = [ V1 V2 ] ;
T = [ T1 T2 ] ;

% Create structure, S, which contains all current variables. ----------------------
W = whos ;

% Create initial string.
e_str = [ 'S = struct(W(',num2str(1),').name,eval([W(',num2str(1),').name])' ];

% Loop that adds on additional strings for the several variables.
for i = 2: length( W )
    e_str = strcat(e_str,',W(',num2str(i),').name,eval([W(',num2str(i),').name])') ;
end

% Ending string.
e_str = strcat( e_str, ');' ) ;

% Evaluate the string, which creates the structure.
eval( e_str ) ;

% ------------------------------------------------------------------------------

% Function call to set_wsr_sim_param.m which goes through the simulink model and
sets
% the values of all the variable blocks.
success = set_wsr_sim_param_22( S, 1 ) ;
success = set_wsr_sim_param_22( S, 2 ) ;

if success == 0
        fprintf('SET_WSR_SIM_PARAM FAILED\n') ;
        mag = 0 ;
        ph = 0 ;
        w = 0 ;
        mV = 0 ;
        bw = 0 ;
        sys_stab = 0 ;
    varargout = { Tmax, 0, 0 } ;
        return
end
```

```
% ------------------------------------------------------------------------------
% Simulate the system at the equilibrium point.
[ A, B, C, D ] = linmodv5( model, [ T1 Yf( 1 ) Yox( 1 ) T2 Yf( 2 ) Yox( 2 ) ], mdot )
;%T2 Yf( 2 ) Yox( 2 )

% Create system from obtained matrices.
sys = ss( A, B, C, D ) ;

% If model has extra outputs, force into SISO.
sys = sys( 1, 1 ) ;

try
    % Compute bandwidth of system.
    bw = bandwidth( sys ) / 2 / pi ;
catch
    bw = 0 ;
    if printing == 1
    fprintf('Bandwidth not available, because system is not SISO.\n') ;
    end
end

% Calculate the poles of the system.
poles = eig( A ) ;

% Calculate zeros of system.
zs = zero( sys ) ;

% Find pole-zero cancellations.
delta = 1 ; % How close to a pole and zero have to be to cancel.
[ zuc, puc, zc, pc ] = pz_cancel( poles, zs, delta ) ;
% ------------------------------------------------------------------------------

% Determine if any of the poles have positive real parts, ie, are unstable poles.
for i = 1 : length( poles )
    if real(poles(i)) > 0
        sys_stab = 0 ;
        if printing == 1
            fprintf('\n#### UNSTABLE SYSTEM #### .\n\n') ;
        end
        mag = 0 ; ph = 0 ; w = 0 ; bw = 0 ; varargout = { Tmax, 0 } ;
    end
end
```

```
% ------------------------------------------------------------------------------
% ---------------------------------- PLOTTING ----------------------------------

if nargout ~= 0
    w1 = 1e-5 ; w2 = 1e15 ;
    [ mag, ph, w ] = bode( sys, { w1, w2 } ) ;
    mag = squeeze( mag ) ;
    ph = squeeze( ph ) ;

else
    w1 = 1e-4 ; w2 = 1e10 ;
    W = logspace(0,6,500) ;
    h2 = figure( fig  ) ;
    clf;
    name_figure( h2, [model,': T1 = ', num2str(T1)] ) ;
    bode( sys, {w1, w2} ) ;
    grid on


end
% ------------------------------------------------------------------------------
% ------------------------------------------------------------------------------




% ------------------------------------------------------------------------------
% Printing Option.
if printing == 1

    Uncancelled_zeros = zuc.'
    Uncancelled_poles = puc.'

    fprintf('\n\n-----------------------------------\n');
    fprintf( 'Mdot = %4.4f\n', mdot ) ;
    fprintf( [vol_str,'\n'] ) ;
    fprintf( 'Volume ratio, V2/V1 = %4.4f\n', Vratio ) ;
    if bw > 1e6
        fprintf('BANDWIDTH = %1.6e Hz\n', bw ) ;
    else
        fprintf('BANDWIDTH = %1.f Hz\n', bw ) ;
    end

    fprintf('Number of poles: %2.0f\n', length( poles ) ) ;
```

```
    fprintf('Number of zeros: %2.0f\n', length( zs ) ) ;
    fprintf('---------------------------------\n\n') ;
end
% --------------------------------------------------------------------------------



% Assign variable output variables.
varargout = { Tmax, sys, Vratio } ;
```

```
function [ Tmax, Yf, Yox, Yo2, mV, rho, solved, varargout ] =  solve_equilib_T32( T1,
T2,T3, phi, fuel, T_in, alpha,beta, printing )
% SOLVE_EQUILIB_T32 solves the equilibrium of a 3-WSR system.
%
%    [ TMAX, YF, YOX, YO2, MV, RHO, SOLVED ] =  SOLVE_EQUILIB_T32( T1,
T2,T3, PHI, FUEL, T_IN, ALPHA, BETA, PRINTING )
%        returns the maximum equilibrium temperature, TMAX, a vector of equilibrium
mass fuel mass
%        fractions, YF and oxygen mass fractions, YO2, the equilibrium mass fluxes, MV,
the density
%        of the system, RHO, and a flag indicating whether or not a solution was found,
SOLVED
%        given the equilibirum temperatures of the WSR's, T1 and T2, the equivalence
ratio, PHI,
%        the fuel, either 'methane' or 'ethane', the inlet temperature, T_IN, and the amount
of
%        recirculation, ALPHA.
%
%    See Also: solve_equilib_T.m, initial_mass_fract.m, wsr_parameters.m
%
% Written by Losh.
% Version 1.4, 4/20/2004 10:39PM.
%

% If no printing preference specified, assume no printing.
if nargin < 7
    printing = 0 ;
end
no = nargout ;

% Initialize solved flag.
solved = 1 ;

% Function call to wsr_parameters.m to retrieve the parameter definitions.
[ MWox, MWo2, MWpr, MWfuel, Ta, Ru, A, cp, delhr, Tin, m, n, a ] = wsr_parameters(
fuel ) ;
```

```
% Calculate initial mass fractions of oxidzier and fuel by function call to
initial_mass_fract.m
[ Yf_in, Yox_in, MWfuel, MWmix, rho_num ] = initial_mass_fract( phi, fuel ) ;

% Calculate the maximum equilibrium temperature for given case of fuel and
equivalence ratio.
Tmax = T_in + Yf_in * delhr / cp ;


% Calculate equilibrium values. - - - - - - - - - - - - - - - - - - - -



% Check to see that the desired equilibrium temperatures are less than the maximum
allowed Temp.
if ( T1 > Tmax ) | ( T2 > Tmax ) | ( T3 > Tmax )
    solved = 0 ;
    if printing == 1
        fprintf('\n\nMAX TEMP = %5.0f\n\n', T1max ) ;
    end

    % Set outputs to zero to signify no solution found.
    Yf = 0 ;
    Yo2 = 0 ;
    Yox = 0 ;
    mV = 0 ;
    rho = 0 ;
    solved = 0 ;
    Tmax = [ Tmax ] ;
    varargout = { 0,0,0,0,0,0 } ;
    return
end

% Calculate fuel mass fraction, Yf1, from T1.
Yf1 = ( cp / delhr ) * ( T_in - T1 ) + Yf_in ;

% Calculate fuel mass fraction, Yf2 and Yf3.
Yf2 = (cp/delhr) *( T1 - T2 ) + Yf1 ;
Yf3 = (cp/delhr) *( T2 - T3 ) + Yf2 ;

Yo2in = 0.233 * Yox_in ;
Yo21 = Yo2in + ( Yf1 - Yf_in ) * a * MWo2 / MWfuel ;
Yo22 = Yo2in + ( Yf2 - Yf_in ) * a * MWo2 / MWfuel ;
Yo23 = Yo2in + ( Yf3 - Yf_in ) * a * MWo2 / MWfuel ;
```

```
Yox1 = Yo21 / 0.233 ;
Yox2 = Yo22 / 0.233 ;
Yox3 = Yo23 / 0.233 ;




%- - - - - - - - - - - - - - - - - - - - - - - - - - - - - - - - - - - - - - - -


% Calculate the rho_num for the systems.
[ fubar, fubar, fubar, fubar, rho_num1, phi1 ] = initial_mass_fract( [ Yf_in ; Yox_in ],
fuel ) ;%[ Yf_in ; Yox_in ]
[ fubar, fubar, fubar, fubar, rho_num2, phi2 ] = initial_mass_fract( [ Yf1 ; Yox1 ], fuel ) ;
[ fubar, fubar, fubar, fubar, rho_num3, phi3 ] = initial_mass_fract( [ Yf2 ; Yox2 ], fuel ) ;

% Calculate the density of the mixture.
rho1 = rho_num / T_in ;
rho2 = rho_num / T_in ;
rho3 = rho_num / T_in ;

Trho = T_in ;

% Calculate the pre-exponential frequency factor, Af.
Af = A * MWfuel / ( MWfuel^m * MWo2^n ) ;

% Calculate mass RR of fuel.
WF1 = Af * exp( -Ta / T1 ) * ( ( rho1 * Yf1 )^m ) * ( ( rho1 * Yo21 )^n ) ;
WF2 = Af * exp( -Ta / T2 ) * ( ( rho2 * Yf2 )^m ) * ( ( rho2 * Yo22 )^n ) ;
WF3 = Af * exp( -Ta / T3 ) * ( ( rho3 * Yf3 )^m ) * ( ( rho3 * Yo23 )^n ) ;
WF = [ WF1 WF2 WF3 ] ;
Qrdot = delhr .* WF ;

% Solve for mdot/V 's:
mV1 = -((delhr/cp)*WF1) / ( T_in + (T3*alpha/(1-alpha-beta)) - (T1*(1-beta)/(1-alpha-
beta))) ;
mV2 = -((delhr/cp) * WF2) / ( T1*(1-beta)/(1-alpha-beta) + (beta*T3/(1-alpha-beta)) -
T2/(1-alpha-beta));
mV3 = -(delhr/cp)*WF3 / ( ( T2-T3 )/(1-alpha-beta) );

vratio12 = mV1 / mV2 ;
vratio13 = mV1 / mV3 ;
vratio23 = mV2 / mV3 ;
```

```
% Assign values to output variables.
Yf = [ Yf1 Yf2 Yf3 ] ;
Yox = [ Yox1 Yox2 Yox3] ;
Yo2 = [Yo21 Yo22 Yo23] ;
mV = [ mV1 mV2 mV3 ] ;
rho = [ rho1  rho2 rho3 ] ;
rho_num = [ rho_num1 rho_num2 rho_num3 ] ;
phi = [ phi1 phi2 phi3 ]  ;
Tmax = [ Tmax ] ;

% If either of the mdot/V values are negative, then the solution is incorrect.
if mV1 < 0 | mV2 < 0 | mV3 < 0
    solved = 0 ;
end

% Calculate Tdot, which should be zero.
Tempstuff = mV2 * ( (1-beta)*T1/ ( 1 - alpha-beta )  +beta*T3/( 1 - alpha-beta ) - T2/( 1 -
alpha-beta ) ) ;
RRstuff = ( delhr / cp ) * WF2 ;
Tdot1 = ( 1 / rho1 ) * ( mV1 * ( T_in + (alpha/(1-alpha-beta))*T3 - (1-beta)*T1/(1-alpha-
beta))  + (delhr/cp)*WF1 ) ;
Tdot2 = ( 1 / rho2 ) * ( mV2 * ( (1-beta)*T1/ ( 1 - alpha-beta )  +beta*T3/( 1 - alpha-beta
) - T2/( 1 - alpha-beta ))  + ( delhr / cp ) * WF2 ) ;
Tdot3 = ( 1 / rho3 ) * ( mV3 * ((T2- T3)/( 1 - alpha-beta )) + (delhr/cp)*WF3) ;
Tdot = [ Tdot1 Tdot2 Tdot3 ] ;


% Print data to command window if desired.
if printing == 1
    if solved == 1
        fprintf('A Solution was found:\n');
    else
        fprintf('ERROR: The solution found used unrealistic values:\n');
    end
    fprintf( '----- First Reactor Volume ----- \n') ;
    fprintf( 'Equivalence ratio of 1st Reactor: %4.4f\n', phi1 ) ;
    fprintf( 'Equilibrium Temperature, T1: %4.9f\n', T1 ) ;
    fprintf( 'Mass fraction of fuel, Yf1: %4.9f\n', Yf1 ) ;
    fprintf( 'Mass fraction of O2, Yo2,1: %4.9f\n', Yo21 ) ;
    fprintf( 'Mass fraction of Oxidizer, Yox1: %4.9f\n', Yox1 ) ;
    fprintf( 'Density, rho1: %4.9f\n', rho1 ) ;
    fprintf( 'Mdot/V1: %4.9f\n', mV1 ) ;
    fprintf( 'Wf1: %4.9f\n', WF1 ) ;
    fprintf( 'Qrdot1: %1.9e\n', Qrdot(1) ) ;
    fprintf( 'Tdot1 check: %1.2e\n', Tdot1 ) ;
```

```
    fprintf( '-------------------------------- \n\n\n' ) ;

    fprintf( '----- Second Reactor Volume ----- \n') ;
    fprintf( 'Equivalence ratio of 2nd Reactor: %4.4f\n', phi2 ) ;
    fprintf( 'Equilibrium Temperature, T2: %4.9f\n', T2 ) ;
    fprintf( 'Mass fraction of fuel, Yf2: %4.9f\n', Yf2 ) ;
    fprintf( 'Mass fraction of O2, Yo2,2: %4.9f\n', Yo22 ) ;
    fprintf( 'Mass fraction of Oxidizer, Yox2: %4.9f\n', Yox2 ) ;
    fprintf( 'Density, rho2: %4.9f\n', rho2 ) ;
    fprintf( 'Mdot/V2: %4.9f\n', mV2 ) ;
    fprintf( 'Wf2: %4.9f\n', WF2 ) ;
    fprintf( 'Qrdot2: %1.9e\n', Qrdot(2) ) ;
    fprintf( 'Tdot2 check: %1.2e\n', Tdot2 ) ;
    fprintf( '-------------------------------- \n\n\n' ) ;


    fprintf( '----- Third Reactor Volume ----- \n') ;
    fprintf( 'Equivalence ratio of 3nd Reactor: %4.4f\n', phi3 ) ;
    fprintf( 'Equilibrium Temperature, T3: %4.9f\n', T3) ;
    fprintf( 'Mass fraction of fuel, Yf3: %4.9f\n', Yf3 ) ;
    fprintf( 'Mass fraction of O2, Yo2,3: %4.9f\n', Yo23 ) ;
    fprintf( 'Mass fraction of Oxidizer, Yox3: %4.9f\n', Yox3 ) ;
    fprintf( 'Density, rho3: %4.9f\n', rho3 ) ;
    fprintf( 'Mdot/V3: %4.9f\n', mV3 ) ;
    fprintf( 'Wf3: %4.9f\n', WF3 ) ;
    fprintf( 'Qrdot3: %1.9e\n', Qrdot(3) ) ;
    fprintf( 'Tdot3 check: %1.2e\n', Tdot3 ) ;
    fprintf( '-------------------------------- \n' ) ;

    fprintf( '\nVolume Ratios:\n' ) ;
    fprintf( 'Volume ratio, V2/V1 = %4.9f\n', vratio12 ) ;
    fprintf( 'Volume ratio, V3/V1 = %4.9f\n', vratio13 ) ;
    fprintf( 'Volume ratio, V3/V2 = %4.9f\n', vratio23 ) ;
    fprintf( 'Check: (V3/V1)/(V2/V1) = %4.4f\n', vratio13/vratio12 )
end

varargout = { rho_num, phi, Tdot,WF, Qrdot, Trho };
```

```
function [ mag, ph, w, mV, bw, sys_stab, varargout ] = wsr32_sim_lineariz( model,
T1,T2,T3, phi, fuel, T_in, alpha,beta, time_delay,printing, fig )
% WSR32_SIM_LINEARIZ linearizes a simulink model of a coupled 3-WSR system.
%
%     [ MAG, PH, W, MV, BW, SYS_STAB, TMAX, SYS, VRATIO ] =
WSR32_SIM_LINEARIZ( MODEL, T1,T2, PHI, FUEL, T_IN, ALPHA,BETA,
TIME_DELAY,PRINTING, FIG )
```

```
%       attempts to linearize model MODEL at equilibrium temperatures T1 and T2 and
equivalence ratio PHI,
%       and fuel FUEL, with an inlet temperature of T_IN, recirculation percent ALPHA,
recirculation, BETA,
%       and a time delay of TIME_DELAY.
%       PRINTING is a flag (0 or 1) that determines if output is printed to the command
window.
%       FIG specifies which figure number is used when graphing is performed.
%
%   WSR32_SIM_LINEARIZ returns the a vector of magnitudes in MAG and the
associated phases PH from a FRF,
%   performed at frequencies, W. It also returns a vecotr of mdot/V's in mV, the
bandwidth in hertz, BW,
%   a system stability flag, SYS_STAB, (0 for unstable, 1 for stable), the maximum
temperature of the system
%   at the given parameters, TMAX, the actual system, SYS, and the ratio of volumes,
V2/V1, VRATIO.
%
% See also: initial_mass_fract.m, wsr_parameters.m, solve_equilib_T32.m,
set_wsr_sim_param32.m, and
%           linmod.m
%
%   Written by Losh.
%   Version 1.2 2/3/2004 1:39PM.
%

% Check number of inputs.
error( nargchk( 10, 12, nargin ) ) ;

% Specify volume of first reactor.
V1 = 1 ;

% For simplified inputs, set flags and parameters. ------------------------
if nargin < 11
% If not inputed, specify the range of the frequency response to be plotted.
    printing = 0 ;
end
% ---------------------------------------------------------------------------

if nargin ~= 12
    fig = 21 ;
end

% Initialize system stability flag to stable,ie,1.
sys_stab = 1 ;
```

```
% Function call to initial_mass_fract.m to compute initial mass fraction of species.
[ Yf_in, Yox_in, MWfuel, FA, rho_num ] = initial_mass_fract( phi, fuel, printing );

% Function call to wsr_parameters.m to retrieve parameters of WSR's.
[ MWox, MWo2, MWpr, MWfuel, Ta, Ru, A, cp, delhr, Tin, nf, no2, a ] =
wsr_parameters( fuel );

% Compute frequency factor for reaction rate of fuel.
Af = MWfuel * A / ( MWfuel^nf * MWo2^no2 ) ;

% Function call to solve_equilib_T.m which returns mdot/V value for 1st reactor.
[ Tmax, Yf, Yox, Yo2, mV, rho, solved, rho_num, phi, Tdot,WF, Qrdot, Trho ] =
solve_equilib_T32( T1, T2,T3, phi, fuel, T_in, alpha,beta, printing ) ;

% If equilibrium could not be solved, set values to zero and return out of function.
if solved == 0
    mag = 0 ;
    ph = 0 ;
    w = 0 ;
    mV = 0 ;
    bw = 0 ;
    sys_stab = 0 ;
    varargout = { Tmax, 0, 0,0 } ;
    return ;

end


% Compute ratio of volumes, Vratio = V2/V1.
Vratio12 = mV(1) / mV(2) ;
Vratio13 = mV(1) / mV(3) ;
Vratio23 = mV(2) / mV(3) ;
Vratio = [ Vratio12 Vratio13 Vratio23 ] ;

% Compute mdot based on mdot/V and volume 1 specified earlier.
mdot = mV( 1 ) * V1 ;

% Compute volume of second reactor segment, V2.
V2 = mdot * mV( 2 ) ^ -1 ;
V3 = mdot * mV( 3 ) ^ -1 ;




V = [ V1 V2 V3 ] ;
T = [ T1 T2 T3 ] ;
```

```
rho_num = rho_num(1) ;

% Create structure, S, which contains all current variables. ----------------------
W = whos ;

% Create initial string.
e_str = [ 'S = struct(W(',num2str(1),').name,eval([W(',num2str(1),').name])' ];

% Loop that adds on additional strings for the several variables.
for i = 2: length( W )
    e_str = strcat(e_str,',W(',num2str(i),').name,eval([W(',num2str(i),').name])') ;
end

% Ending string.
e_str = strcat( e_str, ');' ) ;

% Evaluate the string, which creates the structure.
eval( e_str ) ;

% ------------------------------------------------------------------------------

% Function call to set_wsr_sim_param.m which goes through the simulink model and
sets
% the values of all the variable blocks.
success = 1;
i=0;
while success==1 & i<3
    i = i + 1 ;
    success = set_wsr_sim_param_32( S, i ) ;
end
%success = set_wsr_sim_param_32( S, 2 ) ;
%success = set_wsr_sim_param_32( S, 3 ) ;


if success == 0
     if printing
        fprintf('SET_WSR_SIM_PARAM FAILED\n') ;
     end
        mag = 0 ;
        ph = 0 ;
        w = 0 ;
        mV = 0 ;
        bw = 0 ;
        sys_stab = 0 ;
%         fprintf('Returning\n') ;
    varargout = { Tmax, 0, mdot,0 } ;
```

```
        return
end



% ------------------------------------------------------------------------------
% Simulate the system at the equilibrium point.
[ A, B, C, D ] = linmodv5( model, [ T1 Yf( 1 ) Yox( 1 ) T2 Yf( 2 ) Yox( 2 ) T3 Yf( 3 )
Yox( 3 ) ], mdot ) ;%T2 Yf( 2 ) Yox( 2 )

% Create system from obtained matrices.
sys = ss( A, B, C, D ) ;

% If model has extra outputs, force into SISO.
sys = sys( 1, 1 ) ;

try
    % Compute bandwidth of system.
    bw = bandwidth( sys ) / 2 / pi ;
catch
    bw = 0 ;
    if printing == 1
    fprintf('Bandwidth not available, because system is not SISO.\n') ;
    end
end

% Calculate the poles of the system.
poles = eig( A ) ;

% Calculate zeros of system.
zs = zero( sys ) ;

% Find pole-zero cancellations.
delta = 1 ; % How close to a pole and zero have to be to cancel.
[ zuc, puc, zc, pc ] = pz_cancel( poles, zs, delta ) ;

% ------------------------------------------------------------------------------
% Determine if any of the poles have positive real parts, ie, are unstable poles.
for i = 1 : length( poles )
    if real(poles(i)) > 0
        sys_stab = 0 ;
        if printing == 1
            fprintf('\n#### UNSTABLE SYSTEM #### .\n\n') ;
        end
```

```
        mag = 0 ; ph = 0 ; w = 0 ; bw = 0 ; ;
    end
end

% ------------------------------------------------------------------------------
% ---------------------------------- PLOTTING ----------------------------------
    w1 = 1e-4 ; w2 = 1e10 ;

if nargout ~= 0
    [ mag, ph, w ] = bode( sys, { w1, w2 } ) ;
    mag = squeeze( mag ) ;
    ph = squeeze( ph ) ;

else
    W = logspace(0,6,500) ;
    if fig ~= 0
        h2 = figure( fig  ) ; clf;
        name_figure( h2, [model,': T1 = ', num2str(T1)] ) ;

        bodehz( sys, w1, w2 ) ; grid on
        h3 = figure( fig + 1) ;
        pzmap( sys );
        name_figure( h3, ['PZMAP'] ) ;

    end
end
% ------------------------------------------------------------------------------

% ------------------------------------------------------------------------------
% ------------------------------------------------------------------------------
% Printing Option.
if printing == 1

    Uncancelled_zeros = zuc.'
    Uncancelled_poles = puc.'

    fprintf('\n\n----------------------------------\n');
    fprintf( 'Mdot = %4.4f\n', mdot ) ;

    if bw > 1e6
        fprintf('BANDWIDTH = %1.6e Hz\n', bw ) ;
    else
        fprintf('BANDWIDTH = %1.f Hz\n', bw ) ;
    end

    fprintf('Number of poles: %2.0f\n', length( poles ) ) ;
```

```
    fprintf('Number of zeros: %2.0f\n', length( zs ) ) ;
    fprintf('----------------------------------\n\n') ;
end
% --------------------------------------------------------------------------------

% Assign variable output variables.
varargout = { Tmax, sys, mdot, Vratio } ;
```

Bibliography

[1] Annaswamy, A., El Rifai, O., Fleifil, M, Ghoniem, A. "A Model-based Active-adaptive Controller for Thermoacoustic Instability." *Proceedings of the 1997 IEEE International Conference on Control Applications.* pp. 842 – 847. Hartford, CT, 1997.

[2] Annaswamy, A., Fleifel, M., Ghoneim, Z. and Ghoniem, A. "Active control of thermoacoustic instability in combustion system." *IEEE Conference on Control Applications - Proceedings.* 95CH35764. pp 685 – 690, 1995.

[3] Annaswamy, A., Fleifel, M., Ghoneim, Z. and Ghoniem, A. "A Feedback Model of Thermoacoustic Instability in Combustion Processes." Report 9502, Department of Mechanical Engineering, MIT, 1995.

[4] Annaswamy, A. and Ghoniem, A. "Active control of combustion instability: Theory and Practice." *IEEE Control Systems Magazine.* Vol. 22, No. 6, pp 37-54, 2002.

[5] Bittanti, S., de Marco, A., Poncia, G, and Prandoni, W. "Identification of a Model for Thermoacoustic Instabilities in a Rijke Tube." *IEEE Transactions on Control Systems Technology*. Vol. 10, No. 4, pp. 490 – 502, 2002.

[6] Blust, J. and Ballal, D. "Fuel Effects on Lean Blowout and Emissions from a Well-Stirred Reactor." *Journal of Propulsion & Power.* Vol. 15, No. 2, pp. 216 – 223, 1999.

[7] Dowling, A. and Hubbard, S. "Instability in lean premixed combustors." *Proceedings of the Institution of Mechanical Engineers. Part A, Journal of Power & Energy.* Vol. 214, No. 4, pp 317 – 332, 2000.

[8] Fannin, C. “Linear Modeling and Analysis of Thermoacoustic Instabilities in a Gas Turbine Combustor.” Ph.D. Dissertation, Department of Mechanical Engineering, Virginia Tech, Blacksburg, VA, 2000.

[9] Fleifil, M., Annaswamy, A., Rumsey, J., Kojic, and A., Ghoniem, A., “A Physically Based Nonlinear Model of Combustion Instability and Active Control. *Proceedings of the 1998 IEEE International Conference on Control Applications.* pp. 1185 – 1189. Trieste, Italy, 1998.

[10] Guckenheimer, J. “Multiple Bifurcation Problems for Chemical Reactors.” *Physica D.* Vol. 20, pp. 1 – 20, 1984.

[11] Haber, L. and Vandsburger U. "A global reaction model for OH* Chemiluminescence applied to a laminar flat-flame burner." *Combustion Science and Technology.* Vol. 175, No. 10, pp 1859 – 1891. 2003.

[12] Huang, X. “Development of Reduced-Order Flame Models for Prediction of Combustion Instability.” Ph.D. Dissertation, Department of Electrical Engineering, Virginia Tech, Blacksburg, VA, 2001.

[13] Kee, R., Grcar, J., Smooke, M. and Miller, J., "A fortran program for modeling steady laminar one-dimensional premixed flames." Technical Report SAND85-8240 UC-401 Sandia National Laboratories (1993).

[14] Khanna, Vivek. “A study of the dynamics of laminar and turbulent fully and partially premixed flames.” Ph.D. Dissertation, Department of Electrical Engineering, Virginia Tech, Blacksburg, VA, 2001.

[15] Kinsler, L., Frey, A., Coppens, A., and Sanders, J. *Fundamentals of Acoustics*. John Wiley & Sons, Inc. 2000.

[16] Kruger, I. and Bohn, I. “Combustion Driven Oscillations in Gas Turbines: Theoretical Prediction and Evaluation of Passive Suppression Methods.” ECOS 2000 Proceedings, Universiteit Twente, Nederland, FEBODRUK, Enschede, 2000, pp. 2155-2166.

[17] Lieuwen, T. "Experimental Investigation of Limit-Cycle Oscillations in an Unstable Gas Turbine Combustor." Journal of Propulsion and Power. Vol. 18, No. 1, pp. 61 – 67, 2002.

[18] Lieuwen, T. "Phase drift characteristics of self-excited, combustion-driven oscillations." Journal of Sound and Vibration. Vol. 242, No. 5, pp. 893 – 905, 2001.

[19] Lieuwen, T. "Theoretical investigation of unsteady flow interactions with a premixed planar flame." *Journal of Fluid Mechanics.* Vol. 435, pp. 289 – 303, 2001.

[20] Lieuwen, T., Neumeier, Y., and Zinn, B. "The Role of Unmixedness and Chemical Kinetics in Driving Combustion Instabilities in Lean Premixed Combustors." *Combustion Science and Technology.* Vol. 135, pp. 193 – 211, 1998.

[21] Lieuwen, T. and Zinn, B. "Theoretical Investigation of Combustion Instability Mechanisms in Lean Premixed Gas Turbines." AIAA – 98 – 0641, 1997.

[22] Mohanraj, R., Neumeier, Y., and Zinn, B. "Combustor Model for Simulation of Combustion Instabilities and Their Active Control." *Journal of Propulsion and Power.* Vol. 16, No. 3, pp.485 – 491, 2000.

[23] Nicoli, C. and Pelcé, P. "One-dimensional model for the Rijke Tube." *Journal of Fluid Mechanics*. Vol 202, pp.83-96, 1989.

[24] Park, S., Annawamy, A., and Ghoniem, A. "Heat Release Dynamics Modeling of Kinetically Controlled Burning." *Combustion and Flame.* Vol. 128, pp 217 – 231, 2002.

[25] Raun, R., Beckstead, M., Finlinson, J. and Brooks, K. "A Review of Rijke Tubes, Rijke Burners, and Related Devices." *Progress in Energy and Combustion Science.* Vol. 19, pp. 318 – 384, 1993.

[26] Rumsey, J., Fleifil, M., Annaswamy, A., and Ghoniem, A. "Low-order Nonlinear Models of Thermoacoustic Instabilities and Model-based Control." *Proceedings of the 1998 IEEE International Conference on Control Applications.* pp. 1419 – 1423. Trieste, Italy, 1998.

[27] Schreel, K., Rook, R. and de Goey, L. "The Acoustic Response of a Burner Stabilized Premixed Flat Flame." ECOS 2000 Proceedings, Universiteit Twente, Nederland, FEBODRUK, Enschede, 2000, pp. 2167-2177.

[28] Smith, P., Golden, D., Frenklach, M., Moriarty, N., Eiteneer, B., Goldenber, M., Bowman, C., Hanson, R., Song, S., Gardiner, W., Lissianski,V. and Qin, Z. http://www.me.berkeley.edu/gri_mech 1999.

[29] Thom, R. *Structural Stability and Morphogenese.* W. A. Benjamin, Reading, MA, 1975.

[30] Turns, S. *An Introduction to Combustion.* McGraw-Hill Higher Education. 2000.

Vita

James David Losh was born in Lynchburg, VA, on July 6, 1980, the son of Laurence and Mary Lana Losh. He lived in Poplar Forest, VA, before moving to Lynchburg at age 3. After graduating with honors from E.C. Glass High School in Lynchburg, he attended Virginia Tech in the fall of 1998. Losh graduated Summa Cum Laude with a B.S. in Mechanical Engineering and a B.S. in Mathematics from Virginia Tech in May 2002. Losh then started on his Master's in the fall of 2002. In May 2004, Losh will receive his Master's of Science in Mechanical Engineering from Virginia Tech and take a job in the private sector.